INKJET-PRINTED RF MODULES FOR SENSING AND COMMUNICATION APPLICATIONS

A Dissertation
Presented to
The Academic Faculty

by

Hoseon Lee

In Partial Fulfillment
of the Requirements for the Degree
Doctorate of Philosophy in the
School of Electrical and Computer Engineering

Georgia Institute of Technology
July 2013

INKJET-PRINTED RF MODULES FOR SENSING AND COMMUNICATION APPLICATIONS

Approved by:

Dr. Manos M. Tentzeris
School of ECE
Georgia Institute of Technology

Dr. Benjamin D.B. Klein
School of ECE
Georgia Institute of Technology

Dr. Andrew F. Peterson
School of ECE
Georgia Institute of Technology

Dr. Jud Ready
School of MSE
Georgia Institute of Technology

Dr. Gregory D. Durgin
School of ECE
Georgia Institute of Technology

Date Approved: August 16, 2013

To my wife and daughter, who have been supportive and patient through this process.

ACKNOWLEDGEMENTS

I wish to thank my advisor, Professor Manos M. Tentzeris for his support and guidance. Not only has he has motivated me to seek excellence and novelty in research but he has also been supportive of programs such as ORS and TI:GER at Georgia Tech, through which I gained invaluable experience. I would like to thank my colleagues in our research group, for the many nights of research conversations and moral support.

The TI:GER program for their financial support and the opportunity to understand the synergy effect of applied research, business, law, and commercialization.

Professor Hertling for giving me the opportunity to teach Circuit and Electronics for several semesters which not only gave me valuable teaching experience but also financial support. Professor Peterson and Professor Durgin for being available and their willingness to discuss the theory and concepts related to my research and for lending me their knowledge.

Finally, I reserve this last paragraph to thank my parents and sister, who have given me the foundation from which I could pursue an academic career and to my beloved wife, Yeon J. Lee, and my beautiful daughter, Eun Sang Lee, for their constant love, patience, trust, encouragement, hope and prayer.

TABLE OF CONTENTS

LIST OF TABLES

LIST OF FIGURES

Page

LIST OF TABLES

LIST OF SYMBOLS AND ABBREVIATIONS

RFID	Radio Frequency Identification
CNT	Carbon Nanotubes
PABS	Polyaminobenzene sulfonic acid
AMC	Artificial Magnetic Conductor
PEC	Perfect Electric Conductor
PMC	Perfect Magnetic Conductor
PPM	Parts per million
SRF	Self Resonance Frequency

SUMMARY

The objective of the proposed research is to integrate nanotechnology, applied electromagnetics, and inkjet printing fabrication methods to develop a series of novel inkjet-printed RF modules for sensing and communication applications: wireless gas sensor, wearable RFID tag, and RF inductor.

Passive, wireless sensors have various applications in a wide range of fields including military, industry, and medicine. However, there are issues such as cost, sensitivity of sensors, manufacturing complexities, and feasibility of further miniaturization of these RF modules. One aspect of this research investigates the feasibility of addressing these issues by integrating nanotechnology and applied electromagnetics. The underlying common theme for the three designs is inkjet-printing silver nanoparticles on organic paper substrate.

The research will investigate the characterization of thin film carbon nanotubes and the optimization of inkjet-printing the CNT material on paper substrate followed by the design of a patch antenna based gas sensor. Measurement results from a closed measurement system will be shown. Secondly, an inkjet-printed, conformal, wearable RFID tag on an artificial magnetic conductor is designed and tested using an RFID Reader. Lastly an inkjet-printed high Q RF inductor is designed and integrated with magnetic nanomaterial to evaluate the feasibility of increasing inductance using high permeability nanomaterial. Through the design and testing of the aforementioned three designs, it will be shown that through a multidisciplinary design process, novel, low-cost RF modules can be designed for sensing and communication applications.

CHAPTER I

INTRODUCTION

Today, there is a high demand for novel wireless sensors and RF modules for sensing and communication applications. For example, in the health care industry, there is a need for miniaturized, wireless, flexible bio-monitoring sensors to accurately and conveniently monitor the vitals of patients in the hospital or at home at a very low-cost. There is also a high demand for wireless gas sensors in both the industry and defense. For example, in factories where chemicals are used, toxic gas are present, and for large scale data systems such as Google and IBM, large warehouses of computers need to be cooled in a large scale, for which ammonia is used. In these cases, it is important to be able to detect leakage of toxic gases remotely in a large scale. In defense or homeland security, it is important to be able to detect toxic gases remotely from a safe distance. It is also important to be able to cover a large area, which requires a large network of sensors. Lastly, printed electronics is becoming more and more important as flexible displays are being researched and developed for the mobile telecommunication industry, as well as flexible sensors for robotics and healthcare industry. Samsung has shown prototypes of flexible displays using printed flexible LEDs at the Consumer Electronics Symposium.[1] Beyond the mobile telecommunication industry, flexible electronic paper[2] and curved OLED TVs[3] are other fields that has become technologically feasible.

The commonalities for the above-mentioned demands are as follows:

- Wireless
- Flexible
- Low cost
- Scalable for wireless sensor networks

BCC Research estimated that the sensors industry will be worth $91.5 billion in 2016. According to the research firm's report, "Sensors: Technologies and global markets," the sensors rise will translate to a five-year compound annual growth rate (CAGR) of 7.8%.[4] Biosensors and chemical sensors are at $13.3 billion in 2011, and should hit $21 billion if the segment follows its projected 9.6% CAGR.

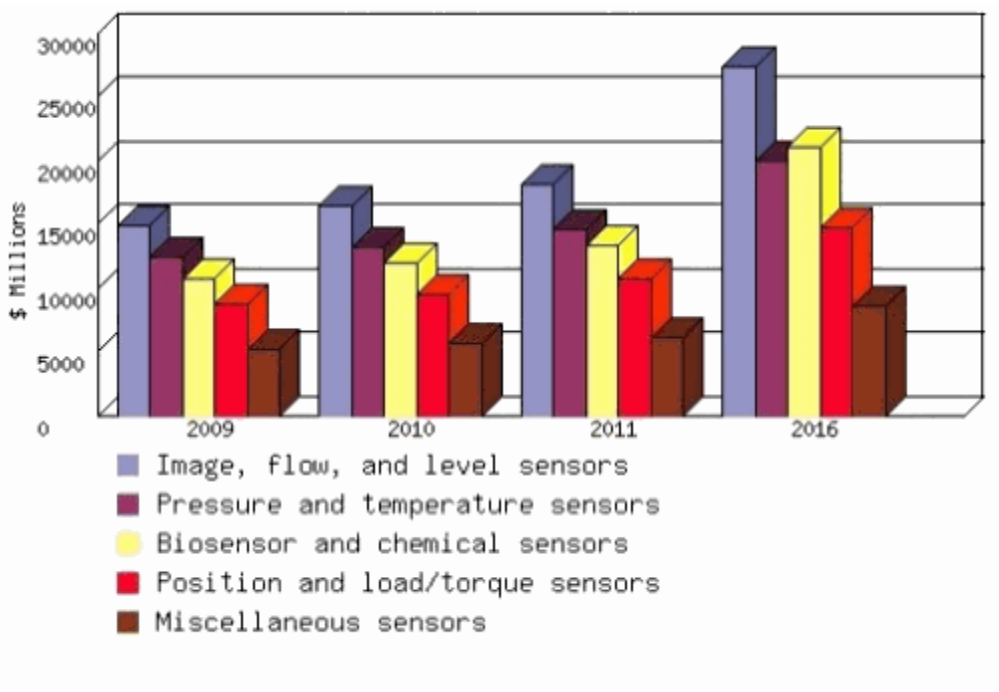

Figure 1. Global sensors market, 2009-2016 in $ millions. (Source: BCC Research May 2011) [5]

To address these needs, a new and different approach is needed to create the hardware devices that meet these specifications. To that end, nanotechnology has been a popular field to help engineer new material that has various sensing capabilities such as gas, strain, humidity, and temperature. However, in all of these cases, the sensed data is converted to a range of DC voltage, current, or impedance values. To create wireless sensors, these DC sensors have to be integrated with a separate wireless module with an antenna that has the capability of transmitting the sensed data wirelessly. This would

increase the size, number of components, number of manufacturing steps, and cost. To create a wireless sensor directly from the nanomaterial, it is necessary to characterize the nanomaterial at high frequencies and understand the properties at the operational frequency bandwidth.

Another important factor is the process of fabrication of these devices for low cost per unit. Printed electronics, and in particular inkjet printing process is used as a low cost fabrication method. In chapter 2, this factor will be addressed in more detail. Ultimately, the systematic process of creating novel wireless sensors and RF modules is illustrated in Figure 2 below.

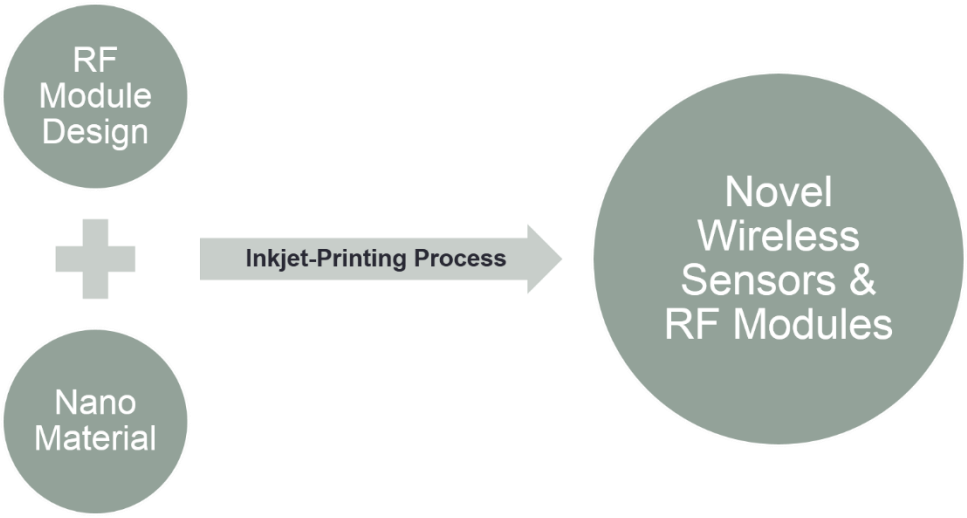

Figure 2. Conceptual overview of designing novel RF modules.

1.1 Wireless bio-monitoring

The global healthcare sector is one of the fastest growing sectors across the globe, accounting for over 10% of the GDP of most of the developed economies. One of the fastest growing segments in this sector is healthcare electronics (including electronics for both, medical and pharmaceutical fields), with rapid developments in various types of

sophisticated electronic devices, equipments and systems fueled by increasing use of new technologies and continuous R&D in this arena.

Bio-monitoring methods have developed substantially since 1965, and wireless technologies of the last few years promise major advances in efficiency by simplifying hospital and home health care. Among various types of sensors, bio sensors can be termed as the biggest game-changers for sensors market in healthcare applications in the past two decades, as it can be undoubtedly said that the current huge market size worth approximately USD 9.9 billion in 2011, and it is expected to grow at a CAGR of 9.6% from 2012 to 2018 to reach a market of USD 18.9 billion by 2018.[6]

$8 billion in 2012 is attained through bio sensors. Bio sensors alone contribute more than 60% of the total revenue and medical sector owing to their phenomenal success in-vitro diagnostics, implantable medical devices, non-invasive surgical tools & equipment, cardiac pacemakers and pharmaceutical drug monitoring systems. But what about communication between the patient and caregiver and between the patient and the environment, as illustrated in Figure 3 below.

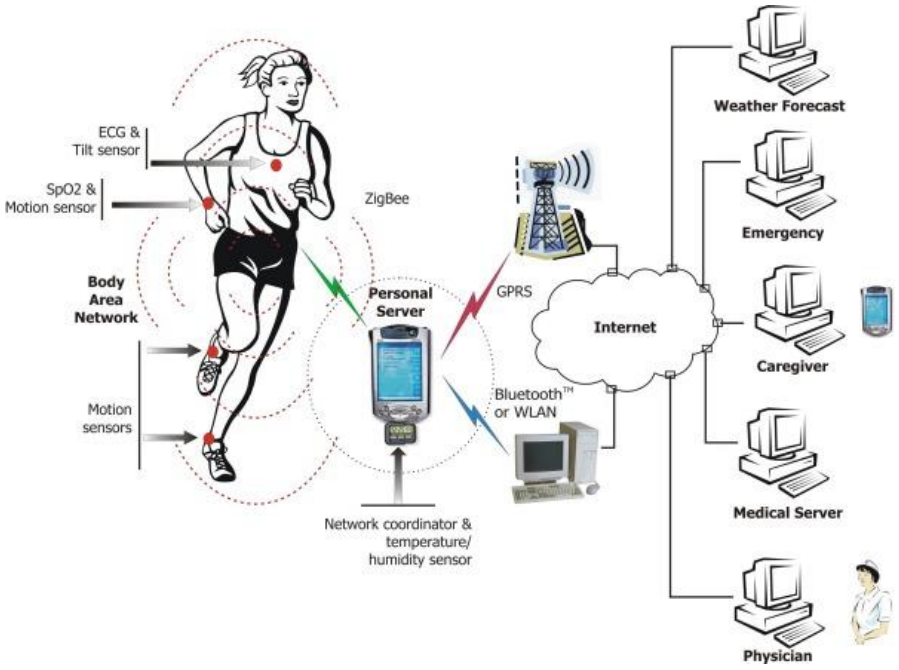

Figure 3. Diagram of wireless bio-monitoring system. [7]

The dawn of IT and multimedia in healthcare revolutionized the field of medical electronics, in turn, affecting the medical sensors market. This has affected the sensors market for smartphone-monitoring in healthcare involving the use of communication technologies for transmission of data acquired through patient monitoring. The field of wireless sensor networking is one of the major focus areas among novel and upcoming fields of research and the latest hot-topic in the field of sensors, the developments of which will drive the sensors market in healthcare applications by a significant extent. The challenge of Bio Signal monitoring is obtaining **accurate measurements** from simultaneous reference points throughout the body while eliminating **interference** (power line, baseline drift, muscle movement, IV-Drip) and also **reducing patient discomfort**.

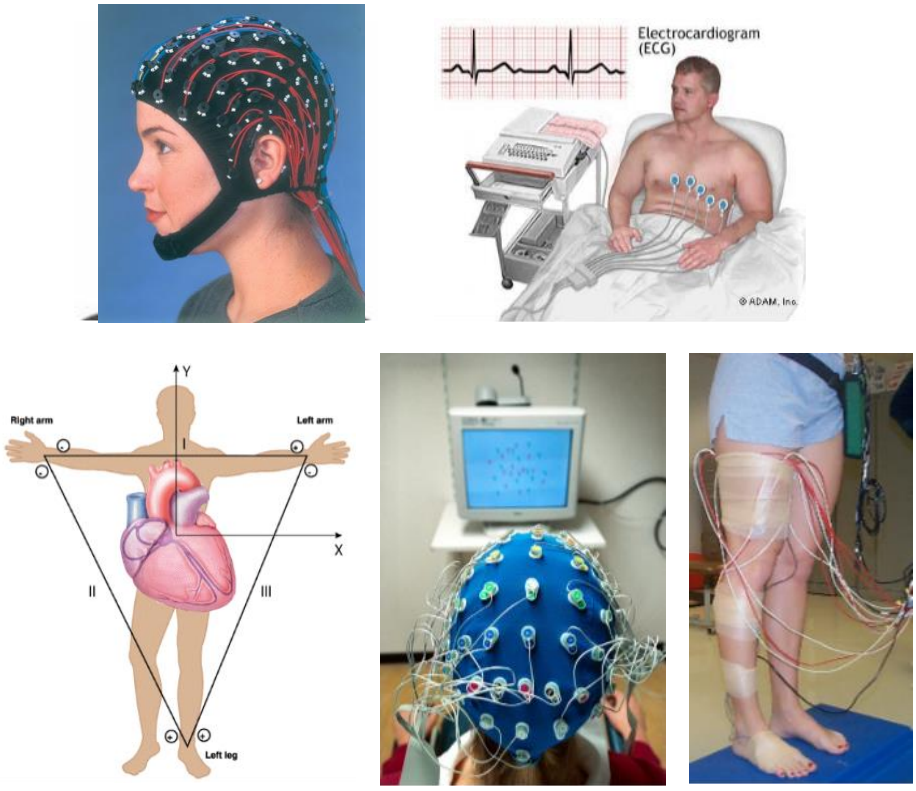

Figure 4. Wired bio signal monitoring.[8, 9]

The pictures in Figure 4 illustrate *wireless* bio signal monitoring where the antenna is mounted directly onto electrodes would eliminate many of these interferences and facilitate *real-time* wireless updates to a portable patient unit.

1.2 Wireless Gas Monitoring

Recently, gas sensing, as a typical application in intelligent systems, is receiving increasing attention in both industry and academia. Gas sensing technology has become more significant because of its widespread and common applications in the following areas: (1) industrial production (e.g., methane detection in mines); automotive industry (e.g., detection of polluting gases from vehicles); (3) medical applications (e.g., electronic noses simulating the human olfactory system); (4) indoor air quality supervision (e.g., detection of carbon monoxide); (5) environmental studies (e.g., greenhouse gas monitoring) (6) homeland security (e.g. detection of IEDs). Globally, the gas sensor market is $250 M/yr, with sensor systems totaling >$1.5 B.[4]

Toxic gas must be sensed in a safe manner from a remote distance. Therefore the sensors need to have wireless capabilities. The sensors must also be small and low-cost so that a network of sensors can be deployed in a target area. However, most conventional gas sensors are bulky and are handheld detection devices, as shown in Figure 5 below. Even for wireless sensors, the size is large, and requires a constant power supply.

Most chemical gas sensors in the market are handheld devices that are expensive and require the sensor element which are also costly and need to be replaced due to the accumulation of chemical residue over time. The chemical residue lowers the sensitivity of these sensors. Furthermore, these sensors are not inherently wireless and would require integration with a wireless module for remote sensing capabilities. Some examples of these sensors are shown in Figure 6 below.

Figure 5. Need for wireless gas sensors for both public safety and defense. [10, 11]

Figure 6. Conventional gas detectors.[12]

BW Technologies provide handheld gas detectors and ammonia sensors, shown in Figure 6.

For low-power, remote gas sensors, it is important to have passive or semi-passive sensors, that operate on a platform such as RFID systems. To create such sensors, conventional sensing materials like metal oxide semiconductors have to deal with the problem of poor sensitivity at room temperature, while carbon nanotubes (CNTs) attract more attention because of their unique properties and have become the most promising materials for high-sensitive gas sensors. As a kind of promising sensing material, CNTs, have been found to possess electrical properties and are highly sensitive to extremely small quantities of gases, such as alcohol, ammonia (NH_3), carbon dioxide (CO_2) and nitrogen oxide (NO_x) at room temperature, while other materials like metal oxides have to be heated by an additional heater in order to operate normally. This high sensitivity eliminates the need of assisting technologies like pre-concentration, and thus contributes to the advantages of low cost, low weight and simple configuration. Besides, CNTs also outperform conventional sensing materials in term of great adsorptive capacity, large surface-area-to-volume ratio and quick response time, resulting in significant changes in electrical properties, such as capacitance and resistance.[13] Moreover, compared with metal oxide semiconductors that require microfabrication techniques, power supply and *ad-hoc* electronics when utilized as sensing material, CNTs possess good corrosion resistance and better bandwidth.[14] Lastly, with small size and wireless capabilities, the sensors can be integrated with RFID or Zigbee protocols battery-less or low-power sensors. These sensors can be used to create a large scale gas sensor network as shown in Figure 7 below.

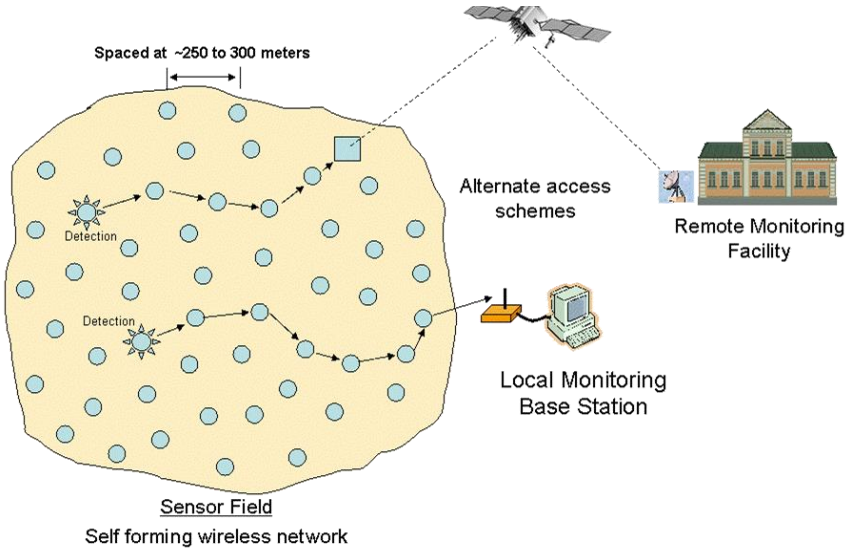

Figure 7. Network of wireless gas sensors.[15]

1.3 Printed Flexible Electronics

Printed electronics is a growing field in both the industry and academia. Various printing processes such as offset printing to gravure up to flexo, screen and inkjet printing are used for applications such as RFID chips, which can be read without contact, and solar cells and displays. The mass production of OLED displays is now already a multi-billion dollar market. There are many different applications for printed electronics. For example, children's books with light switches, wafer-thin illuminated tiles, rolls of solar cells or a handbag with a built-in charging station for the mobile phone. Other areas of application lie in intelligent packaging, medical technology and the pharmaceuticals industry or in the field of consumer electronics. Even classic print products can be upgraded with the new process. For ex-ample, so-called electroluminescent displays are possible, which can be liv-ened up with light and colour effects or animations. For these, several layers of zinc sulphide and copper elements are applied onto the panel film in (screen) printing. The luminescent material lies between these conductor paths, electricity is fed over a programmable circuit board. The different sur-faces can thus be illuminated.

If printed electronics are then combined with 3D printing, three-dimensional objects can even be manufactured in one work step – already fully equipped with electronics.

The new report from IDTechEx titled Printed, Organic & Flexible Electronics: Forecasts, Players & Opportunities 2013-2023 finds that the total market for these technologies will grow from about $16 billion in 2013 to more than $75 billion in 2023. The sector includes profitable large sectors, the majority being OLEDs (organic but not printed) and conductive ink used for a wide range of applications. On the other hand, stretchable electronics, logic and memory, thin film sensors and other components are much smaller segments today, just emerging from R&D.

Organic electronics is a market with major future potential and can take a firm place in our daily lives, for example in intelligent labels on food packaging and solar cells on window panes. Organic and printed electronics is finding a very current application in E-book readers and touch-screens. The continual improvement in printing and production processes combined with cheap materials creates almost unlimited possibilities for applications. Examples of some of these applications are shown in Figure 8 below.

Figure 8. Use of printed electronics in daily life.[16,17,18,19]

Above all else, logistics will benefit from RFID chips which save information and pass this on to a central system via a contact-free reading device. This allows a goods chain, for example, to be monitored in the fight against product piracy. Things will become even more exciting if printed electronics can be sensibly used not only on the surrounding packaging but also on the individual product. There are already examples in the medical industry, and in the near future there will possibly be electronic books with roll-up displays..

To enable this technology, the systematic process of approaching the design of novel wireless sensors and RF modules involves a multi-disciplinary effort of combining RF and antenna engineering with nanotechnology and printed electronics. An example of designing novel gas sensors based on this process is shown in Figure 9 below.

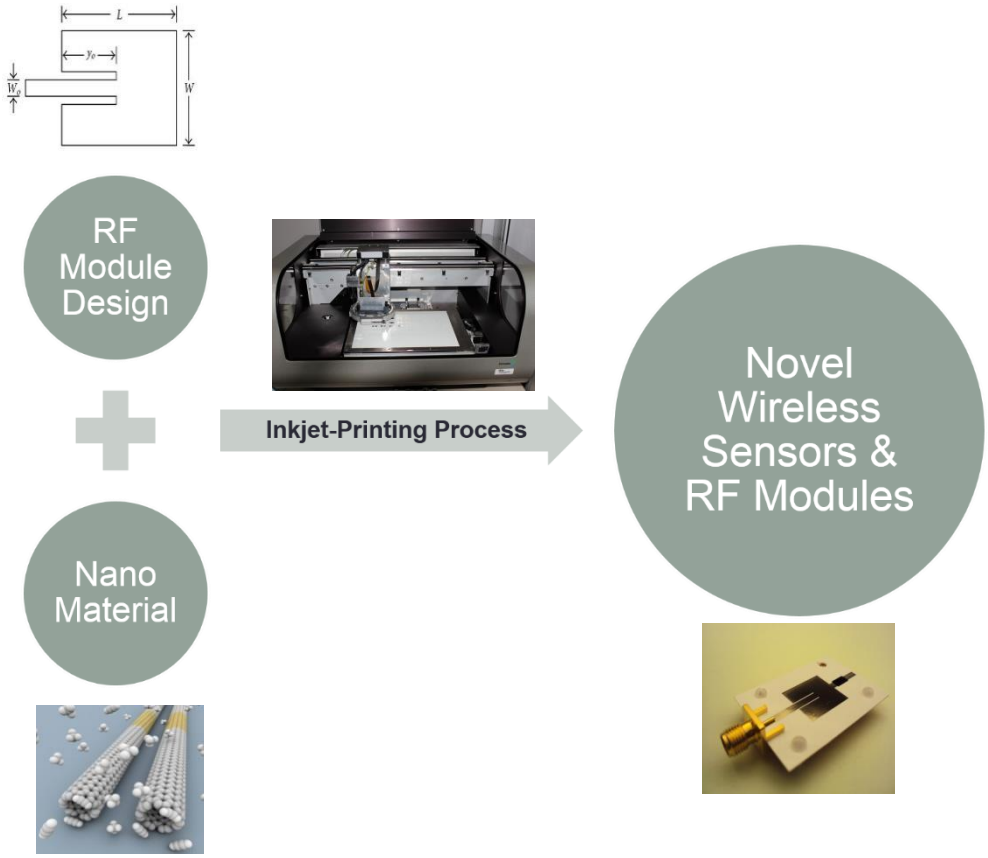

Figure 9. Overview of designing novel gas sensors utilizing nanotechnology and inkjet printing.

CHAPTER II

PLATFORM FOR FLEXIBLE RF MODULES

There are two different platforms that will be introduced, one is the wireless platform and the other is the fabrication platform. For both cases, the key factor is low-cost and scalability for wide area sensor networks.

2.1 Wireless Platforms

Radio frequency identification (RFID) is an emerging compact wireless technology for the identification of objects, and is considered an eminent candidate for the realization of completely ubiquitous ad hoc wireless networks. RFID utilizes electromagnetic waves for transmitting and receiving information stored in a tag or transponder to/from a reader. This technology has several benefits over the conventional ways of identification. Some advantages are higher read range, faster data transfer, the ability of RFID tags to be embedded within objects, no requirement of line-of-sight, and the ability to read a massive amount of tags simultaneously. A listing of applications that currently use RFID are: transportation and logistics, product tracking and inventory systems, access control, library book tracking and management, passports, parcel and document tracking, automatic payment solutions, real time location systems (RTLS), automatic vehicle identification, and livestock or pet tracking. An example of the RFID system with reader and tag is shown in Figure 10.

Whereas a barcode appears printed externally on the object to be scanned, an RFID tag can be embedded within the object itself, or even within a living body – as in the injectable tags which are used for pet identification. The setup for an RFID configuration consists of a scanning antenna which emits radio-frequency radiation, and the tag which is essentially a transponder programmed with the item's information. The use of the radio frequency radiation not only allows the communication between the devices but can also

supply the RFID transponder with a source of energy, meaning that RFID tags do not necessarily need to contain a battery. These tags are called 'passive' RFID tags, and as a result have a long life expectancy. On average an RFID tag can carry up to 2000 bytes of data.

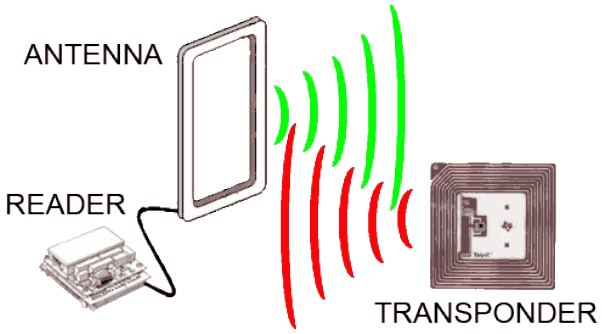

Figure 10. RFID system including reader and tag (transponder).[20]

Because of the technology used the cost of implementing an RFID system is naturally greater than traditional barcoding systems, although the rate of scanning is much higher – typically around less than 100 milliseconds. Additionally, one of the greatest benefits of RFID tagging technology is that an entire bag of groceries; or even your entire shopping cart - could potentially be scanned in moments. The scanning antennas could be incorporated into a door frame or similar channel to scan the persons or objects passing through the field. When a tagged object comes into contact with this field the scanning antenna's activation signal triggers the RFID tag to transmit the data contained in its microchip back to the antenna.

'Active' RFID tags contain their own power source or batteries, meaning that these tags can be scanned at a larger distance, even at several meters away, and still generally have a lifespan of around a decade. High frequency devices are capable of reading tags as far as 20 feet from the scanner. Currently RFID tags are widely used in the automobile production and pharmaceutical industries, as well as for livestock tracking. The technology actually dates back over 50 years. It is only recently however that the costs of

producing the various electronic components has fallen low enough for RFID to pose a viable alternative to ‘disposable’ barcodes. Because of this there has been no real motivation for industry standards to be implemented on a broader scale and for the system to become more widely adopted. Most companies using RFID tags do so internally only, to track their own inventory.

Because RFID technology is designed for very high scanning speeds, issues of “tag collision” and “reader collision” can occur. This happens when signals from multiple readers overlap and the tag is unable to respond to the simultaneous reader queries. Tag collision likewise occurs when many tags are present in a small area and the reader is unable to separate the various return signals.

RFID tags have a few key advantages over traditional barcode systems – mainly the read rates of multiple items, and the fact that no direct line of sight needs to exist between the object and the tag – the tag can be embedded within the product itself. This also means that the durability of the tag is increased because it does not need to be exposed on the outside of packaging.

In addition, data in an RFID tag can be rewriteable if the tag has been designed for this. The new technology means that whereas each item in a shop has been assigned a product barcode, a unique identifier for that type of merchandise – it may now be possible for each separate item of stock to have a unique identifier, which could be linked to the bank card with which the purchase was made. This could be an invaluable tool in police investigations and forensics.

2.2 Low-Cost Fabrication Platform

Low Cost Solutions

There are several different types of fabrication processes for electronics and nanomaterial. For example, chemical vapor deposition (CVD), photolithography, etching, photoengraving, PCB milling, PCB plating, lamination, silkscreen, etc. However, most of these methods do not have the capability of depositing nanomaterials in a controlled manner. CVD method have some control but is complex, costly and cost increases greatly with scale. Printed electronics have become an increasingly popular field for the deposition of nanomaterial, and was chosen as the method of fabrication for the RF module designs in this work.

Inkjet Printing

Inkjet Printing consists of silver nano-particles melting and sintering at low temperatures (100^{o}C). It is economic and convenient compared to wet etching. After melting a good percolation channel is created for electrons flow. This method also provides a better result than traditional polymer thick film material approach. For this research, a Fujifilm Dimatix Materials 2800 Printer was used to fabricate the prototypes. The size of the metal platen onto which the substrate is placed is approximately the size of an A4 piece of paper. The printer requires a cartridge into which the target ink is deposited. Cabot silver nanoink was used as the conductive metal. The cartridge is also used to print carbon nanotubes and magnetic nanoparticles as well. The cartridges have nozzle sizes capable of printing 10 picoliter droplets or 1 picoliter droplets depending on the resolution required and the application. Pictures of the printer and some prototypes are shown in the figures below.

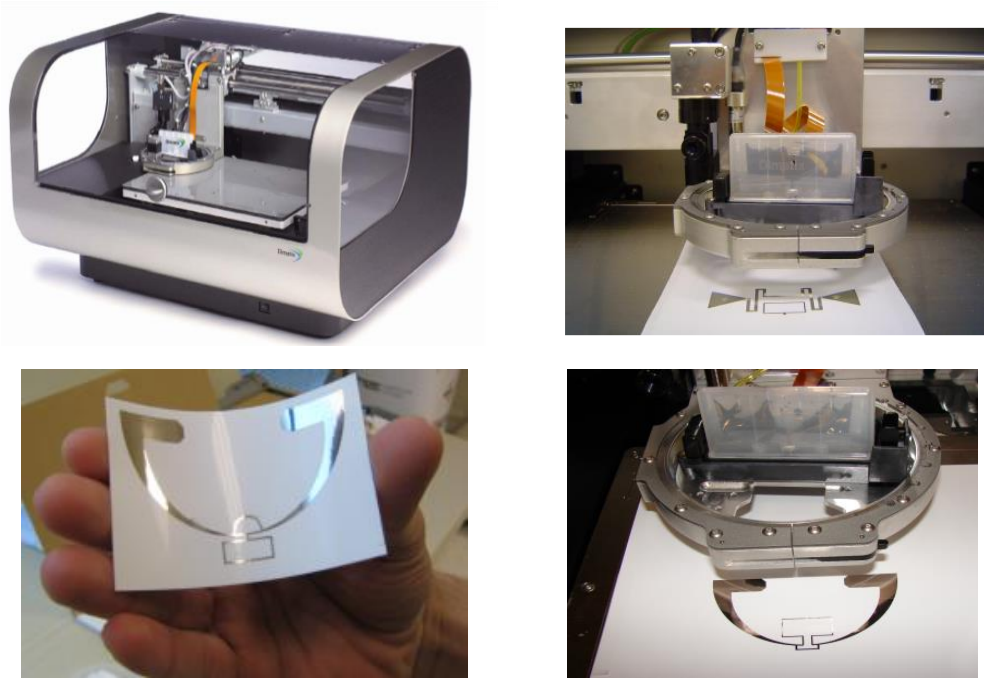

Figure 11. Dimatix materials printer and fabricated prototypes. [21,22]

Figure 11 shows the Dimatix materials printer by Fujifilm Inc. Silver nanoink is printed on paper substrate. The characteristics of the printer are as follows:

- Piezo-driven jetting device to preserve polymeric properties of ink
- 10 pL drops give ~ 21 μm
- Drop placement accuracy ±10 μm gives a resolution of 5080 dpi
- Drop repeatability about 0.5%
- Printability on organic substrates (LCP, paper)

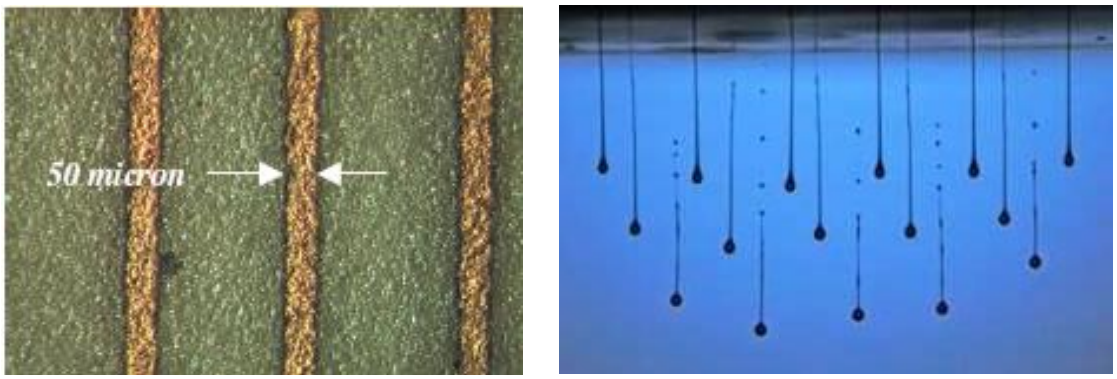

Figure 12. High resolution inkjet printed copper (50 μm).[23]

The printer has high resolution as shown in Figure 12. The jetting profile can be seen in the left picture of Figure 12. The jetting process of the ink in the Dimatix process is outlined in Figure 13. A piezoelectric transducer converts voltage to a decrease in pressure, which draws ink from the fluid supply into an orifice. As the pressure increases again, the ink jets out of the orifice and the ink is deposited onto the substrate. Depending on the surface tension of the substrate, and how hydrophobic or hydrophilic the surface is, the ink has to be formulated so that it deposits onto the surface well.

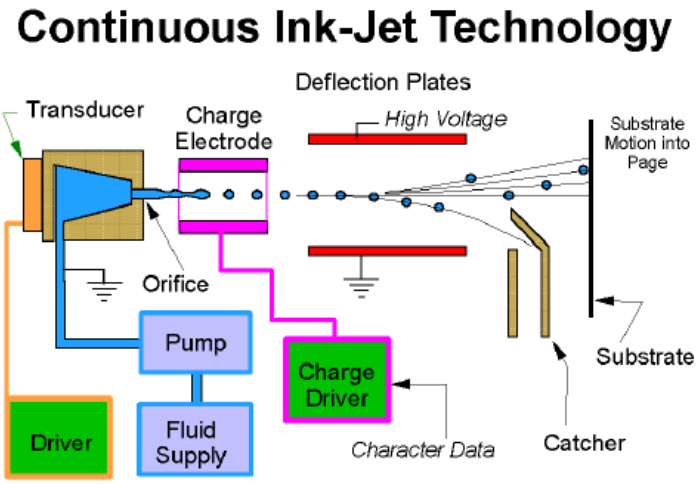

Figure 13. System level overview of ink-jetting process.[23]

Material Considerations

There are many different types of thin flexible substrates available for inkjet printing. Some of the mostly widely used ones are plastics such as polytetrafluoroethylene (PTFE)[24], polyimide (Kapton)[25], and thermoplastic polyetherimide[26], and other substrates such as paper[30]. In considering which substrate material was to be used, it was important to look at what types of applications the RF modules for sensing and communication were to be used for.

Mass deployment of small wireless sensors was an important consideration in this work, in order to detect certain gases in a target location. Therefore it was important to have very low-cost sensors that were biodegradable. Figure 14 illustrates these requirements and the key factors that were considered in selecting the target substrate.

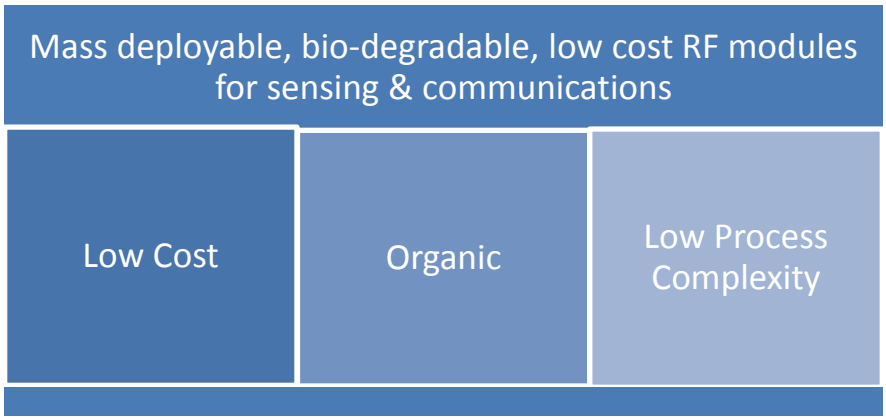

Figure 14. Substrate material requirements and key factors.

The three key factors that were considered were cost, sustainability, and process complexity. The above-mentioned plastics and paper both meet the low cost criteria, however, only paper is organic, and can be recycled. Also, in terms of process complexity, the plastic substrates have higher surface energy and need to undergo surface treatment for high quality printing. The surface energy of the substrate must be matched to the ink for optimal printing, and there are few ways to conduct this surface treatment. One way is to coat the surface with monomers, oligomers, pigments, and photoinitiaters followed by UV curing.[27] This process decrease surface roughness and improves ink-substrate interaction for high quality printing. Another method is oxygen plasma surface treatment which has been found to increase the surface energy of ITO coated substrates used in OLEDs. [28] These extra steps involved in matching the surface energy to the ink adds to the process complexity and ultimately the cost of the fabrication cost.

Taking these key factors into account, paper was selected as the substrate for designing the RF modules.

Figure **15** illustrates the various characteristics of paper substrate including the SEM images of printed silver nano-particle ink, after 15 minutes of curing at 100°C and 150°C. To test the feasibility of silver nano-ink on paper substrate, the paper was characterized by NIST as shown in Figure 16. The properties of paper is as follows:

- Biodegradable
- Low cost
- Large Reel-to-Reel processing possible
- Compatible for printing circuitry by direct write methodologies
- Can be made hydrophobic and can host nano-scale additives (e.g. fire retardant textiles)
- Usable at least up to 20 GHz.

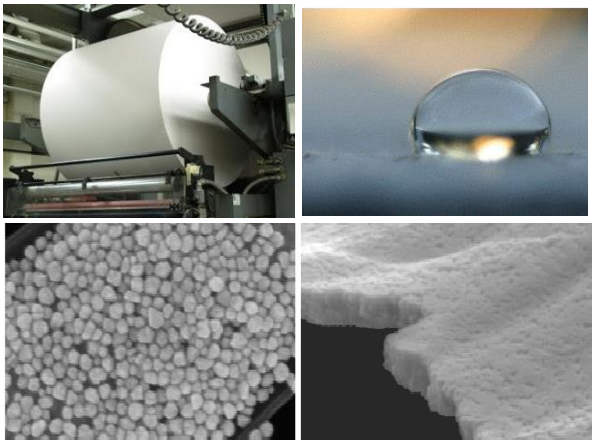

Figure 15. Paper and silver ink used as substrate and conductive ink for designing inkjet-printed RF modules. [29,30]

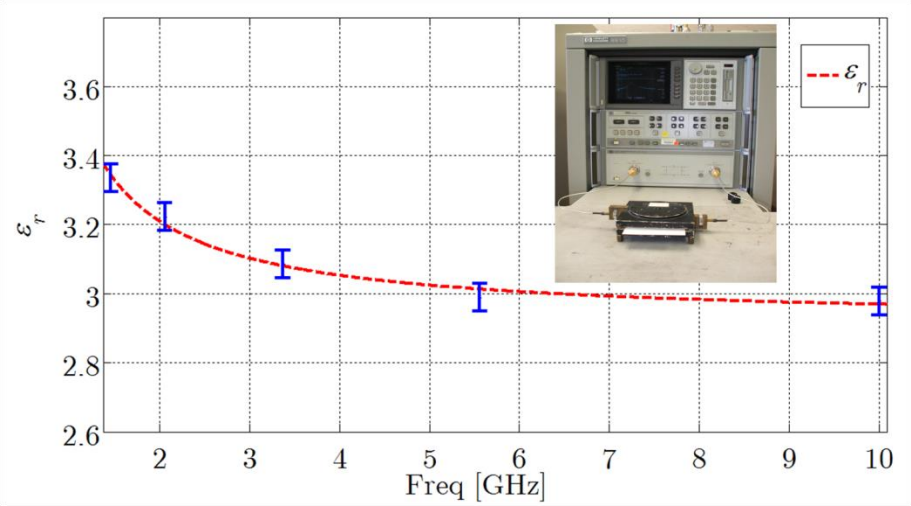

Figure 16. Measurements performed by NIST.[30]

From the characterization process, the permittivity of the paper was measured to range from 3 to 3.3 for RF frequencies. A UWB antenna was measured and compared with simulation based on the characterization results from NIST, and shows good match in Figure 17. Furthermore, the efficiency of the UWB antenna was above 92% up to 10 GHz in

Figure 18.

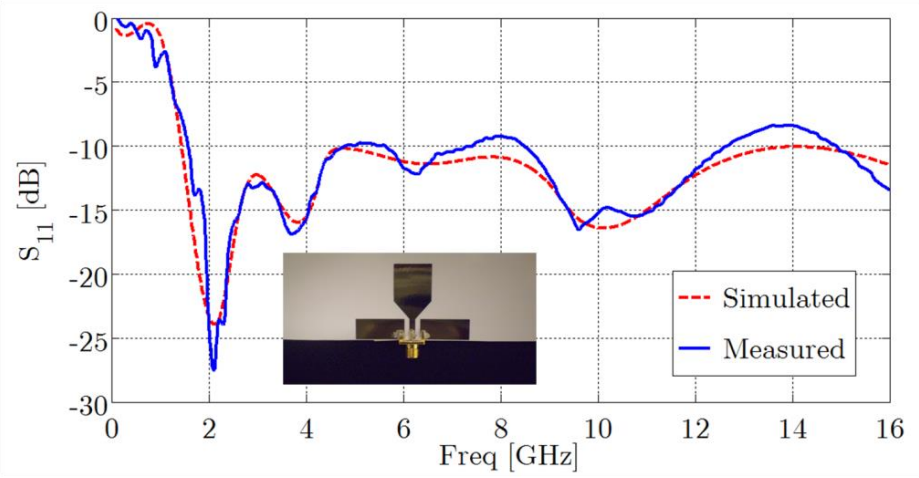

Figure 17. Measurement and simulation results for UWB antenna.[31]

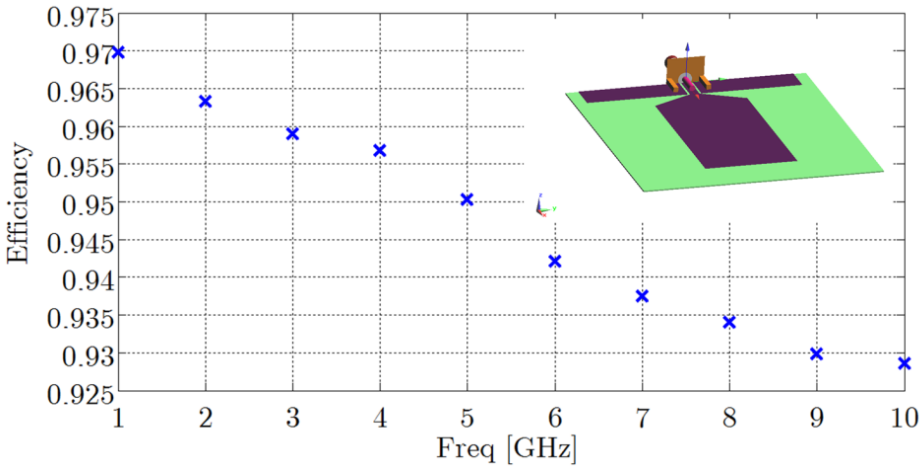

Figure 18. Measured efficiency of UWB antenna. [31]

To test conformability of paper-based antenna designs several tests were conducted, as shown in Figure 19. Several UWB antenna designs were designed and fabricated onto paper substrate then wrapped around a foam cylinder of permittivity close to 1.

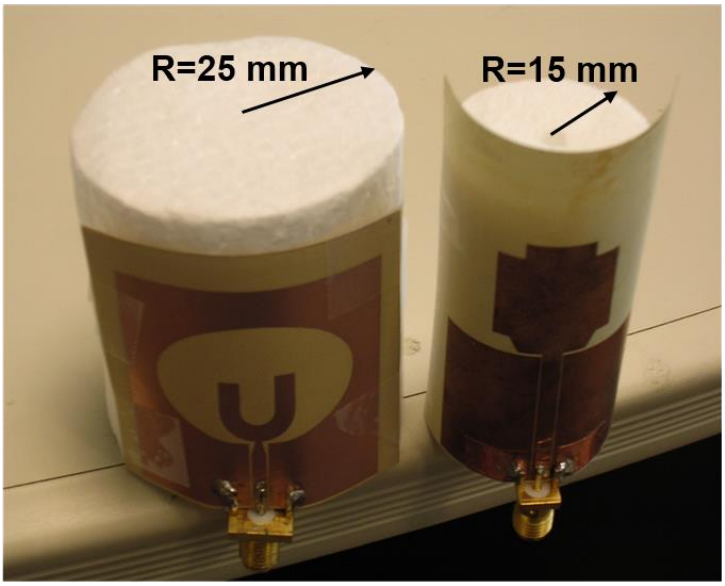

Figure 19. Fabricated antennas on foam cylinder.[32]

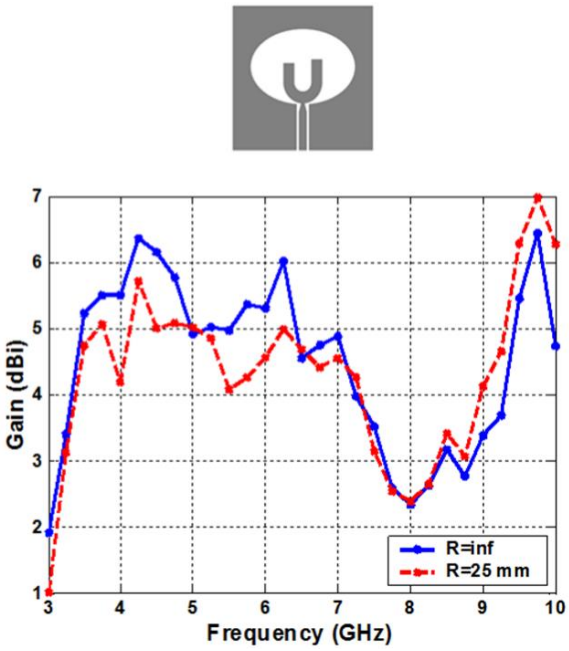

Figure 20. Antenna design with measurements comparing conformal to flattened prototype. [32]

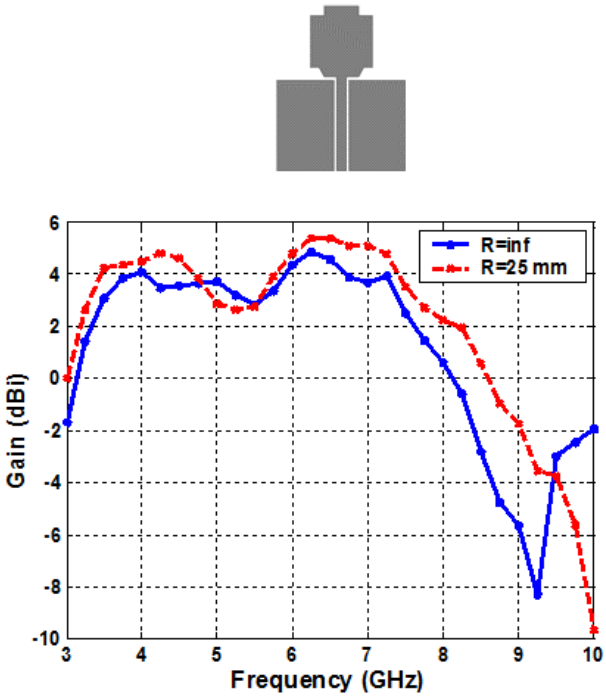

Figure 21. Antenna design with measurements comparing conformal to flattened prototype. [32]

As can be seen from the conformability measurements in the figures above, even when the paper based antenna is flexed, there is little deviation in the gain versus frequency from 3 to 10 GHz. Based on these characterization results, flexible, wearable wireless modules are designed, simulated, and measured in the following chapters. Other benefits for paper is that the material is biodegradable, and therefore for ultra low-cost, temporary, wide area wireless sensor networks, having sensors that is “green” and can be decomposed is another significant benefit compared to other alternatives such as silicon, plastic, or PCBs.

CHAPTER III

HIGH SENSITIVITY ANTENNA-BASED GAS SENSOR UTILIZING CARBON NANOTUBES

3.1 Motivation

CARBON nanotubes (CNTs) have been researched extensively for gas sensing applications due to their unique electrical, chemical, and structural properties. Single-walled carbon nanotubes (SWNTs) have been predominantly used due to their superior electrical conductivity and higher sensitivity relative to multi-walled carbon nanotubes. This work presents the design and characterization of a novel planar sensor fabricated on paper substrate to detect small concentrations of ammonia gas, using the shift in resonance frequency of a patch antenna as the discriminator. Three main design issues have been investigated in depth. First, functionalization of the SWNT's with a polymer is studied in order to enhance the gas detection sensitivity. Second, a thin film of the functionalized SWNT is characterized to create a surface impedance model for the explanation and prediction of the resonance shift due to different gas concentrations. Finally, as a proof of concept, functionalized SWNT's are integrated into a patch antenna design and the return loss is measured in a closed system environment to show high sensitivity for low concentrations of ammonia gas. The proposed antenna-based wireless gas sensor can be utilized in several applications, given its small form factor, light weight, and little to no power requirements.

Carbon nanotubes are long, thin cylinders of carbon (typical diameter ranging from 1 to 100 nm) that are unique for their size, shape, and physical properties. Due to their large tubular surface area comprising a hollow inner core and thin outside cylindrical walls,

CNT's exhibit moderately high surface adsorption and produce appreciable changes in electrical conductivity at room temperature in the presence of various gases .[33,34 ,35 ,36]

This research pertains to the development of a low-cost CNT-based sensor for ammonia detection. Ammonia is found in household cleaning agents, traces of explosives, fertilizers, and as an environmental contaminant in water runoff from streams, estuaries, etc. For the sensor element, we employ a thin film comprising commercially available SWNT's coated with a conductive polymer (at the molecular level) to enhance its chemical reaction with ammonia. In comparison with multi-walled CNT's (MWNT's), SWNT's offer higher sensitivity and produce larger variation in electrical conductivity. For example, by measuring the resonance frequency shift upon exposure to ammonia of a microstrip resonator coated separately with SWNT's and MWNT's, the authors in [48] demonstrated larger shift for the former, and argued that SWNT's provide better surface adsorption of ammonia. SWNT's also depict smaller DC resistances (of the order of 20 to 200Ω) than MWNT's, characterized by high resistances, of the order of kΩ for the same thicknesses.[37] Therefore, in RF applications, where we would like to match the sensor impedance to a transmission line or an antenna with typical impedance values below 100Ω, it is preferable to use SWNT-based sensors. We have also observed that MWNT's require significantly thicker films than SWNT's of comparable resistance, thereby adding to the sensor cost and complexity. Also, SWNT's can be coated with a polymer that can enhance the adsorption of ammonia molecules onto the SWNT.[39] For these reasons, we have chosen functionalized SWNT's as the sensing medium, applied as a film of few microns thickness between electrodes fabricated on paper substrate. Functionalized CNT has been studied to increase the change in DC resistance with adsorption of ammonia molecules.[38 ,39] By coating the CNT with Poly (*m*-aminobenzene sulfonic acid), the CNT has a higher affinity towards H_20 and the CNT does not aggregate together. The polymer also has a higher affinity with NH_x and increases the adsorption rate when compared to CNT that is not functionalized. [40,41]

Chemical gas sensors use the property of binding the gas to some form of electrodes, and detecting the change in both the DC and RF impedance of the electrodes. For example, using SWNTs, [42] introduced a sensitive electronic detector for sensing deadly gases such as the nerve agent sarin, mustard gas, etc. utilizing an array of carbon nanotubes epitaxially grown over a substrate across inter-digitated gold electrodes. Each tube consists of a single-layer lattice of carbon atoms, rolled into a long cylinder with a diameter about 1/50,000 of the width of a human hair, which acts as a molecular wire. When a particular gas molecule binds to this SWNT, the tube's electrical conductivity changes. Each gas affects conductivity differently, so gases can be identified by measuring the conductivity change after binding. The authors in [47] grow CNT film on a silicon substrate between the drain and source electrodes of an FET and observe the change in drain current when the sensor is exposed to alcohol vapor. In the work reported in [54], MWNT's are vertically grown out of a polymer surface at a very high density (about 3×10^9 nanofibers per cm^2) to form a CNT sheet with high flexural strength. Semiconductor growth requires expensive fabrication processes and precludes the development of printable sensors in the form of thin films for low-cost applications.

All these sensors based on growth of CNT's [42]-[50] are designed for stand-alone operation, and need to be integrated with a device which communicates the detection information remotely upon interrogation. Thus, although the gas detector itself is very small and quite sensitive, integration of antenna and sensor electronics with the detector poses serious challenges: (a) impedance mismatch between the antenna and the electrodes, (b) difficulty in interfacing the microelectrodes inside the IC with the antenna terminals, and (c) limiting the power consumption with active devices present. For rapid deployment in buildings, highways, bridges and other infrastructure, it is desirable to have low-cost sensors that can be powered from thin-film batteries or by power scavenging, and *incorporate integration of the sensor and the RF communication device on the same substrate.*

There has been significant work done in wireless CNT-based gas sensors that rely on detecting either change in the resonant frequency or change in the amplitude upon exposure to the analyte of interest. As an example in the first class of sensors, Chopra et al. [48] discuss the design of a resonator, designed at 3.9GHz, fully coated with a mixture of SWNT (in powder form) and a conductive epoxy, for ammonia detection. When the CNT coating is exposed to ammonia, it changes the effective permittivity of the antenna and shifts its resonant frequency. Only 5 MHz shift has been detected even with a high ammonia concentration (1000 ppm). A similar sensor tracking the change in the resonant frequency of a CNT-coated patch resonator is discussed in [43], reporting a shift of 7 MHz when the resonator is immersed in methanol. In references [48], [54], the sensor is used in a laboratory setting to describe phenomenology, and communication of detection information is not addressed. In a remote sensing mode, however, such a small shift can lead to false alarms (in fact, small detuning due to antenna manufacturing tolerances may cause such small changes). In [49], a sensor element comprising of a composite of MWNT's and SiO_2 (which simply acts to bind the MWNT's) is placed over a planar LC-resonator, fabricated by photolithography on a printed circuit board substrate. This sensor detects the change in effective dielectric constant caused by surface interaction with the gas. Due to very small variation observed in the dielectric constant upon exposure to gas, this sensor suffers from low sensitivity too, thus being limited in its practical utility.

Another class of CNT-based gas sensors relies on the change in amplitude of the return loss or transmitted signal for detection. The authors in [50] reported experimental results to demonstrate change in the modulus and phase of transmitted signal when a micro-machined coplanar waveguide (CPW), filled with a mixture of SWNT, is exposed to nitrogen gas. The attenuation constant of the CPW line changes by only a few dB/cm – too small to be of any utility as a wireless sensor node due to potential for multipath interference. Yang et al. [57] loaded a bow-tie antenna at its feeding-gap location with a

SWNT film and utilized the change in the amplitude of the return loss/scattered power as a measure of gas detection. This design requires a very high concentration of gas to get a large variation in the loading resistance, and thus suffers from limited sensitivity and slow detection response detection due to sampling over a wide bandwidth.

Among these different detection mechanisms, the method relying on the shift of the resonant frequency is the most effective for remote sensing, because the amplitude is susceptible to interference and noise, leading to false positives (ammonia detection), while the frequency shift is relatively insensitive to these detrimental factors.

This work focuses on an ammonia gas sensor integrated with a microstrip patch antenna on a thin paper substrate, and utilizes the shift in the resonant frequency as a means of gas detection. The salient novel features of the proposed wireless gas sensor design include (a) incorporation of functionalized SWNT to improve sensitivity, (b) a novel characterization methodology, (c) integration of sensor and communication device (antenna) on the same platform to facilitate wireless detection, and (d) inkjet printing fabrication on paper substrate for low-cost, light-weight wireless sensor nodes.

The work is organized as follows. First, the fabrication of CNT in liquid form from commercially procured functionalized SWNT powder will be introduced. A description of the setup required to print the antennas on paper follows. Next, the characterization of a thin film of functionalized CNT at microwave frequencies using transmission line standards is presented. Then, based on the surface impedance model created through the characterization, a CNT-loaded patch antenna is designed. Finally, the gas detection measurement results are discussed and the sensor performance is evaluated.

3.2 Prior Art

Chemical gas sensors use the property of binding the gas to some form of electrodes, and detecting the change in both the DC and RF impedance of the electrodes. Previous work

shows various different methods of detection such as the change in current in transistors, shift in resonance frequency of circular resonators, LC tanks, and the change in capacitance in inter-digitated capacitors. Table 1 shows the different designs and sensing mechanisms of the prior art.

The authors in [44] grow CNT film on a silicon substrate between the drain and source electrodes of an FET and observe the change in drain current when the sensor is exposed to alcohol vapor. Sensors based on growth of CNT's [44,45] are designed for stand-alone operation, and need to be integrated with a device which communicates the detection information remotely upon interrogation. Chopra et al. [46] discuss the design of a patch antenna, designed at 3.9GHz, fully coated with a mixture of SWNT (in powder form) and a conductive epoxy, for ammonia detection. When the CNT coating is exposed to ammonia, it changes the effective permittivity of the antenna and shifts its resonant frequency. Only 5 MHz shift has been detected even with a high ammonia concentration (1000 ppm). The sensitivity is 0.13% at 1000ppm, which can be extrapolated down to 0.0065% at 50ppm.

Table 1. Prior art of CNT-based gas sensors.

#	Design	Detection Method	Deposition Method	Functionalized CNT	Gas	Detection %Δ @ 50ppm	Radiate	Ref
1	Transistor	ΔI	CVD	No	Ethanol, Methanol	0.3%	No	47
2	Circular resonator	Δfres	Conductive epoxy	No	NH3	0.0065%	No	48
3	LC tank	Δε'	Pipette	No	NH3	2%	No	49
4	IDC, Resistor	ΔZ	Spin coating, Grown	No	NH3	24%	No	50
5	CPW	Δmodulus, Δphase	Tweezer	No	No gas	2~3 dB attenuation	No	51
6	Dipole Antenna	ΔRCS	Inkjet printed	No	NH3	1%	Yes	52
This work	Patch Antenna	Δfres	Inkjet printed	Yes	NH3	5%	Yes	53

A similar sensor tracking the change in the resonant frequency of a CNT-coated patch resonator [54], reports a shift of 7 MHz when the resonator is immersed in methanol. In references [46], [41], the sensor is used in a laboratory setting to describe phenomenology, and communication of detection information is not addressed. In a remote sensing mode, however, such a small shift can lead to false alarms (in fact, small detuning due to antenna manufacturing tolerances may cause such small changes).

A sensor element comprising of a composite of MWNT's and SiO2 (which simply acts to bind the MWNT's) is placed over a planar LC-resonator[55], fabricated by photolithography on a printed circuit board substrate. This sensor detects the change in effective dielectric constant caused by surface interaction with the gas. Due to very small variation observed in the dielectric constant upon exposure to gas, this sensor suffers from low sensitivity too, thus being limited in its practical utility.

The authors in [56] reported experimental results to demonstrate change in the modulus and phase of transmitted signal when a micro-machined coplanar waveguide (CPW), filled with a mixture of SWNT, is exposed to nitrogen gas. The attenuation constant of the CPW line changes by only a few dB/cm – too small to be of any utility as a wireless sensor node due to potential for multipath interference.

Yang et al. [57] loaded a bow-tie antenna at its feeding-gap location with a SWNT film and utilized the change in the amplitude of the return loss/scattered power as a measure of gas detection. This design requires a 5% concentration of ammonia gas, which is 50,000 ppm, to get a large variation in the loading resistance, and thus suffers from limited sensitivity and slow detection response detection due to sampling over a wide bandwidth. Among these different detection mechanisms, the method relying on the shift of the resonant frequency is the most effective for remote sensing, because the amplitude is susceptible to interference and noise, leading to false positives (ammonia detection), while the frequency shift is relatively insensitive to these detrimental factors.

3.3 Material Development

In this work, poly (m-aminobenzene sulfonic acid) (PABS) -SWNT is utilized for the gas detection surface. PABS-SWNT is a water-soluble nanotube–polymer compound, formed by covalently bonding the polymer (PABS) to SWNT's via amide functionalization [39]. The utilized functionalized PABS-SWNT's are 1.1nm in diameter and 0.5-1µm in length.

Chemical functionalization is a method to enhance both processibility and sensing performance of SWNT's. First, it allows the unique properties of SWNT's to be coupled to other materials, such as conducting polymers, metals and metal oxides, to create hybrid sensing materials with enhanced sensitivity, selectivity and faster response time. Second, it can improve dissolution and dispersion of SWNT's in various solvents, including water, which enables cost-effective methods to fabricate sensors by simple dispensing or printing techniques.

Chemical surface modification of nanotubes by attaching functional groups has been utilized as an important step for preparing suspensions and stable solutions.[44] However, the original electrical properties of the nanotubes are not left intact, which should be taken into account when designing a new device.[46] It is recognized that covalent sidewall functionalization is one of the promising methods of modifying electric properties of SWNT for many applications.[58] Sidewall chemical functionalization disrupts the π-*bonding* system and breaks the translational symmetry of SWNT's by introducing saturated *sp3* carbon atoms. As a result, electronic and transport properties of SWNT's are significantly altered.[45] By introducing different chemical groups to the nanotube wall, it is possible to change the interaction between nanotubes and the surrounding environment. This reactivity could enhance the sensitivity and selectivity of CNT-based gas sensor devices.[39,56]

The preparation of well-defined materials through covalent bond formation constitutes the only controlled route for the introduction of chemical receptors into SWNT's that allows for the isolation and characterization of specific compounds of known electrical conductivity.[59] The well-defined composition and properties of covalently functionalized SWNT's provide an opportunity to dynamically characterize the nanotube electronic structure and electrical conductivity in the presence of analyte molecules [[41]].

For this study, PABS-SWNT in powder form was purchased from Carbon Solutions Inc. (www.carbonsolution.com) to prepare our ammonia (NH_3) gas sensing film. The molecular structure and the interaction mechanism of PABS-SWNT with NH_3, proposed by Haddon et al. [[41]], is shown in Figure 22. Aqueous dispersions of PABS-SWNT with a concentration of ~ 5 mg/mL in water were prepared by ultra-sonication for 2 hours, followed by deposition onto a paper substrate using a paint brush technique. About 20 layers of PABS-SWNT were applied for each fabrication to assure the reproducibility of the gas sensor.

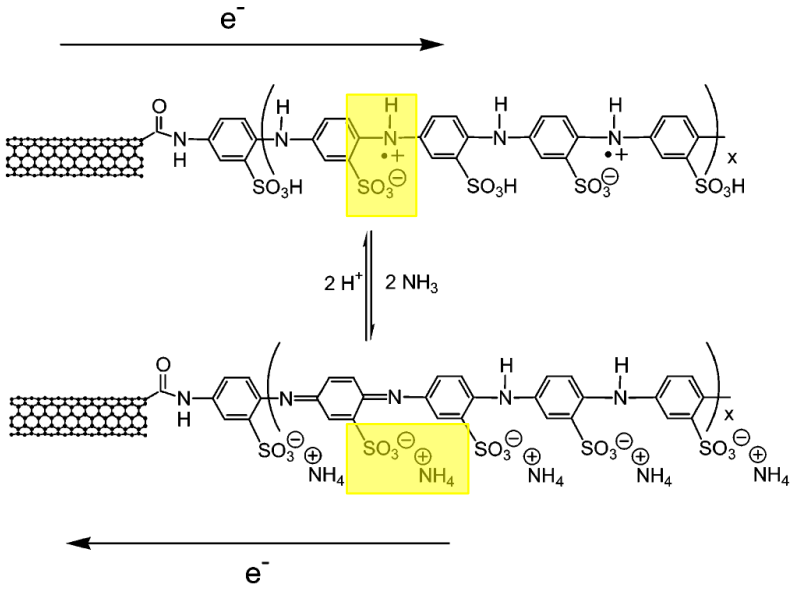

Figure 22. Mechanism of interaction of PABS-SWNT with NH3. The arrows indicate charge transfer between SWNT and PABS [[41]].

The PABS functional group that is attached to the SWNT is chemically sensitive to NH_3. NH_3 sensing occurs by removing a proton (H^+) from the side-chain oligomers (the PABS functional group) as shown in the yellow box in Figure 22, that in turn induces electron transfer between the side-chain and the SWNT's. In effect, conductivity of the PABS-SWNT molecule is decreased, because addition of electrons to the semiconducting SWNT's refills the valence band. Our results have shown that the PABS-SWNT sensing film offers great promise for NH_3 sensing.

A. Printing Setup

To realize low-cost environment-friendly sensors using PABS-SWNT's, we propose the utilization of inkjet printing technologies of conductive inks on paper sheets. Paper possesses a number of intriguing attributes that makes it amenable for low-cost "green" electronics. It is cellulose in nature, thus considered as a renewable resource. Additionally, it can be easily processed in a reel-to-reel fashion enabling low-cost manufacturing solutions. Driven by the fact that it is process- and environmentally-challenging and cost-inefficient to apply photolithography techniques to paper, inkjet printing of conductive particles provides a promising solution.[60,61] It is widely known that one of the most common methods of digital printing is through inkjet printers, almost ubiquitous in home or office applications. Notably, inkjet printing has been recently enhanced with the capability of printing new functional materials, such as conductive and CNT-based inks, leading to an increased deployment in printed electronics, such as flexible displays, RFIDs, sensors, solar panels, fuel cells, batteries, and most recently in antennas.[62,63] Inkjet printing for RF applications is a challenging endeavour, where precise control of the achieved conductivity and surface roughness is required. In general, there are two critical factors that affect the print quality: the ink properties, and the settings of the printing system itself. The most notable ink properties to observe are viscosity, surface tension, and dispersion stability (printing with an ink of high viscosity

and high surface tension at a high contact angle produces smaller sized dot patterns). The most crucial settings of the printing system include the volume of the jetted ink, the travelling velocity of the ejected droplet, the gap distance between each droplet, the printing frequency, the temperature of the jetted ink, the temperature of the substrate, and the sintering/curing mechanism performed on the printed structures. In this work, we utilized a DMP-2800 ink-jet printer shown in Figure 23, a table-top printer available from Dimatix Inc. (www.dimatix.com). To ensure good RF properties of the printed device, an in-house recipe has been developed considering all of the aforementioned parameters. For all devices, the utilized Dimatix 1pL silver nano-ink cartridges (DMC-11601) are kept at a distance of 0.5 mm from the surface of the paper. The printer head is first adjusted to achieve a print resolution of 2540 dpi, which ensures good RF conductivity of above $9x10^6$ S/m, up to several GHz. Cabot conductive ink CCI-300 (www.cabot-corp.com) is then jetted through the cartridges at a temperature of 40°C, with the paper substrate maintained at 60°C. Each printed device is then cured in a thermal oven for two hours at 120°C.

Figure 23. Table-top ink-jet printer used in this work.

B. Paper Characterization

An important contribution of this effort is the introduction of a measurement-based RF surface impedance model for a thin film of SWNT printed on paper. There has been some research in the RF characterization of CNT, but mostly on a model of a single strand of CNT [[64]], or SWNT's grown on a wafer through chemical-vapor deposition.[65] It is possible to incorporate this model as a lumped circuit element in a commercial EM solver to design planar antennas or sensors on paper substrate, which involve CNT loading of some kind.

The dielectric properties of the benchmarking paper substrates are studied through the use of split-post dielectric resonator technique. [66,67,68] Each blank paper sample was cured first in a thermal oven for 2 hours at 120°C to mimic the curing process of the printed ink. The results for the extracted relative permittivity of the 10-mil thick cured paper are shown in Figure 24. The measured dielectric loss tangent values were bounded between 0.06 and 0.07 up to 10GHz.

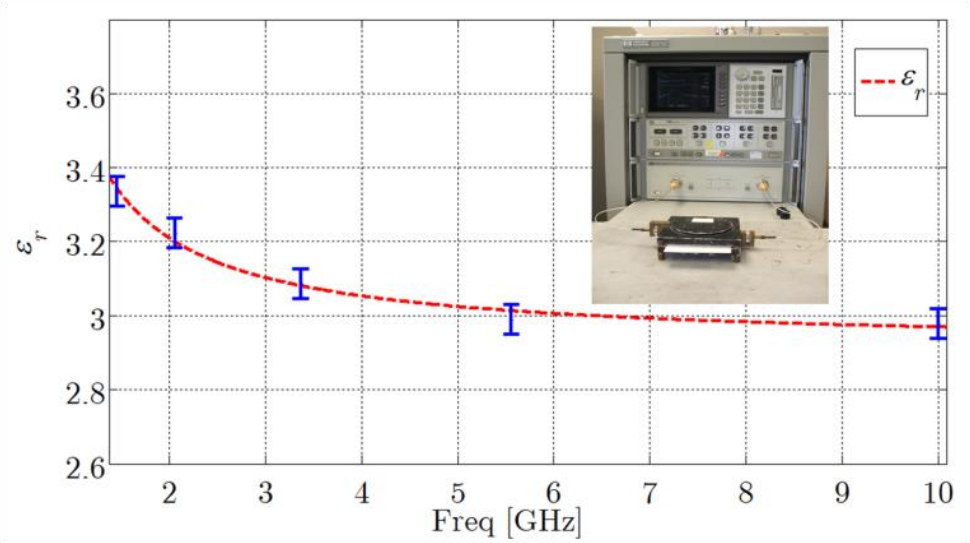

Figure 24. Characterization of the paper material through the split ring resonator method.

C. Silver Ink Characterization

The conductivity of the printed conductive ink was studied through the use of a Signatone Four Point Probe (www.signatone.com). To ensure good RF conductivity, three layers of ink were printed, and then treated in a thermal oven for two hours at 120°C. The resulting ink thickness was measured using the Wyko Profilometer (www.veeco.com). The thickness was around 3 μm with a consistent measured DC conductivity in the range $9x10^6$ S/m – $1.1x10^7$ S/m.

D. CNT Characterization

The RF characterization of the deposited CNT layers was performed using a two-tier calibration process: First, a Short-Open-Load-Thru (SOLT) calibration process was applied up to the coaxial feed of the SMA connector. Next, a custom-designed Multi-Line Thru-Reflect-Line (TRL) calibration set using silver coplanar strip lines was deployed. Figure 25 depicts a schematic of such a custom set, where W1 denotes the strip width, L1 denotes the length up to the calibration reference plane, LL denotes the physical lengths of the line short, and of the load termination. L2 and L3 are different line lengths used in the calibration procedure. A sample of the CNT film deposited between two electrodes on the paper substrate is shown in Figure 26. TRL is utilized to extract the bulk RF behavior of the CNT thin film. The mathematical procedure behind TRL calibration is described in [69]. The silver printed lines form a set of coupled lines, with the CNT layer deposited as a thin film at the TRL reference plane. Using the TRL calibration set, it is possible to de-embed the silver lines up to the reference plane and extract the input admittance at that plane.

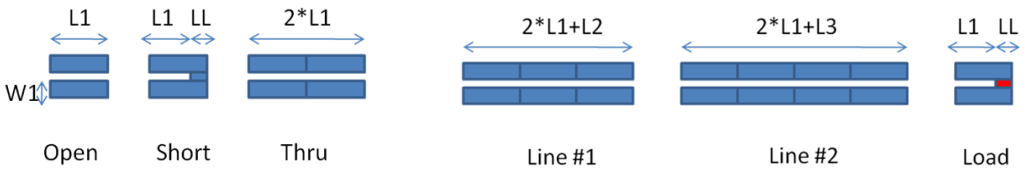

Figure 25. Schematic for the TRL calibration set used in this work.

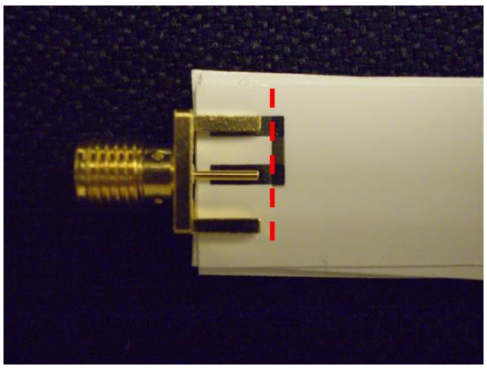

Figure 26. CNT film placed at the edge of printed silver lines.

The fabrication process consists of printing silver nano-ink to form a transmission line coupon of coplanar strip lines on photo paper, followed by the application of SWNT at its edges, as outlined in Figure 25. Multiple layers of paper were stacked to ensure good contact of the transmission line to the connector center pin as well as ground. Note that the dashed red line in Figure 26 defines the reference plane used in the TRL extraction algorithm.

The extraction for various samples with different thicknesses of the SWNT film revealed that the RF behavior of CNT layers can be adequately modeled through a parallel RC tank. Such *R* and *C* values are functions of the frequency, the geometrical configuration, as well as the concentration and material properties of the deposited CNT film. Figure 27 and Figure 28 demonstrate sample results for the extracted resistance and capacitance of a CNT film of dimensions 1 mm x 4 mm deposited at the gap shown in Figure 26. The total thickness of the CNT film (10 layers) is ~11 μm. At higher frequencies, the losses in the SWNT increase as shown in Figure 27. Also, the capacitance decreases as frequency increases. It is important to note that the resulting equivalent resistance and capacitance can be designed to a desired value by altering the dimensions of CNT thin film (width and length), and its concentration (or thickness).

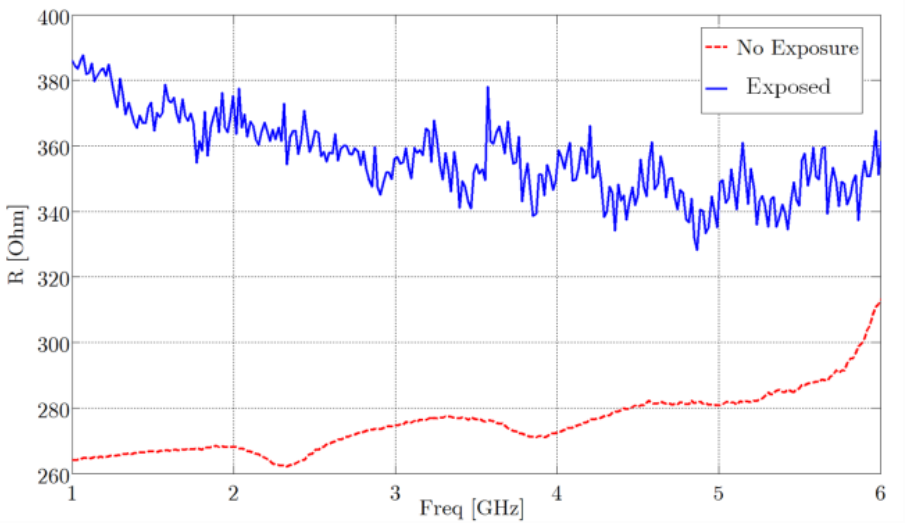

Figure 27. Equivalent resistance of the CNT thin film (before and after gas exposure).

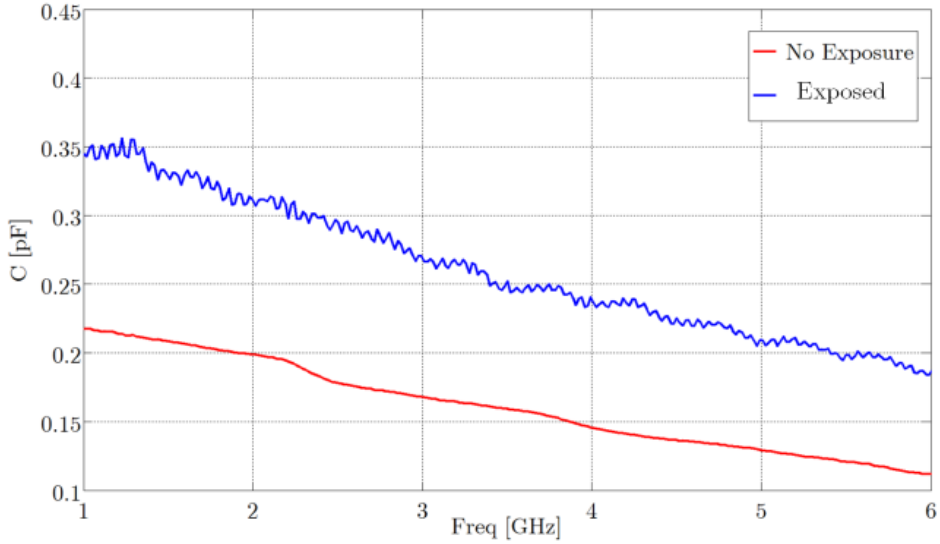

Figure 28. Equivalent capacitance of the CNT thin film (before and after gas exposure).

The increase in the resistance and capacitance can be attributed to two phenomena occurring at the CNT thin film. When the PABS-SWNT is exposed to ammonia, there is electron transfer from the PABS polymer towards the SWNT. When this electron transfer occurs, the electrons fill the valence band of the SWNTs. This in turn decreases the amount of free electrons in the SWNT to flow freely through the SWNT, which increases

the resistance across the nanotube. Therefore, with increased amount of ammonia gas molecules that adhere onto the PABS-SWNT, the higher the resistance across the PABS-SWNT thin film. This mechanism of ammonia detection by chemically functionalized SWNT is explained clearly in Bekyarova [41].

Another phenomena that occurs is the change in capacitance as shown in Figure 28. This is due to the change in the dielectric constant in the thin film. As the ammonia molecules adhere onto the thin film, the dielectric constant increases due to the addition of new material. Since capacitance is proportional to the dielectric constant, the increase in relative permittivity increases the capacitance across the frequencies, as can be seen in Figure 28.

The test fixture shown in Figure 26 was subjected to ammonia of concentration 50 ppm in a closed cell system. Figure 29 shows the reflection coefficient at the coaxial feed of the SMA connector for three distinct cases: without CNT (open-ended transmission line), with CNT before gas exposure, and with CNT after the exposure. It is clear that the RF properties of the CNT thin film are changed upon exposure, resulting in noticeable change in the input reflection coefficient.

The equivalent admittance of the exposed CNT thin-film was extracted using the outlined TRL scheme. The extracted resistance and capacitance values are overlaid in Figure 27 andFigure 28, respectively, and compared to the corresponding parameters without ammonia exposure. Both the resistance and the capacitance of the exposed film increase due to the adsorption of ammonia molecules on the PABS-SWNT thin-film. The losses in the CNT film due to ammonia exposure are higher but not significantly dependent on frequency. The trend in capacitance variation with frequency is similar with and without ammonia exposure.

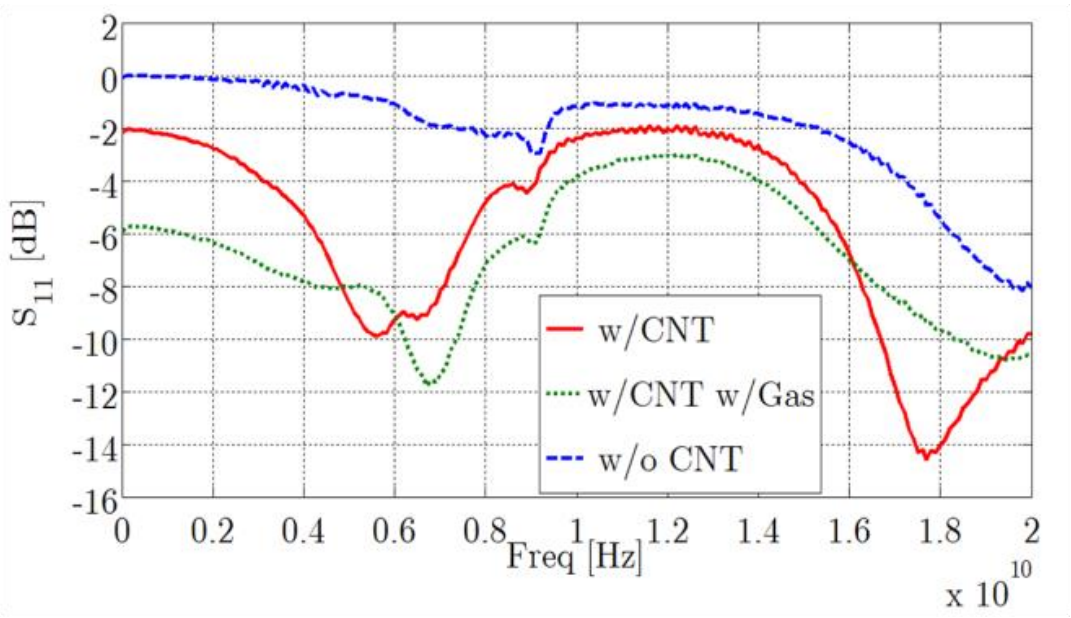

Figure 29. The input reflection coefficient at the connecter coaxial feed in different scenarios (50 ppm ammonia concentration).

E. Fabrication Challenges

The main fabrication challenge was the length of the PABS-SWNT, which was approximately 1-2um. The diameter of the cartridge nozzles were 0.2um, and therefore the length of the nanotube needed to be broken down for the CNT to be deposited onto the paper. The CNT was ultra-sonicated using a probe sonicator to break down the lengths, while a bath sonicator was used to uniformly disperse the particles in the solvent. The dispersion was left overnight to observe suspension stability and sediment at the bottom of the vial, and the top two-thirds of the material was extracted for printing.

3.4 Antenna Design

Given the impedance model of the SWNT film, the sensor was designed with two main objectives: to obtain high RF sensitivity through a high Q/narrow bandwidth design, and moderate gain using a patch antenna. This is achieved by separating the sensing and radiation functions as will be described shortly. Sensitivity from the RF design context means narrow-band sampling of the detection phenomena and does not refer to the chemical sensitivity of the CNT film to ammonia exposure. In contrast to previous efforts where resonators were utilized without incorporating remote sensing, this design focuses on integrating both high sensitivity and remote sensing capabilities within the same structure.

Previously, patch resonators have been designed to sense ammonia by covering the entire patch surface with CNT.[48] However, SWNT retains high conductivity only in single tubular form, and the conductivity decreases significantly when mass-deposited in a random configuration. Therefore, the key to attain high RF detection sensitivity and simultaneously maintain moderate antenna gain, which is required for remote communication, is to minimize the losses in the antenna structure.

Here, we propose using silver ink for the patch antenna realization, with only a small area needed for the CNT film at the tip of the stub (see Figure 30). Thus, silver covers a large part of the antenna surface (namely, the patch), ensuring moderate efficiency and good radiation pattern, while the high *Q* of the sensor element results from minimum losses occurring due to a small CNT film. The idea is that when the CNT impedance changes due to chemical reaction with ammonia, the matching conditions using the loading stub will change, thereby altering the input reflection coefficient at the feed.

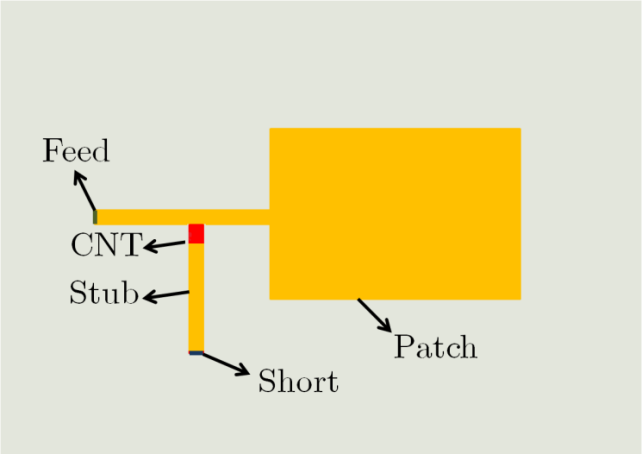

Figure 30. Schematic for the proposed sensor design.

To elaborate on the principle of operation in a simplified manner, let us consider the sensor design case where the equivalent capacitance of the CNT thin film before exposure is 1 pF and resistance *R* is fixed at 1 Ω. Using this lumped element combination to load a parallel stub as shown in Figure 30, a patch antenna was designed (using SPEAG's SEMCAD and Ansoft's HFSS software) to resonate around 4.5 GHz. Based on Figure 27 andFigure 28, we know that the equivalent circuit of the thin film will change upon exposure to ammonia gas. So, we numerically investigate the cases where the equivalent resistance is fixed at 1Ω, and the capacitance changes from 1 pF to 1.1, 1.5, and 2pF. The resulting reflection coefficient at the antenna feed terminal is shown in Figure 31. It is clear that a significant frequency shift is observed, even for a 10% change in the nominal capacitance.

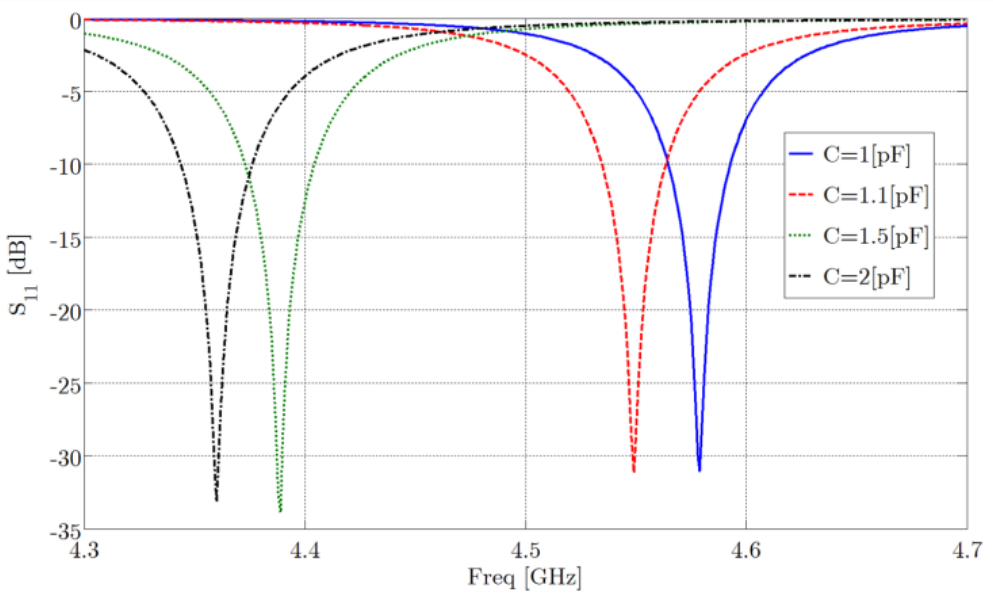

Figure 31. Numerical predictions of the shift in response due to changes in the equivalent capacitance of the CNT layers.

Now, let us consider the case where the nominal (before exposure) equivalent circuit model is a parallel combination of R = 10 Ω and C = 1 pF. Assuming an exposure level that changes R to 20 Ω and C to 2 pF, we get the resonance shift shown in Figure 32. It should be noted that the antenna efficiency in the nominal case will be degraded due to the CNT losses represented by the equivalent resistance. A theoretical calculation shows that the typical antenna efficiency of such design is around 30%.

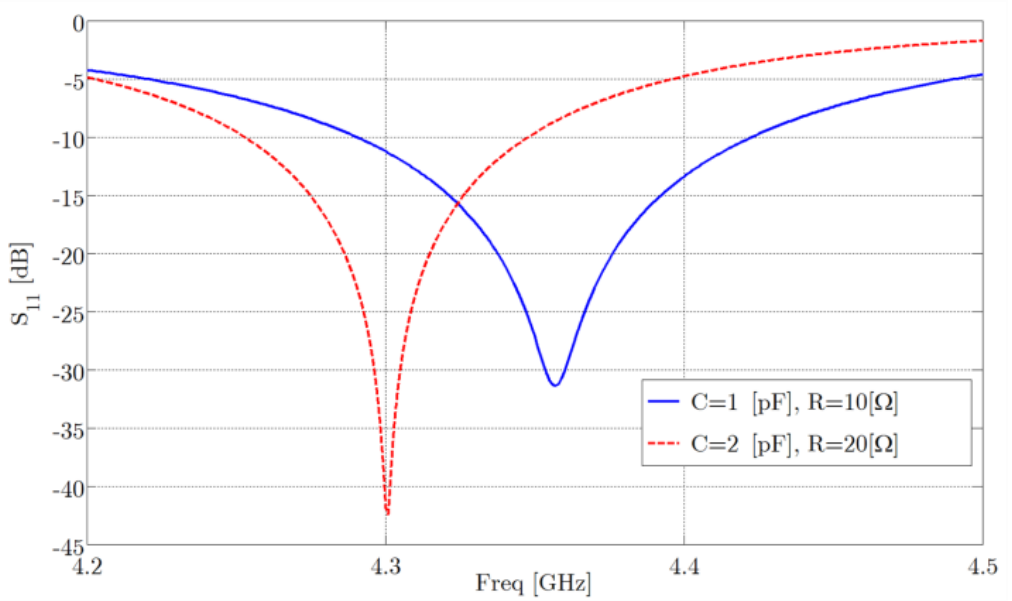

Figure 32. Numerical predictions of the shift in response due to changes in the equivalent admittance of the CNT layers.

Based on the outlined principle of operation, a loaded patch antenna was designed and printed on 10-mil thick paper as shown in Figure 33. The ground plane is made of a thin copper sheet. Conductive epoxy is used to solder the connectors onto silver traces on the paper substrate. The ground pins of an edge-mount connector are connected with the stub end to create the RF short-circuit.

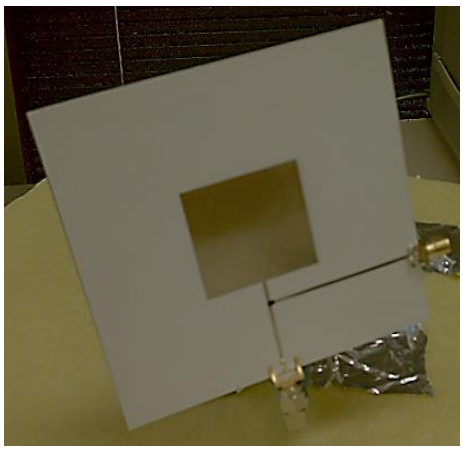

Figure 33. Fabricated patch antenna with loaded PABS- SWNT.

To evaluate the sensor performance, initially we used household ammonia (10% ammonium hydroxide) in a small plastic container, with the antenna placed nearby (Figure 34). The input reflection coefficient was recorded before and after filling the container with ammonia, and the resulting response for these two cases is shown in Fig. 14. Resonance frequency shift of about 120 MHz is observed. Notably, the response time was quick (less than 30 seconds).

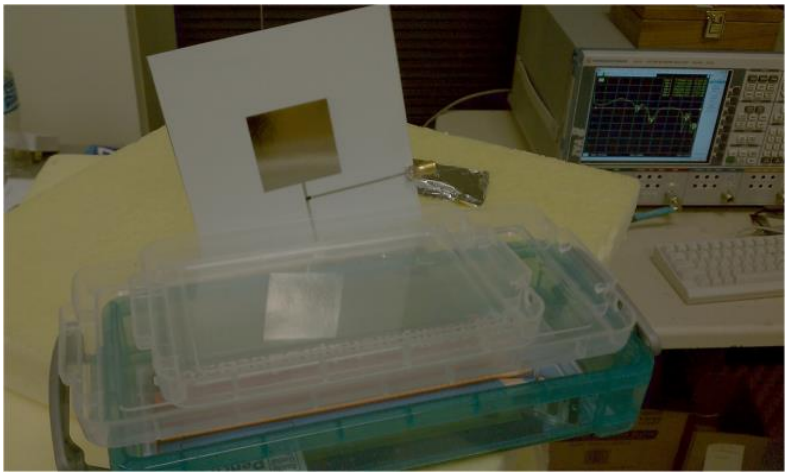

Figure 34. Sensor measurements using household ammonia.

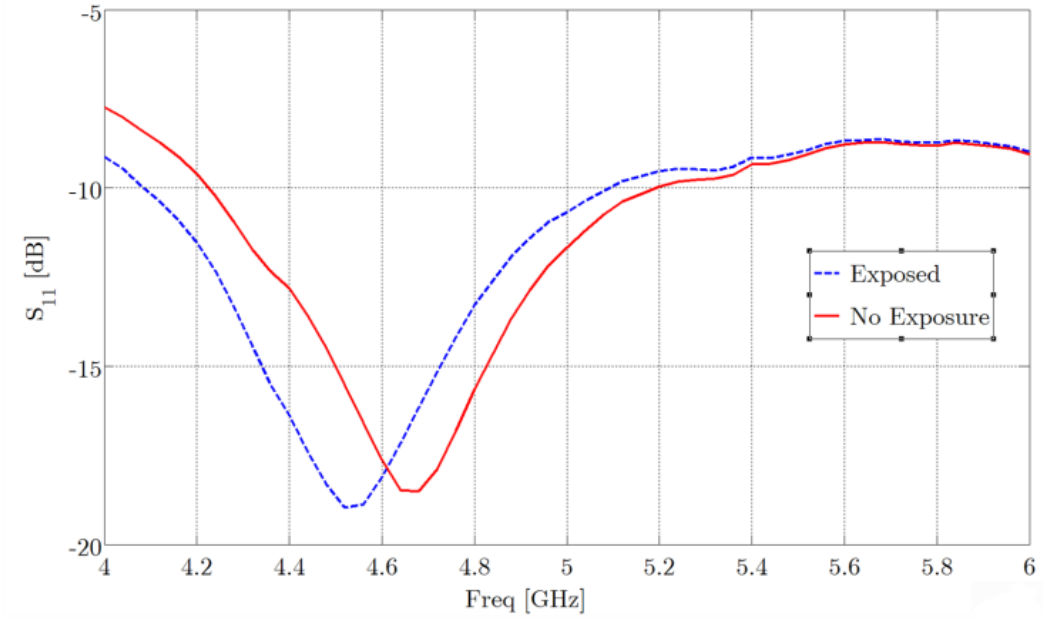

Figure 35. Frequency shift in response after exposure to household ammonia.

Flexibility Analysis

To investigate the effect of bending the sensor for wearable gas sensors, the sensor was simulated in CST with curvatures of 100mm and 60mm radii. The return loss showed a 29MHz upward frequency shift at 3.214GHz, which is less than 3% change for 60mm radii. The results are shown in Figure 36. These changes in resonance frequency for curved sensors can be calibrated to a reference frequency to obtain an accurate measurement for the gas concentrations. The gain simulations were also conducted and showed near constant gain and similar radiation pattern for the different radii, as shown in Figure 37. There was a change of less than 1dB from a flat sensor to a sensor curved with a radius of 40mm.

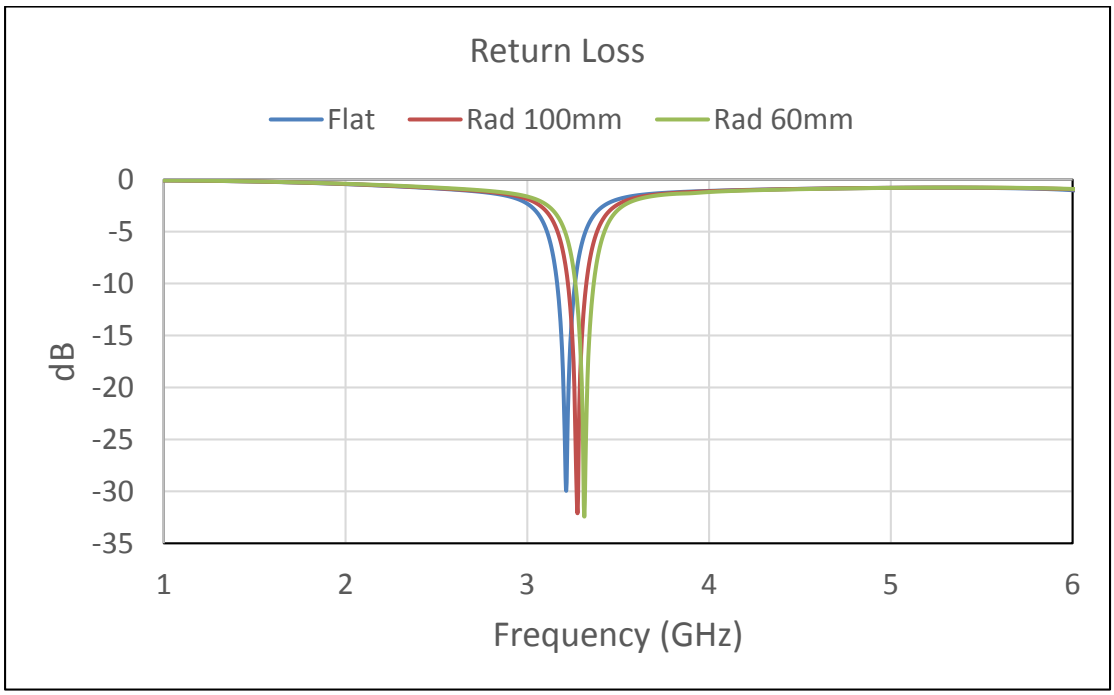

Figure 36. Simulated frequency shift with varying radii of the curved sensor.

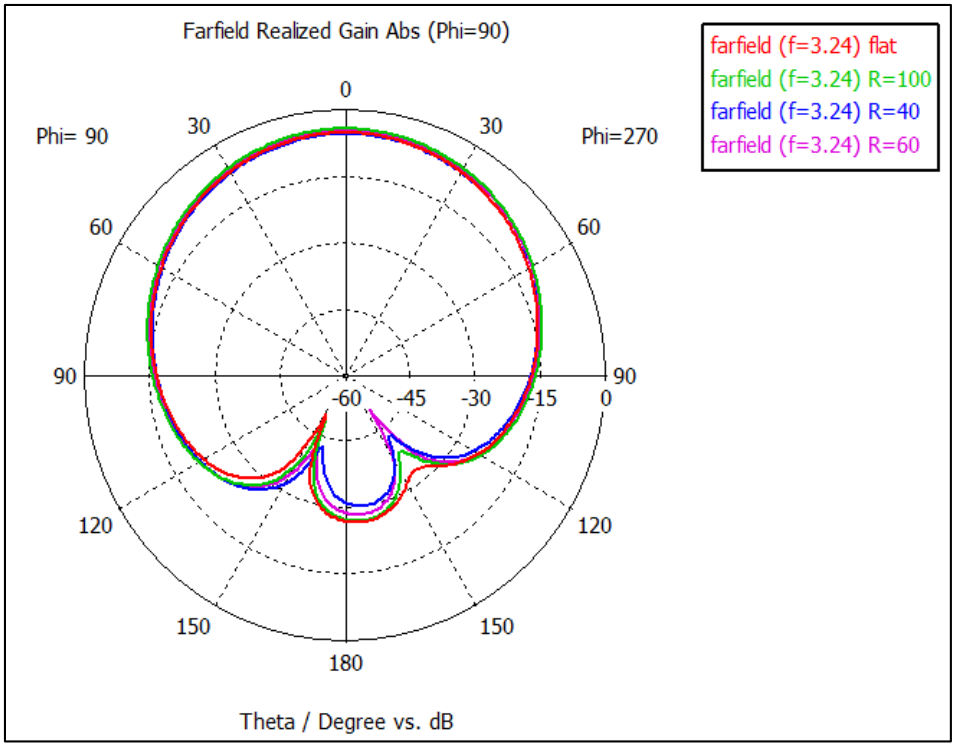

Figure 37. Simulated change in realized gain of sensor curved for varying radii.

3.5 Fabrication & Measurement

The measurements using the setup shown in Figure 34 agree qualitatively with the model presented in Section III-D, which predicts a resonance shift to lower frequencies caused by increase in resistance/capacitance (due to NH_3 interaction with CNT – see Fig. 11). Such measurements verify the principle of operation of the sensor. However, to evaluate the sensitivity, it is desired to determine the gas concentration needed to trigger a noticeable shift in the resonant frequency. To this end, a controlled measurement system is deployed.

Our controlled measurement system consists of five major components: gas generator, NH_3 permeation tube, closed-system sensor cell, Agilent PNA-L N5230A programmable network analyzer (PNA), and data acquisition system. We used the 491M gas generator

and the NH_3 permeation tube, shown in Figure 38, from Kin-Tek Company (La Marque, TX). At all times, this system was used under a chemical fume hood.

The NH_3 permeation tube has a calibrated emission rate under controlled temperature. Dry nitrogen was delivered from an Ultra-High Purity (Grade 5) compressed nitrogen gas cylinder from Airgas. By controlling the ammonia emission rate and the nitrogen flow rate, desired concentrations (in ppm range) of ammonia were generated from the gas generator. Before each ammonia exposure test, the NH_3 permeation tube was installed in the gas generator and heated to a predetermined temperature for around 4 hours in order to obtain a stabilized ammonia concentration. The accuracy of gas concentration output is ± 4% according to the calibration results from Kin-Tek.

Figure 38. (left) 491M gas generator (right) ammonia permeation tube.

The sensor was installed inside a closed test cell, depicted in Figure 39. The concentrated NH_3 stream was delivered into the test cell via a Teflon tube. The CNT film was placed near the gas inlet port, so that the ammonia stream was allowed to interact with the sensor surface first. For the RF measurement, expendable connectors and a precision phase-steady cable assembly was used to interface between the PNA and the antenna under test. An SOL 1-port calibration was conducted with coaxial standards.

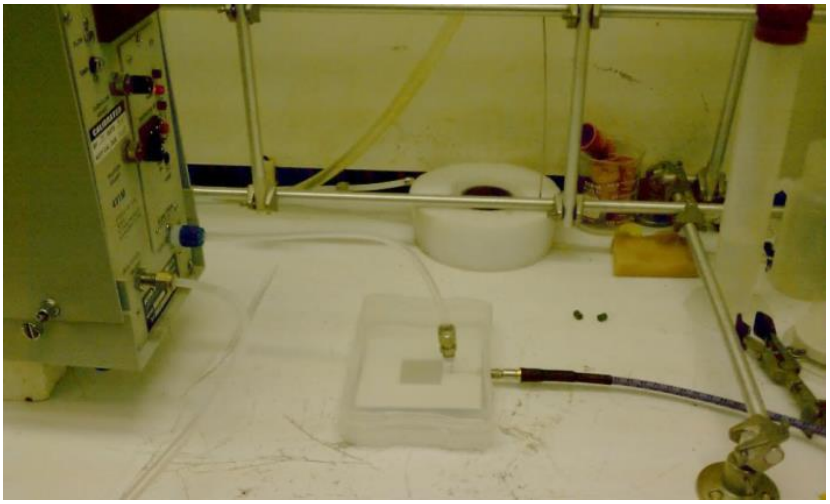

Figure 39. Closed test cell connected to gas generator and PNA.

Measurements were made at three different concentrations: 50ppm, 75ppm, and 100ppm. For each measurement, the data was saved automatically every 10 seconds. Also, each measurement consisted of several minutes of baseline recording (exposure to pure nitrogen), followed by exposure to ammonia, after which the system was purged with nitrogen gas to bring the sensor back to the baseline.

Based on the measured data for the three concentrations, we conclude that the resonance frequency shift increases with ammonia concentration until the sensor eventually saturates. The resonant frequency shift is summarized in Table 2 along with the nitrogen flow rate required to maintain appropriate ammonia concentration from the 491M Gas Generator during the exposure and reversion (back to ambient) phases. In Figure 40, the frequency shift as a function of time is plotted during these two phases.

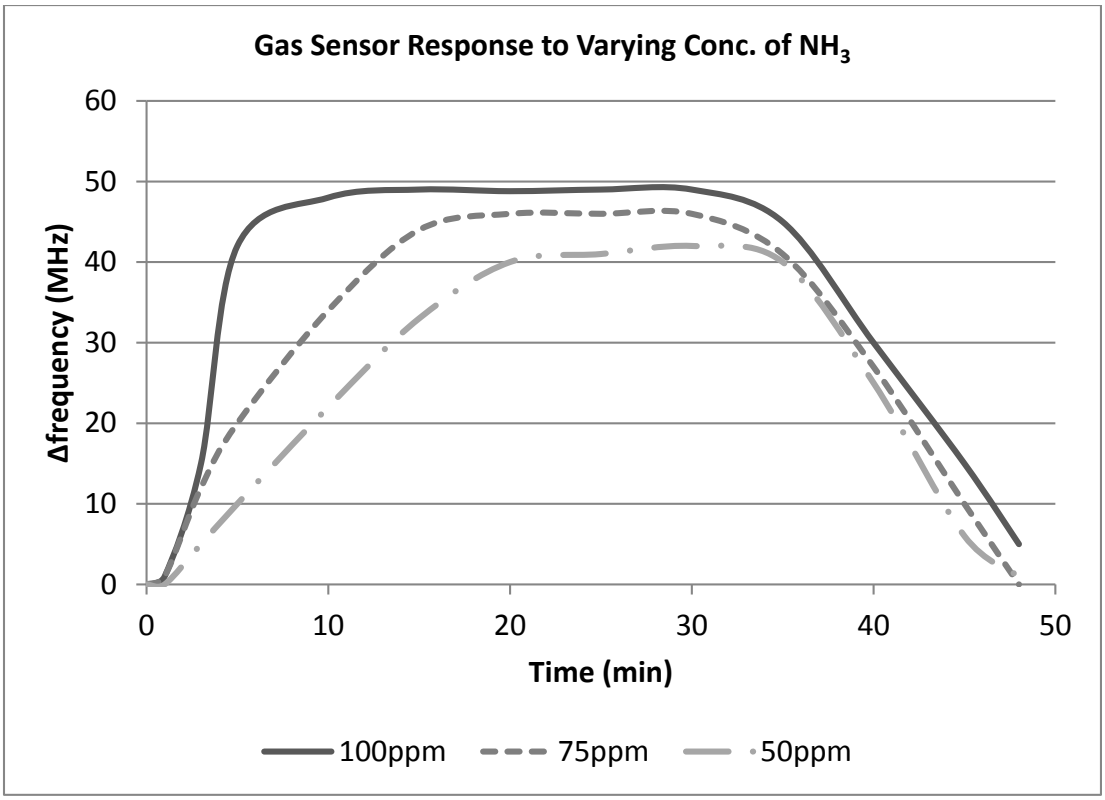

Figure 40. Measurement of frequency shift versus time for three different concentrations.

From Figure 40, it can be observed that the gas concentration affects two things: the time it takes to reach saturation, and the saturation level itself (or the maximum frequency shift). The 100ppm concentration showed the steepest slope to saturation as well as highest shift at 48.75 MHz, while the 50ppm showed the slowest response as well as the lowest shift at 43.125 MHz.

Table 2. Measurement results for ammonia gas sensor.

Conc. Ammonia (ppm)	Exposure Flow Rate (L/min)	Reversion Flow Rate (L/min)	Δfres of S11 (MHz)
50	0.46	0.5	43.125
75	0.31	0.5	46.875
100	0.23	0.5	48.750

After exposing the sensor to ammonia for approximately 18 minutes, the closed system was purged of ammonia using nitrogen gas. In the third column of Table 2, reversion flow rate indicates the flow rate of nitrogen gas to flush out the closed cell system so that the input reflection coefficient of the antenna returns to its baseline.

In Figure 41, the maximum shift in frequency is plotted against ammonia concentration, showing that higher concentration yields larger resonant frequency shift. Also, the plot shows a decreasing amount of shift for incrementally higher concentrations past 80 ppm level, indicating a trend towards saturation of the sensor with ammonia. Repeatability measurements showed there was approximately 1 to 2MHz deviation in the frequency shifts. The lower concentration required higher flow rate compared to the higher concentrations, which created more turbulence in the measurement cell, leading to higher deviation in the repeatability measurements.

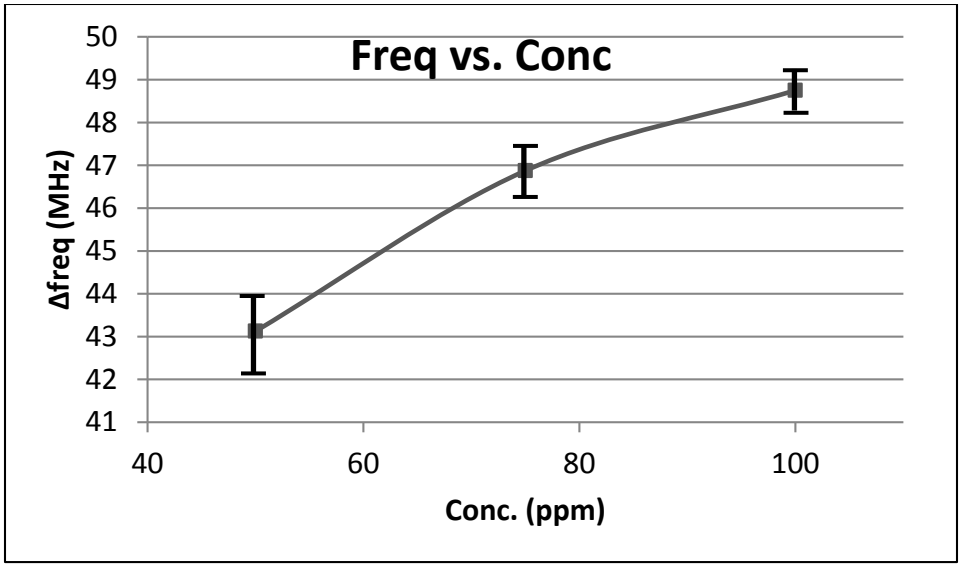

Figure 41. Measurement plot of resonant frequency shift versus concentration of NH3 gas.

3.6 Chapter Summary

This is the first reported design and characterization of a highly sensitive antenna-based CNT sensor which responds to interaction with ammonia by shift in resonant frequency. We have conducted RF characterization experimentally on a patch of thin-film PABS-SWNT and derived a surface impedance model for the SWNT. The impedance model for SWNT is equivalent to a parallel *RC* circuit, of which both the *R* and *C* values changed with exposure to ammonia. Utilizing the derived impedance model, we have designed a sensor using a loaded patch antenna topology. Measurements showed a frequency shift of 43-49 MHz shift for ammonia concentrations ranging from 50 ppm to 100 ppm. The change in the resonant frequency with ammonia exposure qualitatively validated the characterization model, and the sensor demonstrated both high sensitivity at low concentrations and fast return to baseline. The proposed design can be used for remote sensing and can be integrated with RFID or WISP tags for low-cost, wireless gas sensing applications.

- Dual functionality of sensing and communicating with one device
- Lower cost and fabrication complexity with inkjet printing
- Integrate nanomaterial directly with RF module for high frequency sensing capabilities

3.7 Support

- This research was supported by Georgia Tech Research Institute (GTRI)
    - Funding for two semesters for this research.
    - Use of the following equipment:
        - Gas generator
        - Fume hood
        - Power Network Analyzer

CHAPTER 4

WEARABLE RFID TAG

4.1 Motivation

RFID tags have evolved from Mario Cardullo's passive radio transponder with memory[70], which is considered to be the first true ancestor of modern RFID[71], to modulated backscatter RFID tags[72] (both passive and semi-passive), to the first patent to be associated with the abbreviation RFID[73]. RFID tags have been used in many different applications such as commerce, transportation and logistics, passports, animal and human identification, institutions (hospitals, libraries, museums, and schools), sports, complement to barcode, and telemetry.[74]

However, RFIDs have a major limitation when placed in close proximity to metal or the human body. Since the human body can be modeled as a lossy conductor, the following references pertain to RFID tags on both metal ground planes and lossy dielectric material. For example, Durgin et al. have shown effects of a metal ground plane on RFID tags with folded dipoles as the tags move towards the metal ground plane.[75] This work shows that the real and imaginary impedance decrease as the tag moves closer to the ground plane, causing mismatch and degradation in antenna performance. Lingfei et al. deduced the optimal distance of the tag from a metal ground plane through simulation using finite element method as well as experimental verification.[76] Ruyle et al. have investigated the placement sensitivity of meandered dipoles for RFID systems[77] and have also introduced a slot antenna design that mitigates the effect of the ground plane.[78]

RFID tags that can be mounted on any surface has significant potential for a number of different applications such as wearable tags for wireless bio-monitoring[79,80] and metal mount tags for mass shipping of container cargos.[81,82] The two main challenges for

wearable RFID tags are overcoming the loss of gain when placed on the human body or metal surfaces and conformability to the curved surfaces of the body. The subsection 3.1.2 Wearable RFID Tag in Chapter III addresses these two challenges by using inkjet-printing as the fabrication method and artificial magnetic conductors (AMC) for increased gain. The following section introduces the AMC, how it operates and its benefits for wearable RFID tags.

An inkjet-printed AMC-backed RFID tag has been designed and tested for wearable and metal mount applications. An array of dual split-ring resonators backed by a ground was used as the AMC structure. A dipole antenna matched to an RFID chip at 915 MHz was designed and inkjet printed on paper substrate. Measurements were conducted in both a controlled environment and a realistic environment outside the antenna chamber. Measurements show that the required reader's minimum transmit power for successful tag reading decreases by 6 dB compared to the case without AMC. Also, for on-body and on-metal measurements, the read range increases by approximately a factor of 2. The proposed RFID tag is flexible since it is easily fabricated by inkjet printing nano-silver particles on paper or plastic substrates. There are numerous applications ranging from wearable antennas for bio-monitoring or military applications to metal-mount tags for transportation and container cargos for mass shipping. One main challenge for universally mountable tags is overcoming the loss of gain when placed on the human body or metal surfaces. Another important challenge is the conformability of tags to various non-flat surfaces.

To resolve the issue of gain degradation due to the antenna proximity to metal or lossy material, patch antennas have been reported in the past [89]-[91] as a solution for wearable RFID tags. Since the gain for a patch antenna is highly directive away from the body, it is a natural choice for wearable RFID tags. Dipole or monopole antennas, on the other hand, has a wider bandwidth compared to a patch antenna and can be matched more

easily. However, they have not been an ideal choice for wearable applications due to the effect of the radiation toward the body, and also the loss of gain due to body effect.

As a solution to shield the effect of a surface from a dipole antenna, an AMC structure can be used. An example of an AMC cell is shown in Figure 42. There has been previous work utilizing AMC or high impedance surfaces. AMC designs are considered in [83], however they require the use of vias which limit the flexibility, reduce the ease of fabrication and limit the ruggedness of the derived wearable RFID tag. Different designs are proposed to mitigate the effect of metal but they lack in flexibility for a truly wearable RFID tag [84]. Previously, a dipole integrated with a commercially available RFID chip placed over an AMC structure has been proposed [85] for metal-mounted applications. In this work, a conformal RFID tag over AMC is investigated with measurements conducted with a Tagformance Reader in free space, on metal, and on body. A comparison is made with and without the AMC-backing to see the effect of the AMC.

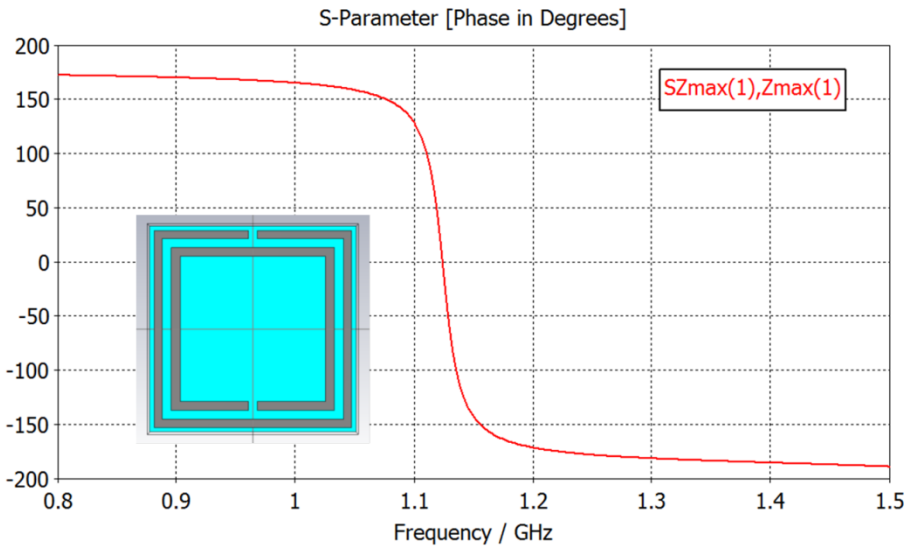

Figure 42. Phase reflection of a split-ring resonator cell.

In order to design a conformal wearable tag, inkjet-printing is a desirable solution due to the ability to print metal on flexible substrates. There has been previous work on inkjet-printed antennas for wearable applications [86] as well as inkjet-printed AMC

structures [87]. In [87], the AMC structure is a split ring resonator array inkjet-printed on paper substrate with a dipole antenna placed on top, designed at 400MHz. In this design, the dipole antenna was fed with a coax cable through the AMC and measured results showed 1dB increase in gain due to the effect of the AMC.

Presented herein is a design for an inkjet-printed dipole, matched to a commercially available RFID chip and printed on photo paper substrate, which is placed above a dual split-ring resonator AMC structure, printed on photo paper substrate. Photo paper was chosen as the substrate due to its conformability and characterized electrical properties [88]. Also, inkjet-printed silver traces on photo paper substrate allows for the tag to be mounted on non-flat, rugged surfaces, due to its flexible nature. Furthermore, it is a low-cost, low fabrication complexity solution for roll-to-roll mass production of tags.

The contribution of this work is twofold: first to present an alternate solution to patch antenna-based wearable tags. By using AMC structures, there is no longer a limitation to the type of antenna that can be used for wearable tags, and opens the door to dipoles or monopoles which can be miniaturized even further. The second contribution is the introduction of a completely inkjet-printed AMC-backed dipole tag for conformal, flexible tags. This fabrication process allows for mass production of printed wearable tags, especially because there are no vias in the design, which reduces the fabrication complexity.

The organization of the paper is as follows. In section II, the design of the prototype is explained starting with the design and optimization of the AMC unit cell. Then an optimal array size was determined and the finalized design is presented matched to a commercially available RFID chip. In section III, the inkjet-printing fabrication on photo paper substrate is described. Presented in section IV are the measurement results for three different cases to demonstrate feasibility. First, a controlled measurement was taken in an anechoic chamber comparing the performance of the tag with and without the AMC backing. Second, a real environment measurement was conducted outside the chamber

demonstrating read range over various different distances, for both body mount and metal mount scenarios. Third, conformability of the tag was investigated by measuring in free space on curved on the body and the superior performance of the AMC-backed tag was confirmed.

Applications can range from wearable antennas for factory workers in industry and patients in the hospital to plastic water bottles and metal containers. In the following sections, the AMC design and fabrication is introduced followed by measurement results and conclusion.

The proposed research is to investigate the feasibility of using an RFID tag over an AMC surface to target four different goals:

- Low fabrication complexity and cost
- Disposable (“Green”) tags
- Readable when mounted on body
- Flexible tags

4.2 Prior Art

Various different methods for creating wearable RFID tags such as using embroidered conductive thread, patch antennas, and adhesive metal sheets, are detailed in Table 3.

Table 3. Prior art of wearable RFID tags.

#	Design	Freq	Realized Gain	Material	Dimensions (mm)	Conformal	On body measurement	Ref
1	Folded patch	870 MHz	-1.5 dB	Copper on FR4	6x9 cm	No	Yes	[89]
2	Folded patch	868 MHz	-7 dB	Al adhesive sheet	45x35 cm	Yes (no analysis)	Phantom	[90]
3	Loop Antenna	2.45 GHz	N/A	Embroidered electro-thread				[91]
4	Dipole	870 MHz	-6 dBi	Embroidered conductive thread	19 x 12 mm	Yes (no analysis)	No	[92]
5	Meandered dipole	866 MHz	-6 dBi -7 dBi (body)	Printed or embroidered on textile (er 1~1.5)	68x22mm	Yes (no analysis)	Yes	[93]
6	Folded dipole	866, 915, 955MHz	Not reported	Printed or embroidered on fabric	100x10mm	Yes (no analysis)	No	[94]
7	Folded dipole	910 MHz	Not reported	Embroidered conductive thread	78mm x 39mm	Yes (no analysis)	Yes	[95]
8	Dipole on EBG	915 MHz	RCS 0.09 sm	Copper on FR4, foam	152x152mm	No	No	[96]
This work	Dipole on AMC	915MHz	3.8 dB	Inkjet printed on paper	157x125mm	Yes	Yes	[97]

In works 3-7, the fabrication method was embroidery, and the realized gain was low. The folded patch on FR4 [89], had the highest realized gain among the prior work, however the tag is no flexible due to the rigid substrate. The folded patch using adhesive aluminum sheet showed flexibility but had a low realized gain of -7dB. The dipole on AMC had an RCS of 0.09 m^2, but the fabrication was on FR4 substrate and thus is not flexible. This work showed the highest gain with a cost and time effective fabrication method for flexible tags, by using inkjet-printed silver nanoink on paper substrate.

4.3 Artificial Magnetic Conductor

Artificial magnetic conductors, also known as high impedance surfaces, are structures that are capable of reflected the incident waves at zero reflection phase, unlike metals or any electric conductor that enforces phase reversal for reflected waves. This feature has been studied in the literature thoroughly for its potentials in realizing low-profile antennas. On the other hand, split ring resonators (SRRs) have been considered as means for producing metamaterial surfaces when integrated with a wire medium for applications in the microwave frequencies.[80-82]

An artificial magnetic conductor (AMC) is a type of metallic electromagnetic structure that is characterized by having high surface impedance at a certain frequency band, and capable of reflecting the incident waves at zero phase reflection phase, unlike metals or any electric conductor that enforces phase reversal for reflected waves.[98,99] This feature has been studied in literature thoroughly for its potentials in realizing low-profile antennas. AMC surfaces are made of continuous metal, and conducts dc currents, but it does not conduct ac currents within a forbidden frequency band. Unlike normal conductors, this new surface does not support propagating surface waves, and its image currents are not phase reversed. The geometry is analogous to a corrugated metal surface in which the corrugations have been folded up into lumped-circuit elements, and distributed in a two-dimensional lattice. This unique material is applicable to a variety of electromagnetic problems, including new kinds of low-profile antennas.

Figure 43 helps illustrate the significance of using an AMC surface for on metal or on body applications through image theory. Unlike a PEC surface, for which a point source above the PEC surface creates an image of itself on the other side of the surface with a 180 degrees phase shift, the PMC surface creates an image with a 0 degree phase shift.

δ : phase shift
λ : wavelength
h : height of source from surface
θ_{max} : angle of max. gain

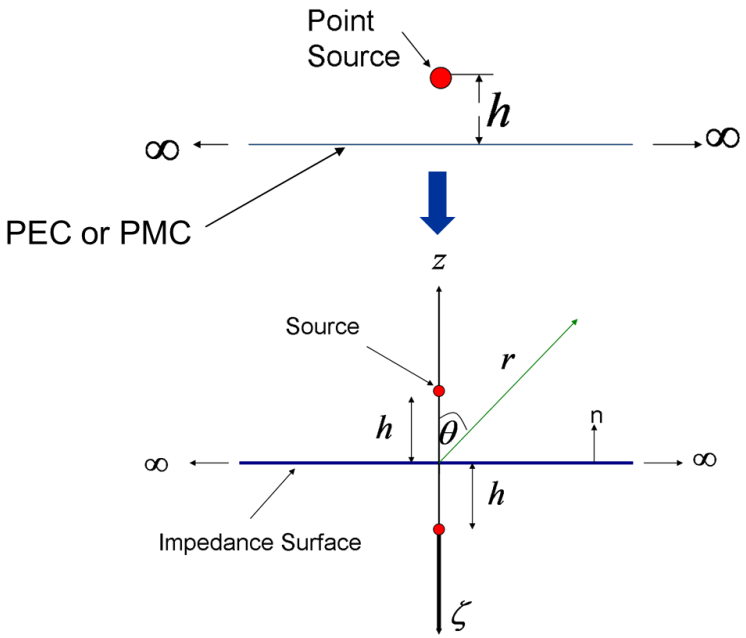

Figure 43. Image Theory

According to the gain equation (Equation 1), the phase shift of 0 degrees increases the gain by two fold, whereas a phase shift of 180 degrees reduces the gain to nearly zero, depending on the height of the point source away from the surface.

$$G_r = 2\cos^2\left(\frac{2\pi h}{\lambda}\cos\theta_{\max} - \frac{\delta}{2}\right) \qquad \textbf{Equation 1}$$

δ : phase shift
λ : wavelength
h : height
θ_{max} : angle of maximum gain

Furthermore, in Figure 44 it is illustrated why an AMC surface is needed especially if the RFIDs are mounted on the human body. Since, the radiation from the source needs to be away from the boy, a dipole antenna for example, will radiate towards the body, and therefore needs to be mounted on an AMC surface.

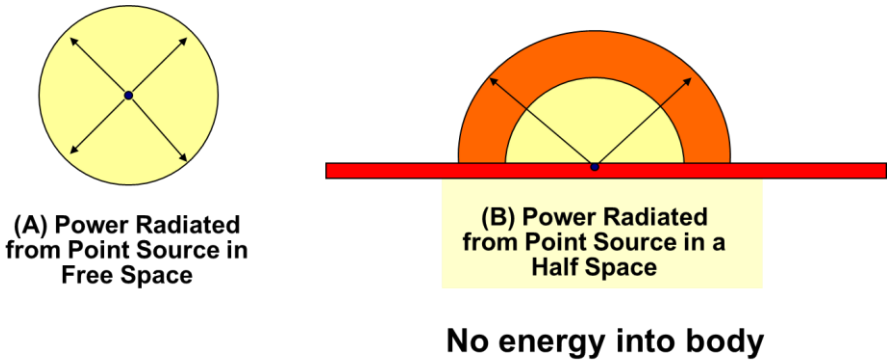

Figure 44. Comparison of radiation from point source.

Several different designs for AMC surfaces have been investigated in the past, [100,101] including a mushroom-like (electromagnetic band gap) AMC, uni-planar compact AMC (UC-AMC), Peano curve, and Hilbert curve, as a ground plane for a low-profile antenna. Depending on the design, the gain and bandwidth of the operating region can vary. The measured data show that all the AMC surfaces act as good ground planes for a low- profile antenna, yet the bandwidth and gain of the mushroom-like AMC structure are broader and larger, respectively, than those of the other structures.

Among these different designs, split ring resonators (SRRs) have been considered as means for producing metamaterial surfaces when integrated with a wire medium for applications in the microwave frequencies.[102] Unlike square patches, or loops, SRRs have the advantage of half the length in perimeter due to the resonance at $\lambda/2$ instead of λ, effectively reducing the size by half. SRR behave as an LC resonant tank that can be excited by an external time-varying magnetic field applied parallel to the particle axis, thus producing a quasi-static resonant effect. By utilizing the advantage of increased gain

of an antenna over an AMC surface, this work investigates the feasibility of integrating a flexible, inkjet printed RFID tag with a SRR-based AMC surface to create a wearable RFID tag.

AMC Based Antenna

To illustrate the effect of an AMC based antenna, we utilize split ring resonators backed by a conductive metal plane to form a high impedance surface. The overall structure is relatively compact. In addition, it has the potential of extending the functionality to multi-band through the addition of multiple SRRs in the middle of the unit cell. Fig. 1 shows the SRR unit cell modeled and optimized for operation at in the low UHF band (300-400MHz) using a finite element solver (Ansoft HFSS). The numerical model accounted for the actual silver ink conductivity $1*10^7$ $S*m^{-1}$. As in [103], the dielectric constant (3.1) and loss tangent (0.06) of a 254micron sheet of paper were used. The unit cell has a size of 150mmX150mm. The SRR structure on paper was backed by a 25mm thick foam layer on top of a metallic ground plane. The resulting reflection phase is also shown in Figure 45. Split ring resonator unit cell printed on paper, simulated in CST..

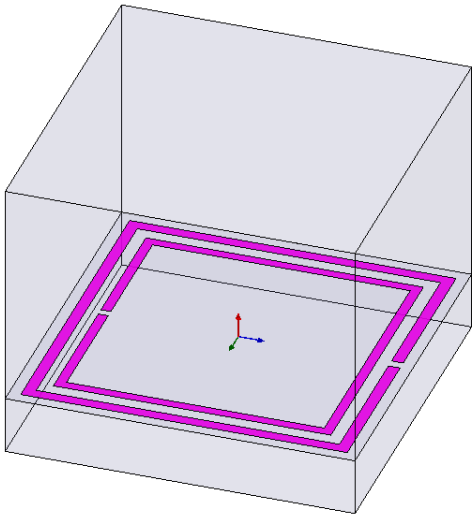

Figure 45. Split ring resonator unit cell printed on paper, simulated in CST.

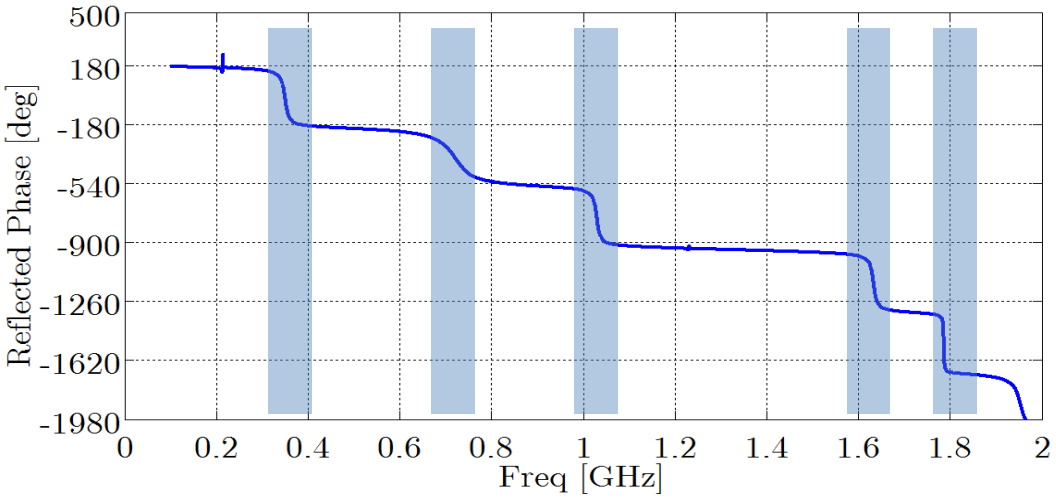

Figure 46. Split ring resonator unit cell printed on paper, and the resulting reflection phase.

Figure 46 shows the resulting reflection phase of a unit cell split ring resonator printed on paper. The extra gap in the loop aids in miniaturization of the unit cell. For demonstration purposes, and to realize a low profile antenna, a 300 mm dipole is placed horizontally 10 mm from a grid of 4X4 SRR unit cells (See Figure 47). A technique similar to that presented in [89] is used in the design and optimization process. Simulated reflection coefficient and gain values are presented in Figure 47Figure 48Figure 49. In Figure 47, a dipole is placed on the structure (feeding not shown) and the resulting antenna reflection coefficient is plotted. In Figure 48, a 4x4 split ring resonator array with a dipole placed on the surface (feeding now shown) and the resulting simulated antenna reflection coefficient. Optimal dimensions of the antenna and relative distance from the surface are found through optimization. Figure 49 shows the simulated antenna gain in two vertical cuts (Φ=0, 90^o). Note that the traditional placement of a horizontal dipole on metallic plane requires a quarter wavelength separation (187.5mm at 400MHz). This is much larger than the presented structure which has a combined height of 30mm. A gain of about 3.5dBi is observed at 400MHz.

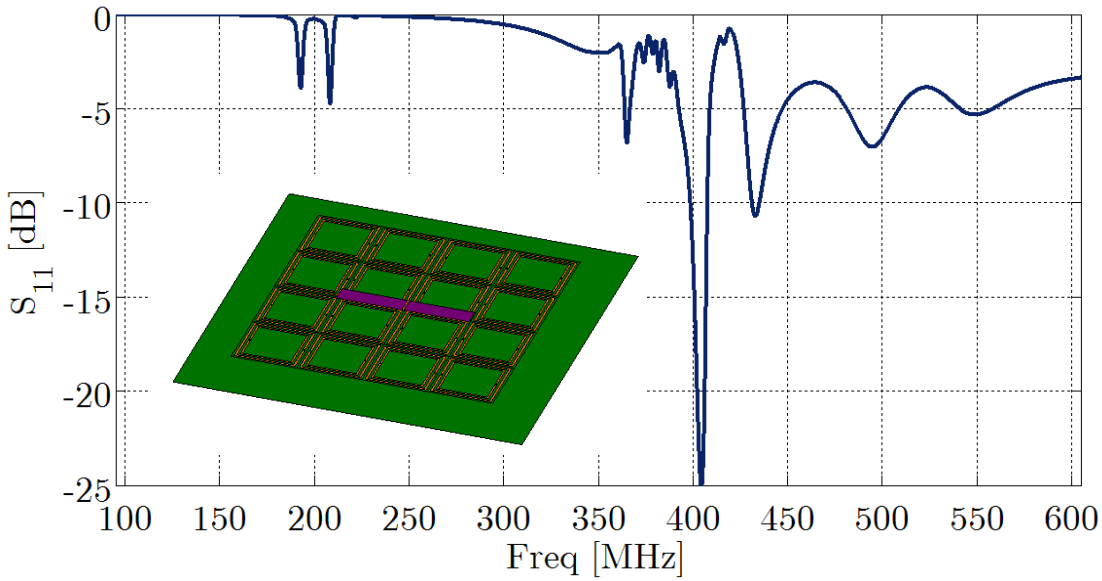

Figure 47. Split ring resonators (4X4) unit cells forming a high impedance surface.

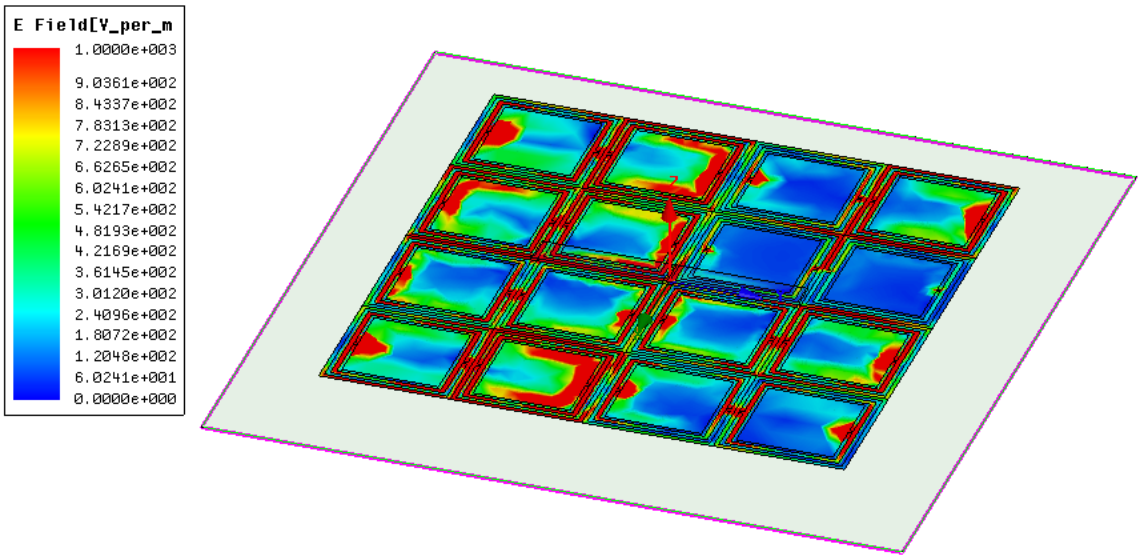

Figure 48. Simulated Electric Field of AMC in Ansoft HFSS.

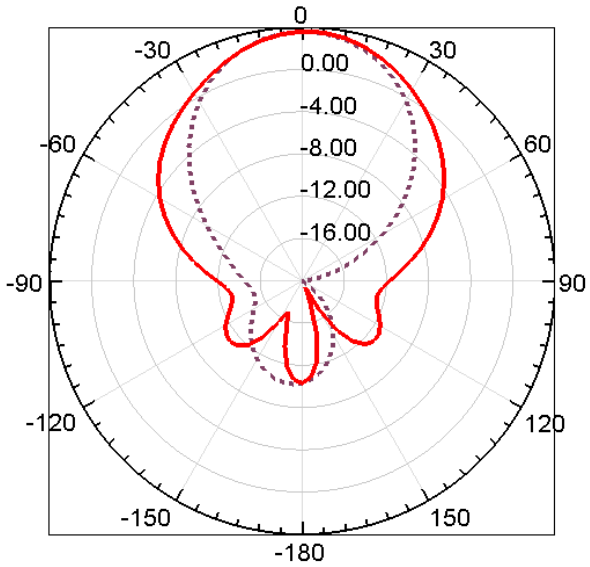

Figure 49. The resulting gain of the antenna in the two vertical cuts to the HIS surface.

To fabricate the prototype, 16 dual split ring resonators were printed on paper substrate using the Dimatix printer. Then, they were assembled together to form the AMC surface using small amount of tape. Two pieces of foam, 81cm x 81cm x 5cm, were used, where one piece of foam was placed between the dipole and the AMC and the other was placed between the AMC and copper plane. Adhesive glue was used to keep the structure intact. Figure 50 shows a picture of the fabricated prototype, minus the dipole antenna.

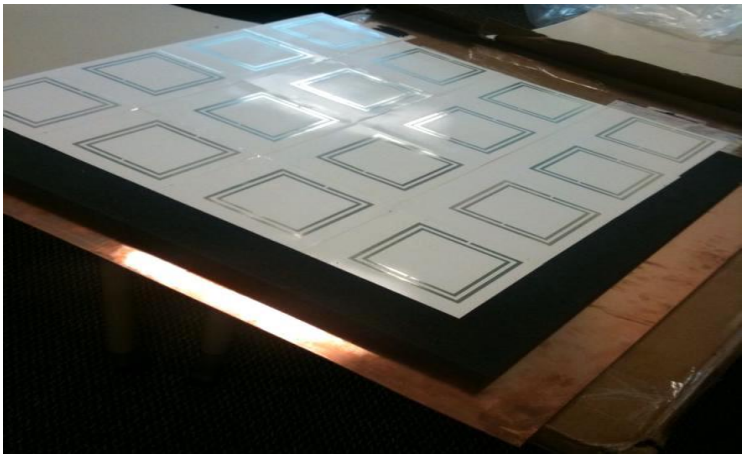

Figure 50. Fabricated prototype of AMC surface.

The antenna (Dipole + AMC) was measured at Satimo with the dipole fed by a coaxial cable that went vertically from the bottom copper plane through the center of the AMC to the dipole. Figure 51 shows a picture of the measurement setup with the antenna.

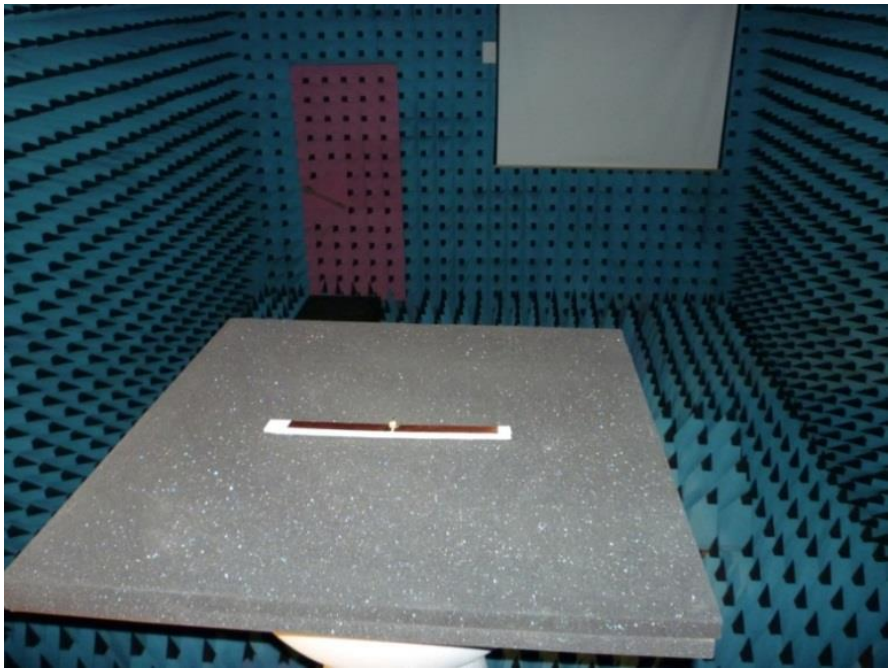

Figure 51. Measurement conducted at Satimo with dipole antenna on top of AMC separated by foam.

The return loss measurements in Figure 52 show that although the magnitude of the return loss decreases, the loss is only 12% when the AMC is added. More importantly, the resonant frequency shifts by 40MHz (10%). The gain measurements in Figure 52 and 53 show a clear 3dB increase in gain when the AMC surface is added. However, the efficiency in Figure 54 show that the efficiency decreases by 40% when the AMC is added. This can be attributed to the loss tangent of the paper, for which there is a large square area due to operational frequency of 400MHz.

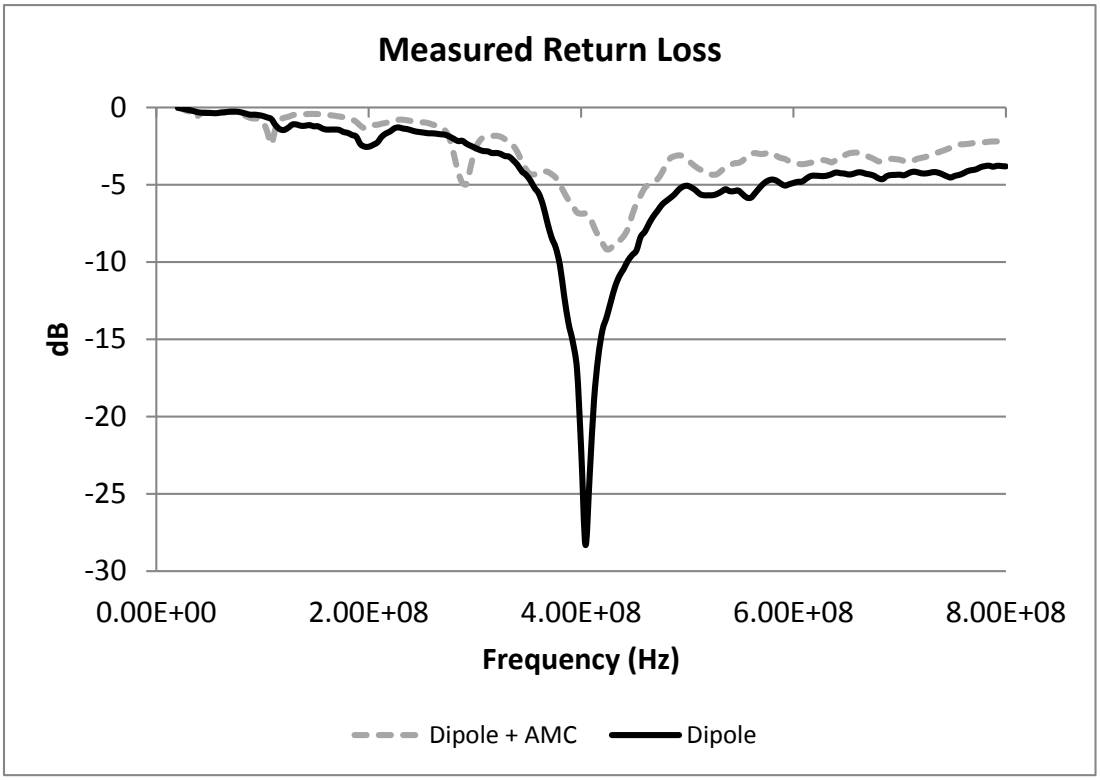

Figure 52. Measured return loss of Dipole with AMC and without AMC.

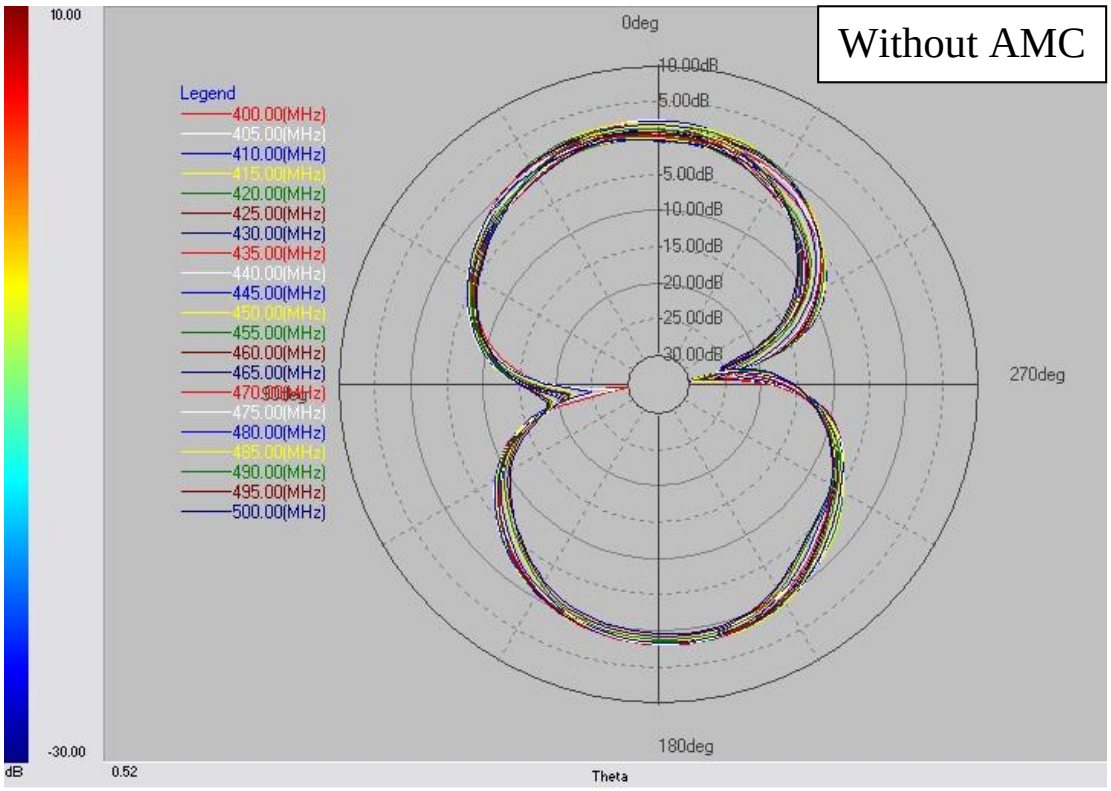

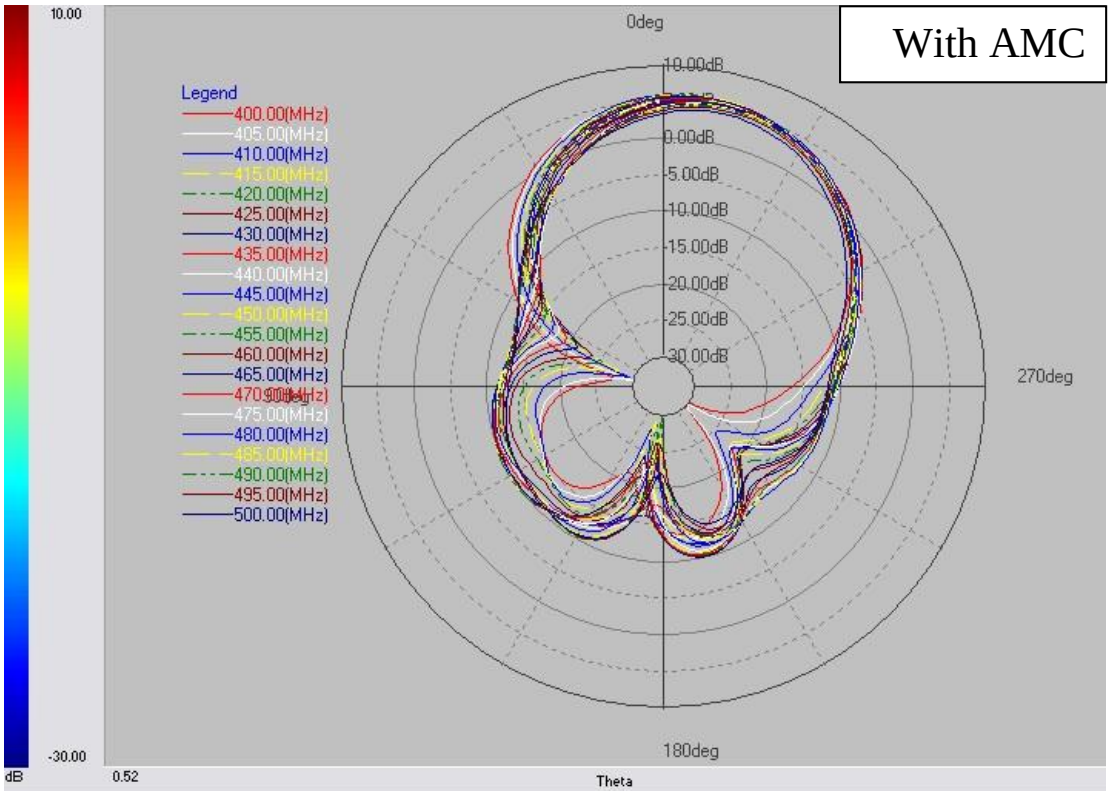

Figure 53. Measured radiation pattern and E Total. dB Phi=0 deg for (top) dipole without AMC (bottom) dipole with AMC.

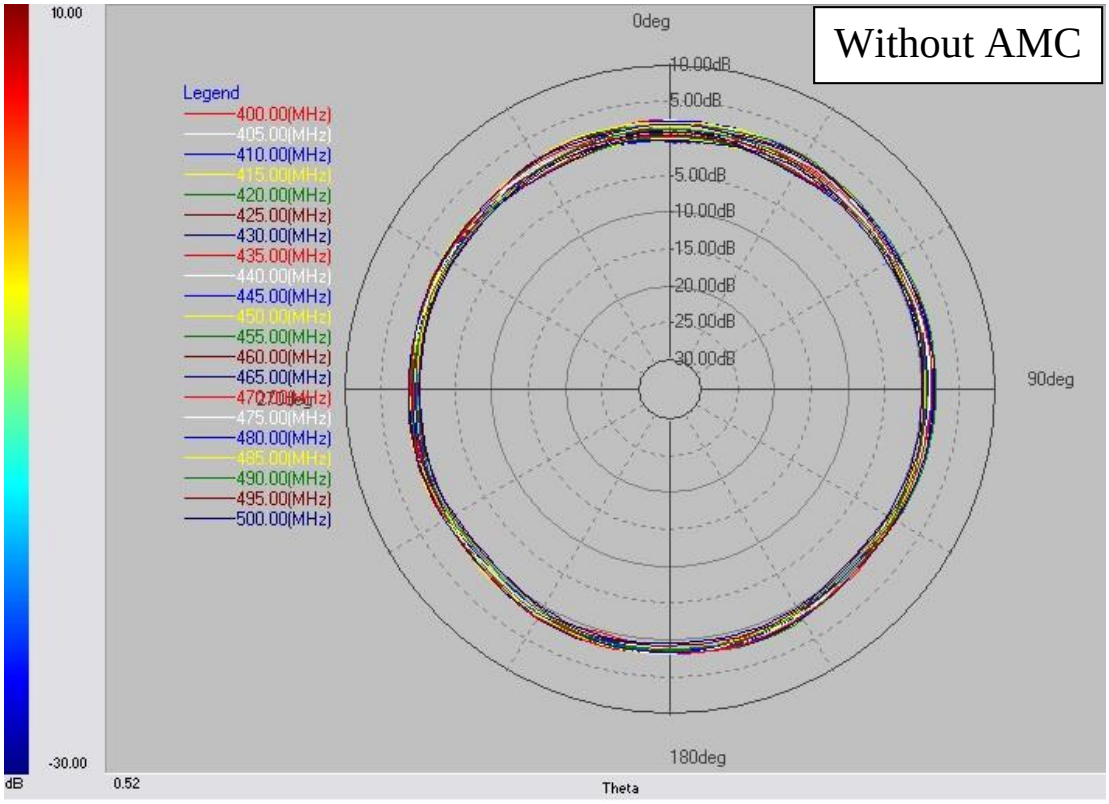

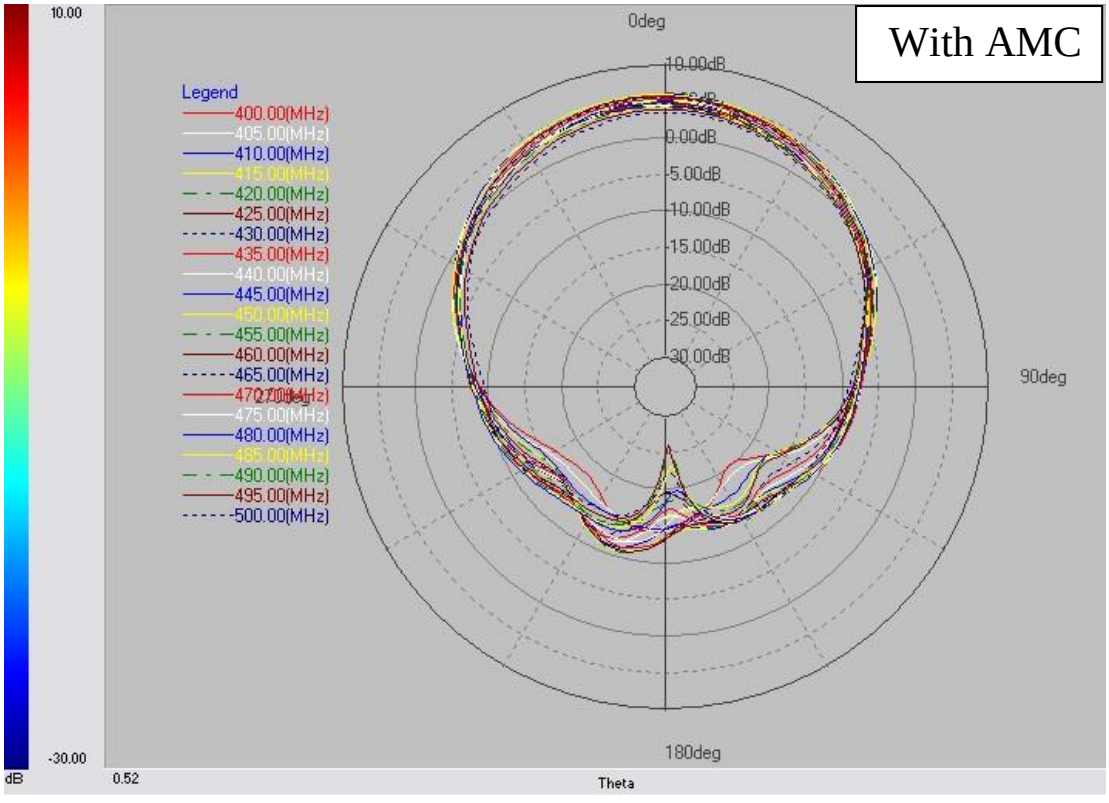

Figure 54. Measured radiation pattern and E Total. dB Phi=90 deg for (top) dipole without AMC (bottom) dipole with AMC.

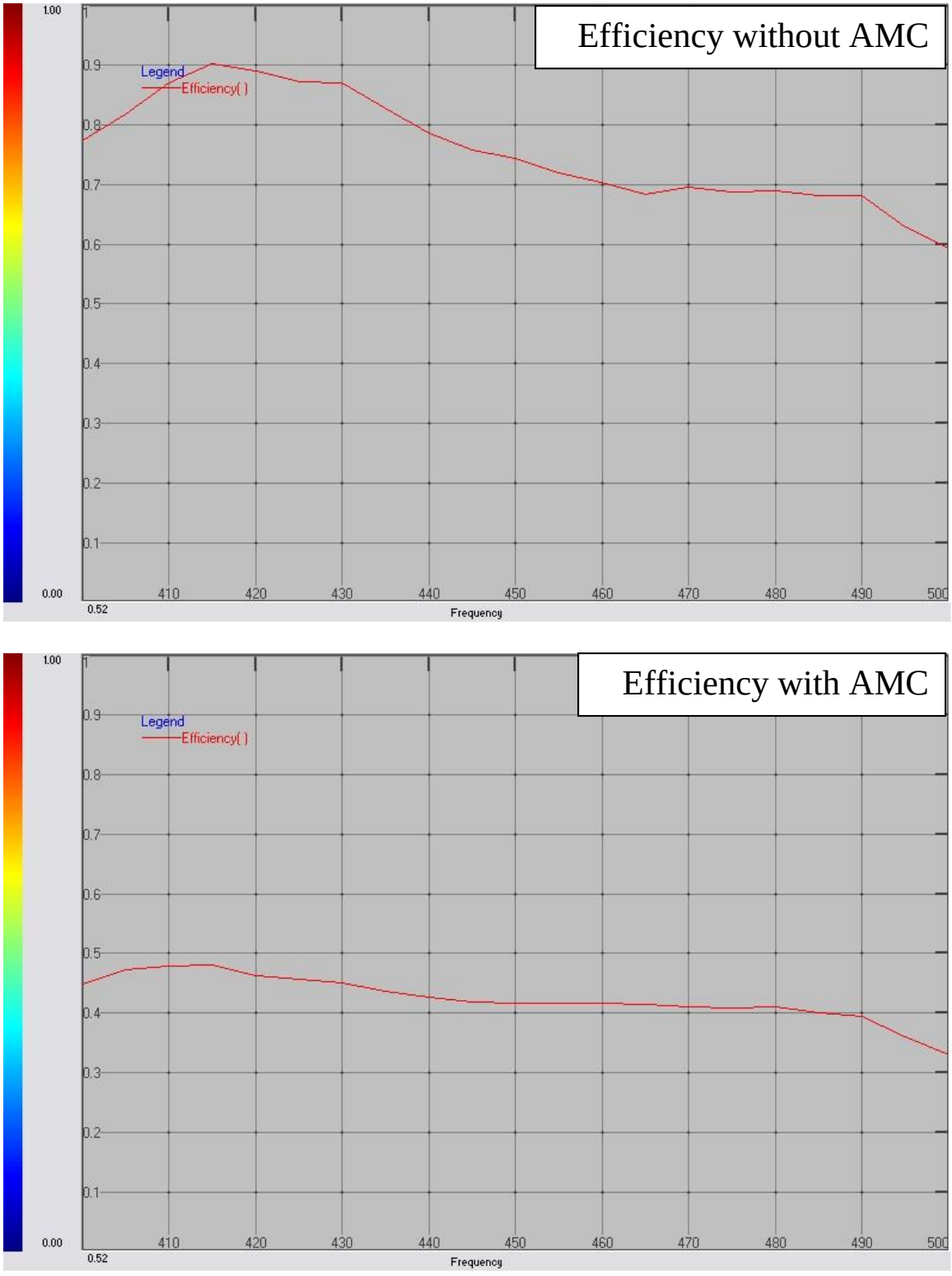

Figure 55. Measured efficiency of dipole (top) without AMC (bottom) with AMC.

A low-profile antenna on AMC surface was developed for UHF applications. The surface is inkjet-printed on paper which produces a low-cost, light-weight, and environment-friendly solution. More compact unit cells (and thus smaller overall size) and/or wider antenna bandwidth can be realized using alternative unit cells/antenna configurations as discussed in [89-90].

- A low-profile antenna on AMC surface was developed for UHF applications.
- The surface is inkjet-printed on paper which produces a low-cost, light-weight, and environment-friendly solution.
- More compact unit cells (and thus smaller overall size) and/or wider antenna bandwidth can be realized using alternative unit cells/antenna configurations

4.4 Antenna Design

Unit Cell

The design process started with the simple concept of figuring out what type of surface is needed beneath the dipole antenna to shield the body from radiation effects and to have sufficient antenna gain. Based on the well-known image theory gain (Equation 1) of a point source above a surface, two different extreme cases can be considered. One is when the surface is a perfect electric conductor (PEC) and the other when it is a perfect magnetic conductor (PMC) surface. If the surface is a PEC, there is a phase shift of π between the source and image, and for a PMC surface, the phase shift is zero.

Therefore, assuming the height of the antenna from the surface, h, is very small, the gain of the antenna is zero for an infinite PEC surface and 2 for an infinite PMC surface. There have been past studies done [104,105] on how to make PMC surfaces or artificial magnetic conductors (AMC) using high impedance frequency selective surfaces. Split ring resonators (SRR) were first proposed by Pendry *et al.* [106], and have been applied in the synthesis of AMC surfaces with negative effective permeability based on periodic arrangements of these resonators. A dual split ring resonators have been chosen due to the relatively large value of the edge capacitance achievable, which helps reduce the electrical size of the overall circumference at resonance.[107] Also, in terms of fabrication, compared to patch-based designs for high impedance surfaces, the split ring resonators require less metal for the inkjet printing process.

In the design of the SRR cell, the reflection phase needs to be investigated as shown in Figure 56 [108], to optimize the AMC cell to operate at the desired frequency operation. In the proposed design, the operating frequency is 915MHz for RFID bands in the U.S. For a single split ring resonator, the theoretical circumference of the ring would be approximately 23.2cm assuming a dielectric constant of 3 for the paper substrate. However, with the dual SRR, there is an added edge capacitance between the inner and outer rings, which decreases the electrical length at the resonance frequency, which reduces the circumference to 17.8cm.

The advantage of this dual split ring resonator compared to a ring resonator is miniaturization based on two key points. First, by placing a gap in the ring, each split ring acts like a meandered dipole, with electrical length of $\lambda/2$. This is as oppose to the ring resonator which acts like a folded dipole with electrical length of λ. Second, having two split rings, there is an added capacitance between the two rings, which reduces the circumference even further.[109] However, the tradeoff in the miniaturization is the introduction of linear polarization to the split ring, compared to the previous non-polarized loop.

The unit cell shown in Figure 56 has been simulated in CST Microwave Studio, and tuned to 915MHz with paper used as the substrate. The design of this particular SRR was different from the past work in that the shape was elongated to reduce the number of cells to cover the dipole antenna to be placed on top. If a square SRR array was used, more cells would be needed to cover the length of the dipole.

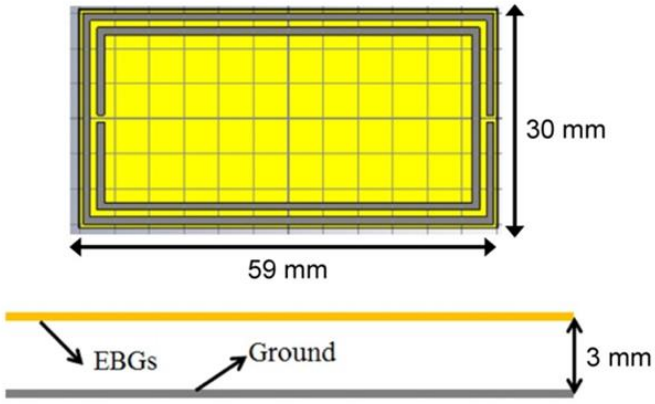

Figure 56. Optimized AMC unit cell (top) and the resulting simulated reflection phase (bottom).

An air gap was placed between the unit cell and ground and the height of the gap was tuned to 3mm so that the bandwidth of the reflection phase shift was wide enough for impedance matching. The phase shift shows an operating region of 20MHz from 900 to 920MHz. Although the thickness can be reduced even further, due to the increase in Q of the resonant cavity, the bandwidth becomes smaller, and the AMC becomes even more sensitive to de-tuning. So, to take into account possible margin of error in fabrication, a sufficient gap was placed between the SRR and ground.

The gap between AMC and ground plane is kept by inserting flexible microwave foam with dielectric constant 1.03 and loss tangent 0.0001.[110] This provides more flexibility, low losses and reduced difference between paper substrate and air dielectric constants. The reflection coefficient at the paper-foam interface is 0.5, a small value because the dielectric constants of paper and foam are 3 and 1, respectively. In other words, 75% of

power can be transmitted to AMCs to make in-phase reflection. Different materials can be considered to fill the AMC-ground-plane gap. For example, with high dielectric materials like ceramics the tag loses its benefits in terms of flexibility and weight. With paper substrates, maximum power transfer is achieved but the AMC loses its property of increased gain due to high loss tangent and the overall flexibility is degraded by the structure thickness. The rectangular shape was used instead of a square shape in order to decrease grating issues when a broad read angle was used and to reduce the size of the array by minimizing the capacitance between the AMC cells and the dipole antenna on top. Figure 57 shows the phase of reflection coefficient on the AMC structure. The reflection phase has a value between -90° and +90° in the RFID frequency band. The AMC is designed by means of reflection phase characterization. [111,112] A plane wave is illuminated onto the infinite AMC surface and the phase of reflection coefficient on the surface of the AMC is observed. The AMC surface can be considered as an AMC reflector if the reflection phase is within range of [-90°, +90°] since the reflected waves will be constructively added to radiated waves.

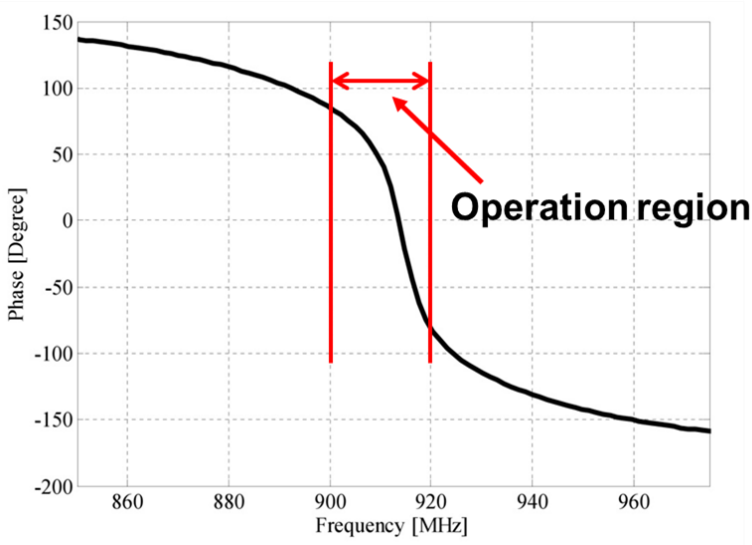

Figure 57. Broad read angle versus the number of AMC cells.

Optimal AMC Array

For the final design, an optimal array size for the AMC needed to be determined, taking into account minimal size for wearable applications, gain, and operating frequency. Although a small array, such as a 1x2, would be generally desired, the coupling between the SRRs is not enough to create a high impedance surface that induces the desired phase shift of 0 degrees between the source and image, according to Equation 1. Since there is no radiation at the ends of the dipole antenna, there is no added gain due to an AMC surface at the ends, and therefore, two rows are sufficient for an optimal array size. However, in order to determine the optimal number of cells for the width, the change in θ_{max}, from Equation 1, was analyzed for each added cell starting with one, as shown in Figure 58.

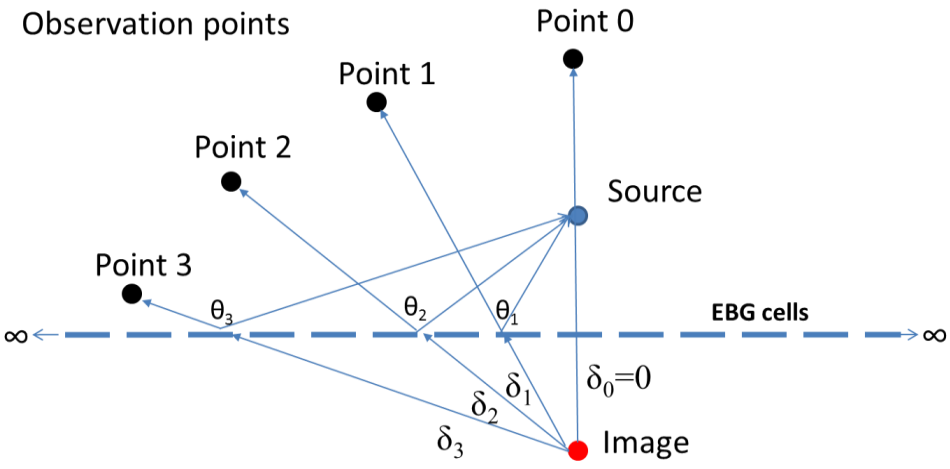

Figure 58. Broad read angle versus the number of AMC cells.

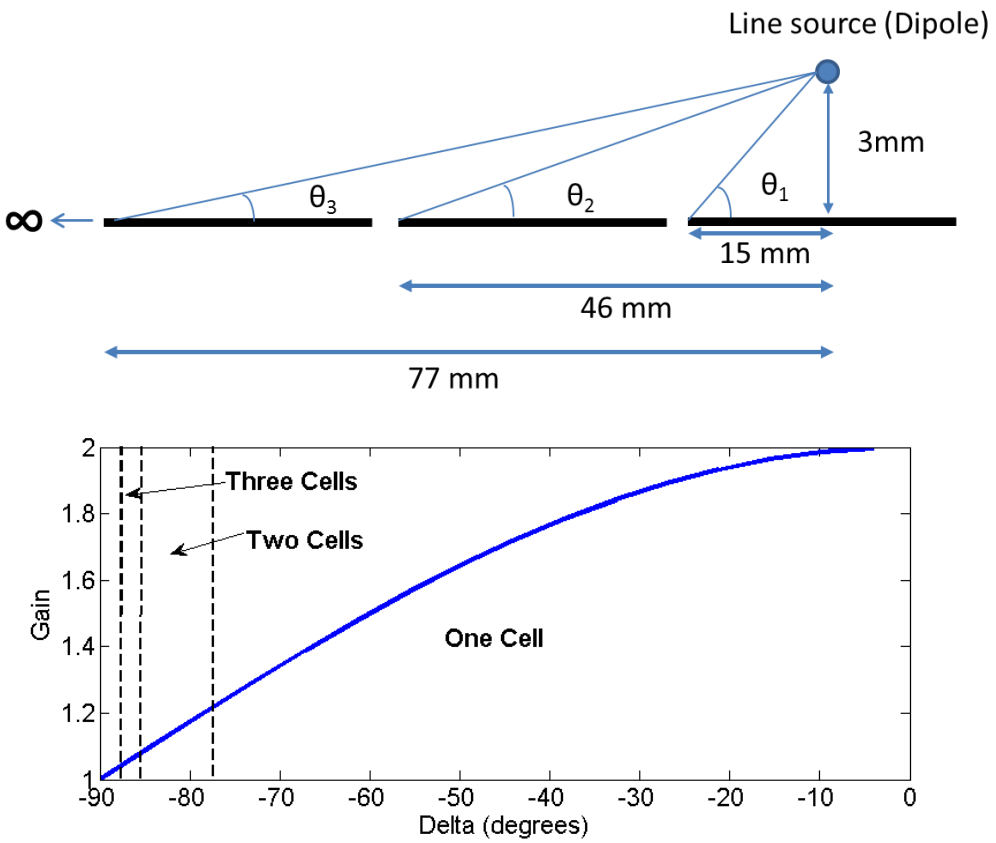

Figure 59. Three unit cells (in the half plane) and the corresponding gain versus observation angle.

Depending on the position of the observation point, the angle at which the gain is maximum changes. At observation Point 0 in Figure 58, the angle from the image to Point 0, δ_0 is zero degrees. However, as the observation point moves away from the center to point 1, 2, and 3, the angle δ_0 increases. Given the dimensions of the unit cell of our design, the observation angle versus the number of cells can be analyzed. In Figure 59, three unit cells are placed, with each cell at 30mm in width, and the dipole antenna placed 3mm away from the surface. Using Equation 1, the gain for each angle was calculated in Matlab software. With one unit cell, the observation angle is from 78 to -78 degrees, which is a total angle of 156 degrees. With two unit cells, the observation angle increases by 16 degrees to 172 degrees. However, with a third unit cell, the incremental increase in observation angle is less than 3 degrees, for a total of 175 degrees. Therefore

the added benefit of a third column of cells (in the half plane, meaning five columns overall) compared to the added total size of the tag is not enough to justify making the overall tag larger, especially for wearable RFID tag applications. It can also be seen that when the observation point is directly above the dipole, then the theoretical max gain of 2 can be achieved, and this gain decreases with observation angle.

Next, a dipole antenna was designed and matched to a commercially available NXP RFID SL3ICS1002 chip with a T-matching network. The impedance of the chip with an aluminum strap packaging was 13.3-j122 Ω and Figure 60 shows the finalized design with the dipole antenna matched to the RFID chip over an AMC surface.

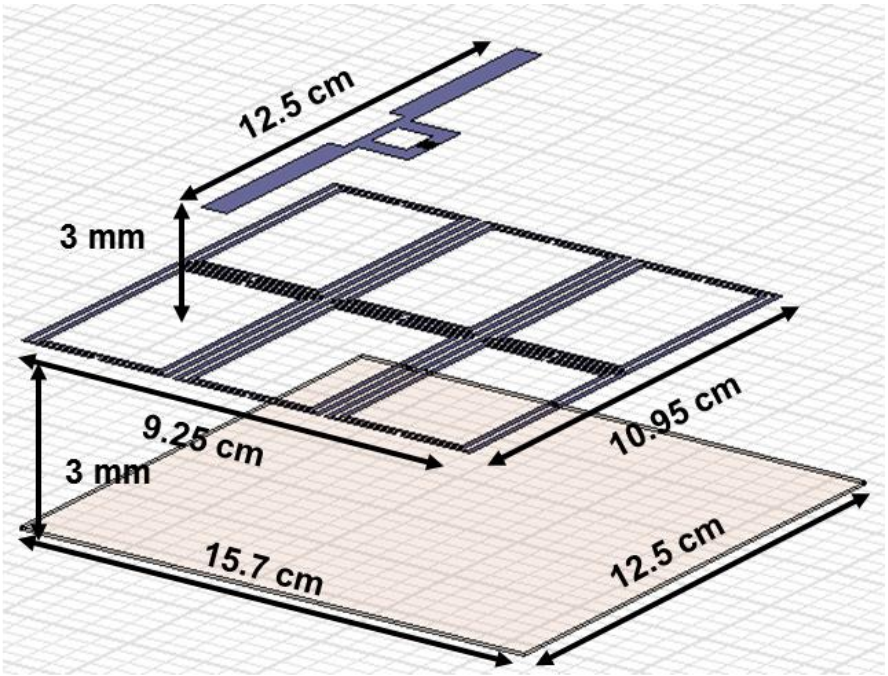

Figure 60. Dipole antenna matched to the RFID chip on top of the designed SRR-based AMC surface, with the bottom layer as the ground plane.

Simulation

The simulation is largely divided into two different categories. One is the analysis of the effect of the AMC surface when placed on the body or a metal surface. The other analyzes the effect of conformability of the AMC-backed tag. To analyze the effect of the AMC surface on the body and on a metal surface, four different cases were simulated. The simulated 3D radiation pattern of the AMC-backed shows that there is higher gain with the AMC compared to a dipole tag without the AMC. Two scenarios were simulated, as shown in Figure 61, one with the tags on a body and one with the tags on the metal. In both cases, there was a higher gain with the AMC structure.

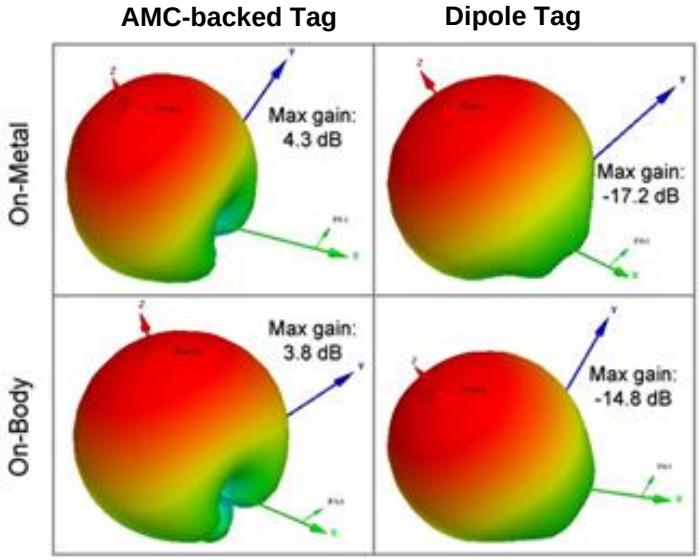

Figure 61. Simulated 3D radiation patterns of the AMC-backed and dipole Tags on both metal and body.

Next, to analyze the effects of conformability, the tag was wrapped around a foam cylinder with permeability of 1 and simulated in CST, as shown in Figure 62. Measurements were conducted to demonstrate the effect of a conformal AMC-backed tag, and is shown in the Measurements section below.

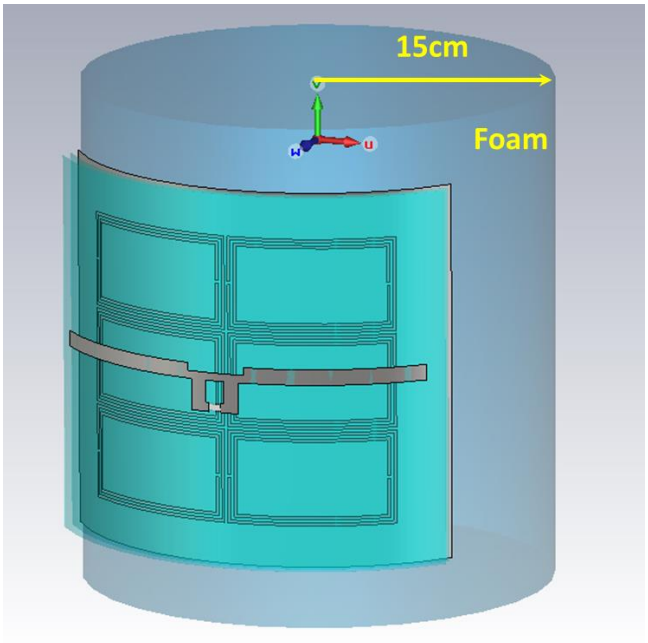

Figure 62. Simulation of prototype curved on foam in CST.

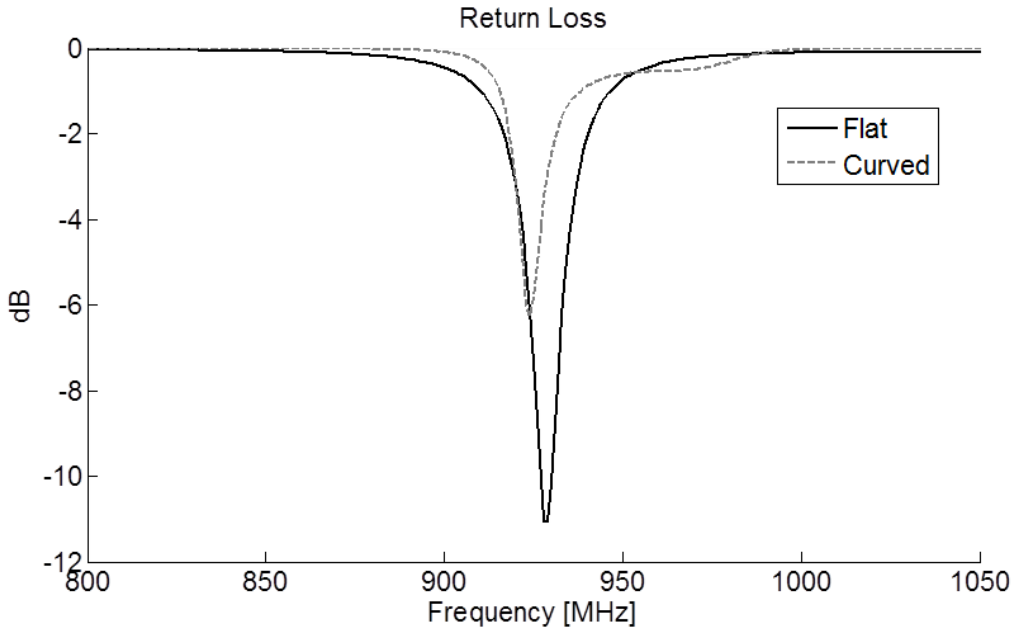

Figure 63. Simulated return loss of curved tag compared to a flat tag in CST.

The simulation results in Figure 63 shows that the return loss shifts downward slightly by 5MHz when the tag was curved, which is only a 0.54% change. This can be attributed to a slight increase in capacitance at the center of the AMC where the cells meet. A curved structure effectively gives a 3D structure in which the cells have more capacitance between them.

To analyze the change in gain, first the return loss was taken into account to get the realized gain. The curved tag has a return loss of -6.272dB at the resonance frequency, which introduces a corresponding mismatch loss -1.17dB, which lowers the realized gain. Second, in the curved case, the gain was -7dB. This can be attributed to the fact that as the tag is curved there is a phase difference of the incident wave hitting the center of the tag compared to hitting the curved edges. If the angle of observation is 90 degrees at the center, then a curved surface will have a lower angle at the edge compared to that of a flat surface at the edge. According to Equation 1 and Figure 59, this lowers total gain for the curved tag.

4.5 Fabrication

For the fabrication, inkjet printing was chosen as the method due to several reasons. One reason is that the feasibility of printing lends itself to the possibility of roll-to-roll printing which helps lower the cost per unit tag. The second reason is that a truly flexible and bendable tag was desired, and conventional copper etching would not suffice for this wearable tag. Inkjet printing would allow fabrication on flexible substrates, which is the main reason behind choosing inkjet printing as the desired fabrication method.

For the printing process a Fujifilm Dimatix 2800 printer was used. Commercially available silver nano-ink was used as the conductive ink. The conductivity of the ink is 4.7×10^6 [S/m]. Photo paper was selected as the substrate due to several reasons. First, much work has been done to optimize the inkjet printing process of silver nano-ink on

photo paper. Second, the dielectric properties of the photo paper have been characterized [23]. Third, it can be easily bent and flexed to measure the effect of a bendable AMC antenna on the body. The inkjet printed prototype of the SRR array on paper substrate is shown in Figure 64. The paper is also commercially available photo paper. The finalized prototype consisting of the dipole on top of the AMC is shown in Figure 65.

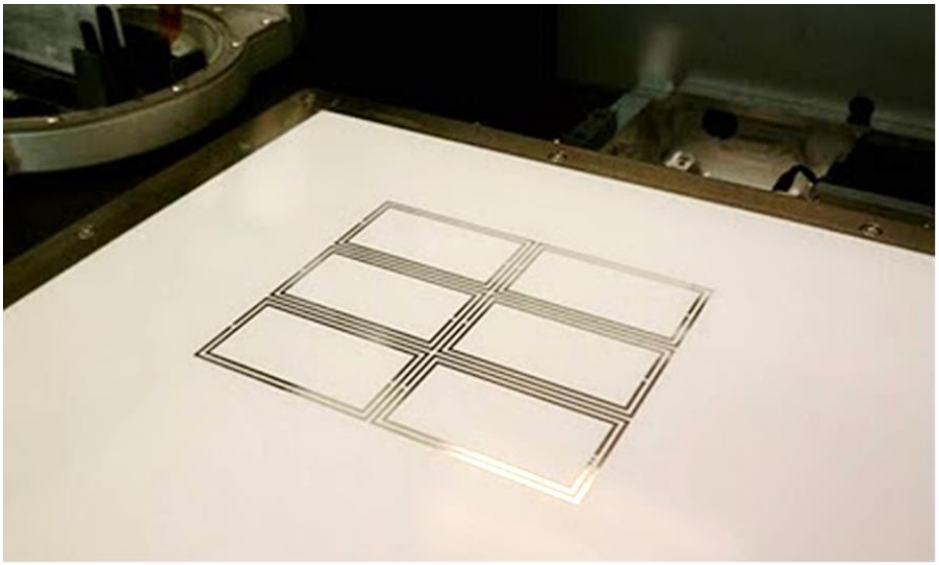

Figure 64. Inkjet-printed AMC array on paper substrate with Dimatix material printer.

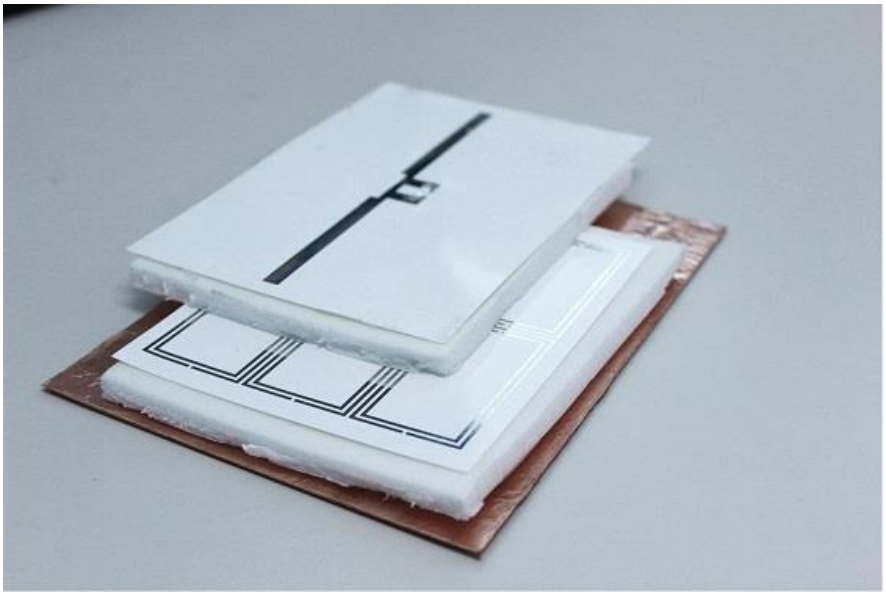

Figure 65. Finalized prototype fabricated with foam and flexible copper ground.

For the 3mm air gaps, flexible foam was used that were highly porous to closely match the properties of air, and also to be bendable for wearable applications. The ground plane was made using copper tape on photo paper, also for maximum flexibility. However, due to the de-tuning effect of the AMC, another dipole antenna was designed and printed to take into account this de-tuning effect. For the dipole antenna to be measured in free space, the length of the dipole was 13.75cm, whereas the dipole tuned to be placed on the AMC was 12.5cm.

4.6 Measurements

The AMC-based RFID Tag was extensively tested in order to assess its capability to work regardless of the surface where it is mounted. Three different measurements were performed. First, a controlled measurement was conducted within an anechoic chamber to see the effect of the AMC-backed dipole to without. Second, a real environment scenario was investigated outside the chamber and detecting the RFID tag as it was placed further and further away from the reader. Both on-body and on-metal cases were considered. Lastly, conformal measurements were conducted in which both free space measurements and conformal on-shoulder measurements were taken inside an anechoic chamber.

Controlled Measurements

In the first experiment, a sensitivity analysis in anechoic chamber was performed when varying the interrogation frequency. The AMC-based Tag was mounted on a polystyrene sheet and placed 1 meter away from a circularly polarized antenna (8 dBi gain) connected to the Voyantic Tagformance Reader. The minimum power required to communicate with the Tag was recorded at different frequencies in the 840-1000 MHz band with 1

MHz step. Figure 66 shows the comparison between an AMC-based Tag and an inkjet-printed dipole Tag in terms of minimum transmit power from the Reader. Both Tags exhibit a broadband behavior with best performance achieved in the U.S. UHF RFID band (902-928 MHz). Here, the AMC-based tag outperforms significantly the dipole which requires about 6 dB more power to communicate with the Reader. Since current RFID systems are forward-link limited [113] and therefore the maximum read range exclusively depends on the Reader EIRP, a sensitivity gain of 6 dB in free space allows to double the read distance of the AMC-based Tag over the dipole.

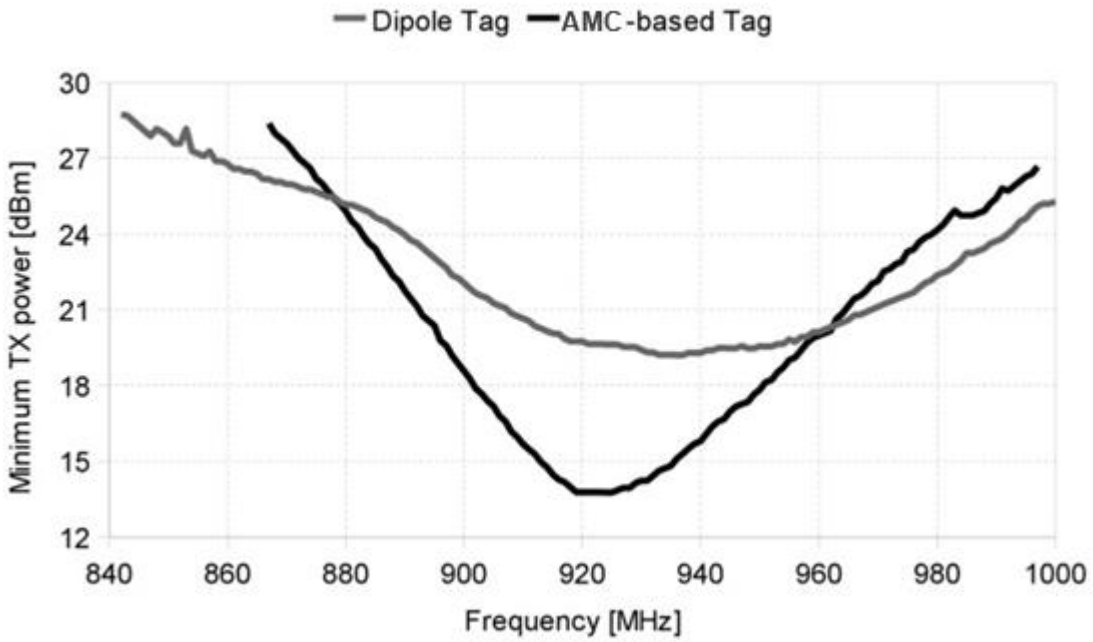

Figure 66. Measurement comparison of dipole tag with and without AMC backing in an anechoic chamber.

Real Environment Measurements (Body, Metal)

In the second experiment, the reliability of the Tag-Reader communication in real application scenarios was evaluated. The AMC-based Tag was attached both to a metal surface and to a human body for future applications like container tagging and bio-monitoring. The Impinj Speedway Reader (operating frequencies 902-928 MHz) was used to interrogate the Tag in a standard office room.

Error! Reference source not found. shows the measured packet loss, i.e. the ratio between the numbers of lost Tag replies to the total number of performed interrogations, at the Reader. The AMC-based Tag can be reliably read up to 4.5 meters and 2.5 meters when attached to metal and human body, respectively. The difference in range between metal and body is due to the lossy dielectric properties of the human body close to 0.3 for the loss tangent.[114] There is less constructive reflection off of the body which contributes less to the gain compared to metal. The dipole Tag instead exhibits extremely poor performance on both surfaces: it is never read on metal and can communicate with the Reader up to 1 meter away when attached to human body. The measurement results are in perfect agreement with simulations performed by HFSS: the maximum gain of dipole Tag is extremely poor both on-metal and on-body while the AMC-based Tag exhibits excellent performance on both surfaces (see Figure 61). This clearly demonstrates the inappropriateness of commonly adopted RFID Tags in harsh application environments. In such situations, ad-hoc Tags like the AMC-based one here presented are required in order to ensure a reliable communication with the Reader.

Conformal Measurements

In the third experiment, the tag response in a conformal setting was measured. The tag was placed on a foam cylinder 30cm in diameter, and measured in an anechoic chamber. This measurement is compared to the flat tag in free space shown in Figure 67. The

measurement results show a downward shift in the resonance frequency of 5MHz, which matches the simulated results in Figure 62. Furthermore, the minimum transmitted power from the reader increases, due to the loss in realized gain when curved. Lastly, for a conformal, on-body measurement, and the tag was measured while wrapped around the shoulder of a person. Two different measurements were taken; one with the AMC backing and the other without. In the latter case, the Tagformance reader was not able to read the tag at all, because there is no magnetic surface, and thus no added gain without the AMC backing. The measurement results are shown in Figure 68.

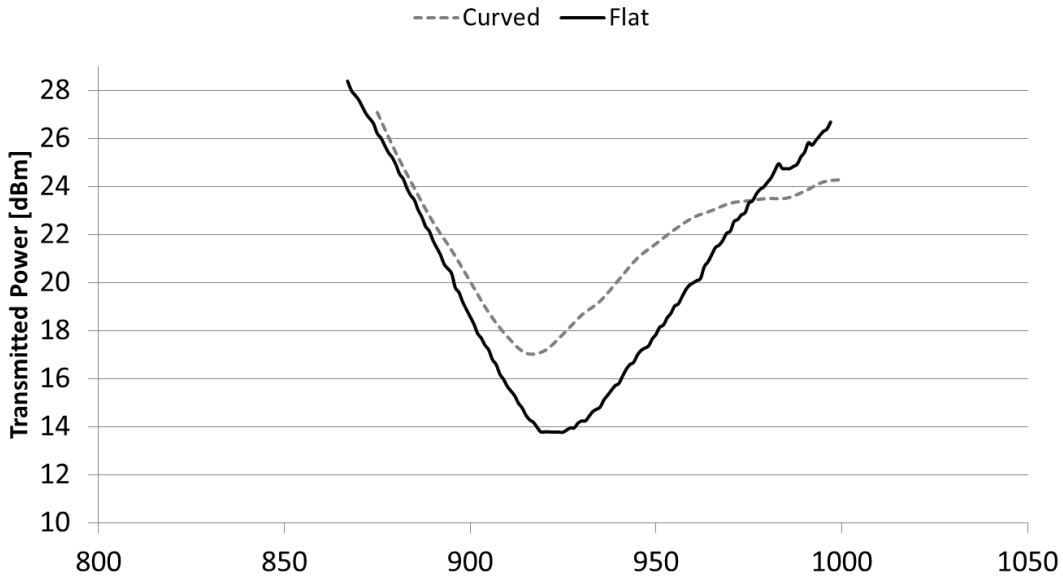

Figure 67. Measurement results of AMC-backed tag curved on cylindrical foam versus a flat foam in free space.

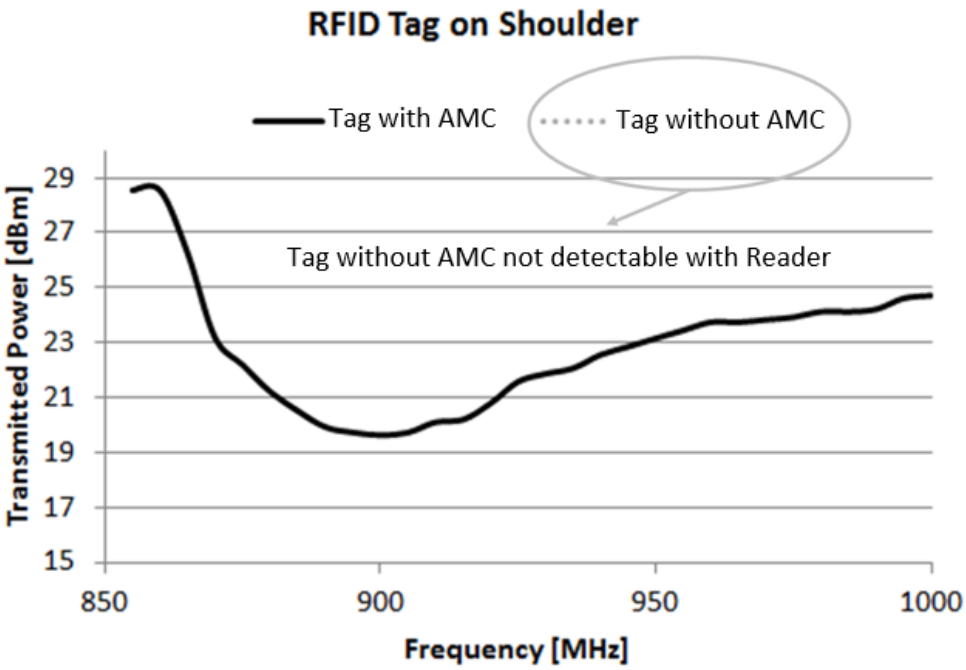

Figure 68. Measurement of conformal, wearable tag. Two measurements were taken, one with AMC-backed tag and the other without the AMC.

Due to the relatively small ground, there are some added effects of the body at the edges of the plane. With a larger ground plane, the body effect would be less. With the added lossy conductor effect, due to the body at the edges of the plane, the loss reduces the Q of the resonator, and increases the bandwidth. As can be seen in Figure 68, only one curve is shown, since the reader was not able to read the tag that did not have the AMC backing. This clearly demonstrates that the proposed AMC-backed tag has superior gain performance over the tag without the AMC.

4.7 Chapter Summary

This is the first reported design and development of an inkjet-printed RFID tag on an AMC surface printed on paper substrate. Compared to patch antennas which have limited, narrow bandwidth, AMC surfaces have various shapes, bandwidths, and miniaturization techniques which can open up the possibility of new wearable RFID tag designs for varying design specifications. Furthermore, as tags need to be low-cost, the feasibility of inkjet-printed tags on paper demonstrate the possibility of low-cost, environmentally friendly, flexible RFID tags.

A flexible, fully inkjet-printed, AMC-backed RFID tag has been introduced as a solution for wearable and metal-mount applications. An analysis on AMC array size optimization was conducted and simulations for various scenarios such as body mount, metal mount, and conformal tags show viability in gain performance of the AMC-backed tag. Extensive measurements in a controlled chamber, in a real environment with data packet transfer, and conformal tag measurements in free space and on the body show that the AMC-backed tags perform better than tags without the AMC. On body can be read at approximately twice the distance compared to a tag without AMC on body. Both in chamber and real environment measurements demonstrate the increase in gain and range due to the AMC structure. Furthermore, a curved measurement on the shoulder showed that the AMC-backed tag can be read easily whereas a tag without AMC could not be read at all. With more precise manufacturing and fabrication, the thickness can be reduced even further, and with a lower loss flexible substrate such as LCP, the range can also be improved. This demonstrates that an inkjet-printed AMC-backed RFID tag on photo paper substrate shows higher gain and thus greater read range compared to a tag without the AMC backing, and can be used for wireless bio-monitoring applications or metal mount applications.

4.8 Support

- Received support from Dr. Yang Wang's Research Group
    - Use of Tagformance RFID Reader to conduct RFID measurements
    - People who helped:
        - Sangkil Kim
        - James Cooper

Chapter V

INKJET PRINTED RF INDUCTOR WITH MAGNETIC NANOMATERIAL

5.1 Motivation

Printed electronics have shown tremendous growth in recent years, and the demand for faster, smaller, cheaper, and more efficient printed devices is ever increasing. Inkjet printing is a technology which has demonstrated the ability to fabricate electronic components in a rapid, additive manner which can be scaled to mass production in roll-to-roll processing to meet these needs.

Recently, there has been a push for inkjet-printed RF passive components such as multi-layer capacitors and inductors to remove the requirement for mounted discrete components in printed systems.[22] Currently, only low-frequency and low Q inductors have been demonstrated in the literature. Inkjet printing allows for the deposition of a wide variety of materials including magnetic material which can be integrated with printed inductors increase the inductance.

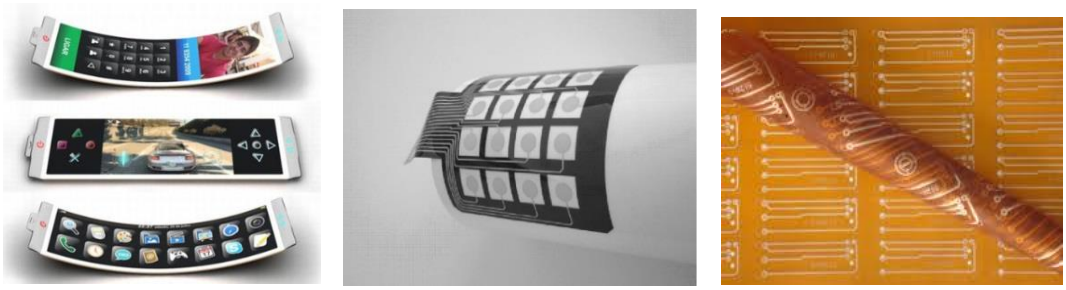

Figure 69. Examples of printed electronics.

Current techniques to deposit magnetic nanomaterial on printed inductors include dc magnetron sputtering [115], epoxy paste application [116], or substrate impregnation of magnetic particles [117]. These techniques result in rigid and brittle components which cannot be used in flexible or wearable applications. However, the ability to print magnetic nanoparticles allows for thin, conformal layers of material to be deposited rapidly and at low-cost.

This work demonstrates an improvement in the performance compared to previous works with inductances of up to 8 nH while maintaining a high quality factor of 25, and an SRF of 8 GHz. The inductors are integrated with printed magnetic nanoparticles to investigate the high frequency performance of printed nanoparticle-based magnetic material for the first time.

In this work, the RF characterization of the magnetic nanomaterial for complex permittivity and permeability is first performed. The meander RF inductors are then designed and fabricated for high inductance, Q, and SRF. Measurements for the printed inductors with and without printed magnetic nanomaterial are then compared with simulation.

For the first time, high quality factor (Q), meander inductors are demonstrated utilizing inkjet-printing on organic paper substrates. Quality factors of up to 25, which is an order of magnitude greater than previous works, and inductance values of up to 8 nH are achieved. The high self-resonance frequency (SRF) of 8 GHz makes it possible for the inductors to be used in the 900 MHz and 2.4 GHz RFID bands, and in 5 GHz Wifi band. Furthermore, a study into the performance and miniaturization effects of inkjet-printing magnetic nanomaterial onto the inductors shows increases in inductance of up to 5%. Applications for inkjet printed inductors include all-printed flexible and wearable filters, resonators, and microwave matching networks.

In this work there are two main goals behind inkjet-printed RF inductors with magnetic nanomaterial. The first goal is to demonstrate high Q inductors that can be

inkjet-printed on paper substrate. The second goal is to investigate the feasibility of inkjet-printed magnetic nanomaterial and observe increase in inductance. The main challenges for this work are as follows:

- Optimize the inkjet printing of the magnetic nanoparticles
- RF characterization of the magnetic nanoparticles
- Fabrication of the RF inductors with and without the magnetic nanoparticles

5.2 Prior Art

Printed electronics have shown tremendous growth in recent years, and the demand for faster, smaller, cheaper, and more efficient printed devices is ever increasing. Inkjet printing is a technology which has demonstrated the ability to fabricate electronic components in a rapid, additive manner which can be scaled to mass production in roll-to-roll processing to meet these needs.

Table 4. Prior art of printed inductors.

#	SRF	L	Q	size	Fabrication	substrate	Magnetic material	Ref
1	1MHz	220nH 230nH	n/a	11x11mm	Inkjet Printing	Polyimide	4.5% increase (thickness n/a)	118
2	18GHz	2nH	3.5	1.8x2mm	Inkjet Printing	Kapton	No	119
3	10GHz	1.4nH	10	0.13x0.13mm	DC Magnetron Sputtering	Silicon	7% increase (0.2um)	120
4	1MHz	16.2nH	10.5	0.1x0.1um	Electroplating / Photolithography	Ferrite plate	Ferrite plate (0.5mm)	121
This work	8GHz	7.8nH	25	3.3x7mm	Inkjet Printing	Paper	5% increase (5um)	

Kang et al. demonstrates an inkjet-printed spiral inductor, which is characterized up to 1 MHz.[118] Menicanin et al. introduces an inkjet-printed meander inductor on Kapton with inductances of up to 2 nH, and quality factors of up to 3.5 with a SRF of 6.865 GHz for a single loop meander inductor.[119] Viala et al. demonstrated inductors fabricated on silicon

substrate with SRF at 10GHz, and has also demonstrated increase in inductance using magnetic material.[120] However, the inductance value is low and the fabrication method is DC magnetron sputtering which is more costly than the proposed inkjet printing method. Furthermore, preliminary simulations have shown higher Q of close to 30 using silver nanoparticles on paper substrate compared to the Q of 10 as the author has demonstrated. Zhang et al. has shown an inductor directly fabricated on ferrite substrate.[121] The inductor showed improvement of inductance from 16nH to 80nH at 1MHz compared with coreless inductors, and the increment of inductance is larger than the magnetic thin-film inductor. However, the frequency of operation is at 1MHz and is not applicable for RF inductors.

5.3 Magnetic Nanomaterial

RF magnetic material has many useful applications in high frequency devices such as RF inductors and antennas due to the permeability value of the magnetic material. The higher permeability value helps to increase the inductance of inductors and lower the resonance frequency of antennas, effectively reducing the size of antennas. However, magnetic material has a fundamental limitation called Snoek's limit[122], which states that higher permeable magnetic material have a lower cutoff frequency than lower permeable magnetic material. However, recent studies have shown new magnetic material that has been developed for high frequency applications.[123,124,125,126,127] For example, cobalt magnetic nanocomposites[128,129] have shown permeability value of 2 and permittivity value of 7 up to 1GHz. The studies indicate that the increased inductance is due to the interparticle exchange coupling effect. The exchange interaction, which leads to magnetic ordering within a grain, extends out to the neighboring environments within a characteristic distance, l_{ex}. For Fe or Co, l_{ex} is 30 nm.[130] The exchange interaction in nanocomposites also leads to the cancellation of magnetic anisotropy of individual particles and the demagnetizing effect, leading to reduced remanent fields.[131]

Remanence or remanent magnetization is the magnetization left behind in a magnetic material (such as iron) after an external magnetic field is removed.

Magnetic nanoparticles commonly consist of magnetic elements such as iron, nickel, and cobalt and their chemical compounds. While nanoparticles are smaller than 1 micrometer in diameter (typically 5–500 nanometers). Of the different kinds of magnetic nanoparticles that are being produced and used, ferrite nanoparticles are the most explored up to date. Once the magnetic particles become smaller than 128 nm[132] they become superparamagnetic which prevents self-agglomeration since they exhibit their magnetic behavior only when an external magnetic field is applied. With the external magnetic field switched off, the remanence falls back to zero. Just like non-magnetic oxide nanoparticles, the surface of ferrite nanoparticles is often modified by surfactants, silicones or phosphoric acid derivatives to increase their stability in solution.[133,134]

Table 5. Different types of magnetic material and their susceptibility.

Class	Structure on atomic scale	Magnitude of χ
Diamagnetic	Atoms have no permanent dipole moments	~ -10^{-6} to -10^{-5}
Paramagnetic	Atoms have permanent dipole moments. Neighboring moments do not interact.	~ 10^{-5} to 10^{-3}
Ferromagnetic	Atoms have permanent dipole moments. Interaction produces ↑↑ alignment.	Large
Antiferromagnetic	Atoms have permanent dipole moments. Interaction produces ↑↓ alignment.	~ 10^{-5} to 10^{-3}
Ferrimagnetic	Atoms have permanent dipole moments. Interaction produces ↑↓ alignment, but moments are unequal.	Large

Adapted from [135]

As shown in Table 5, ferromagnetism (including ferrimagnetism) is the strongest type. A substance is said to be ferromagnetic when it possesses a spontaneous magnetic moment

in the absence of any applied magnetic field.[136] The benefits and potential applications of ferrites for microwave devices have been known for decades, but their application in thin-film form has been hampered due to complicated problems in processing them. [137] Defects in ferrite films, such as dislocations, cracks, voids, compositional inhomogeneity, impurities, strain, and vacancies will increase losses and degrade performance.

The magnetic nanomaterial used in this work is based on a commercially available fine oxide-passivated cobalt nanocluster synthesized via laser evaporation. The magnetic nanoparticles which are ~30 nm in diameter are first coated with a surfactant in a solvent medium and milled for 24 hrs in order to form a stable particulate suspension. Suitable amount of epoxy polymer was then added to maintain a metal-polymer ratio of 40:60 and milled for another 4 hours to form the nanoparticle ink. The polymer matrix AOT (Sodium Dioctylsulfosuccinate), in conjunction with the thin native oxide formed on the particles, prevents further oxidation during handling and is also demonstrated to make the printed magnetic material composite less brittle and of lower loss.[138]

The nanoparticle ink is formulated for the Dimatix DMP 2800 series of materials printers which requires that the viscosity be near 10-12 cP and the surface tension near 30 dynes/cm^2. Figure 70 shows a scanning electron microscope image of the polymer coated cobalt nano-clusters dispersed in an aqueous solution.

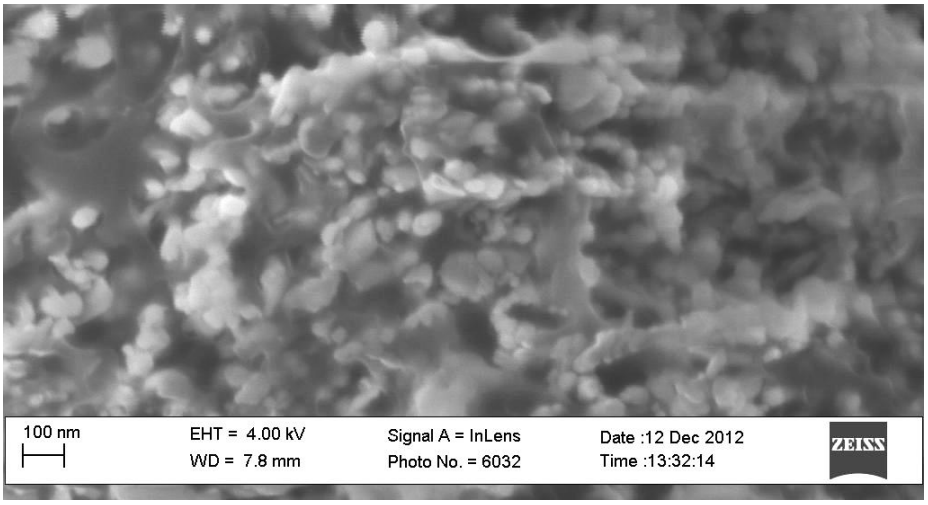

Figure 70. SEM picture of polymer coated cobalt nanomaterial in solution.

The material is characterized using an HP4291A impedance analyzer to obtain the complex permeability and permittivity over 200 MHz to 1 GHz. A mu sample holder is used to hold a bulk toroid shape of the magnetic nanomaterial to extract the permeability. An epsilon test head is used to hold a bulk slab of magnetic nanomaterial to extract the permittivity. The pictures of the equipment are shown in Figure 71Figure 72, and Figure 73.

Mu Sample Holder

Mu test head connected to system

Figure 71. Sample holder for characterization of permeability.

Epsilon test head

Eps test head close-up of connection area

Figure 72. Sample holder for characterization of permittivity.

Figure 73. Network analyzer used for characterization.

5.4 Inductor Design

Several designs for realizing printed inductors can be used such as meanders or spirals. Spiral inductors, while able to achieve a higher inductance than meander inductors, require the use of vias to connect to the inside of the spiral. Currently, inkjet-printed vias have high resistance and will drastically lower the Q of the inductors. For this reason, a CPW-based meander inductor is chosen for this work as shown in Figure 74.

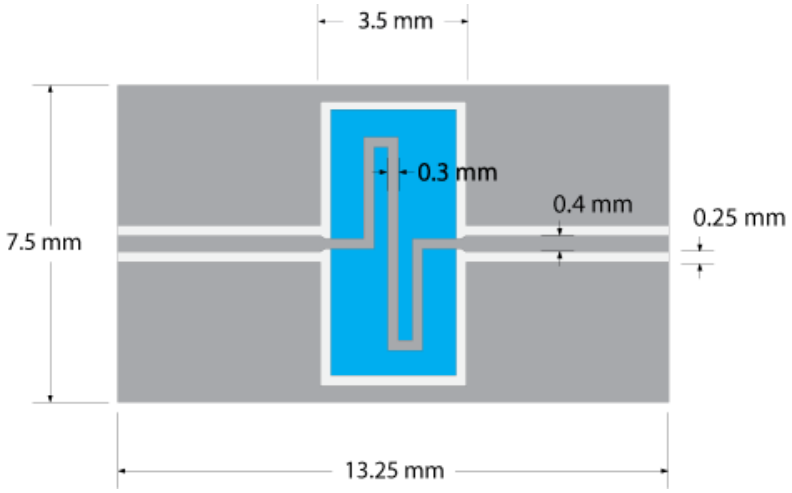

Figure 74. Layout of fabricated inductor.

A single turn was used to increase the SRF for RF applications and the width and spacing of the inductor was chosen to maximize the inductance within the limitation of the printing resolution. The inductors are designed for a commercially available photo paper substrate with thickness 220 um. The paper substrate has a permittivity of approximately 2.9 and a loss tangent of 0.06 below 10 GHz.[22]

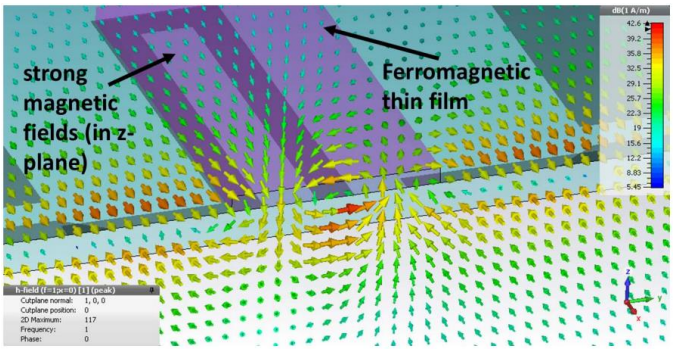

Figure 75. Magnetic field distribution seen from cross section simulated in CST.

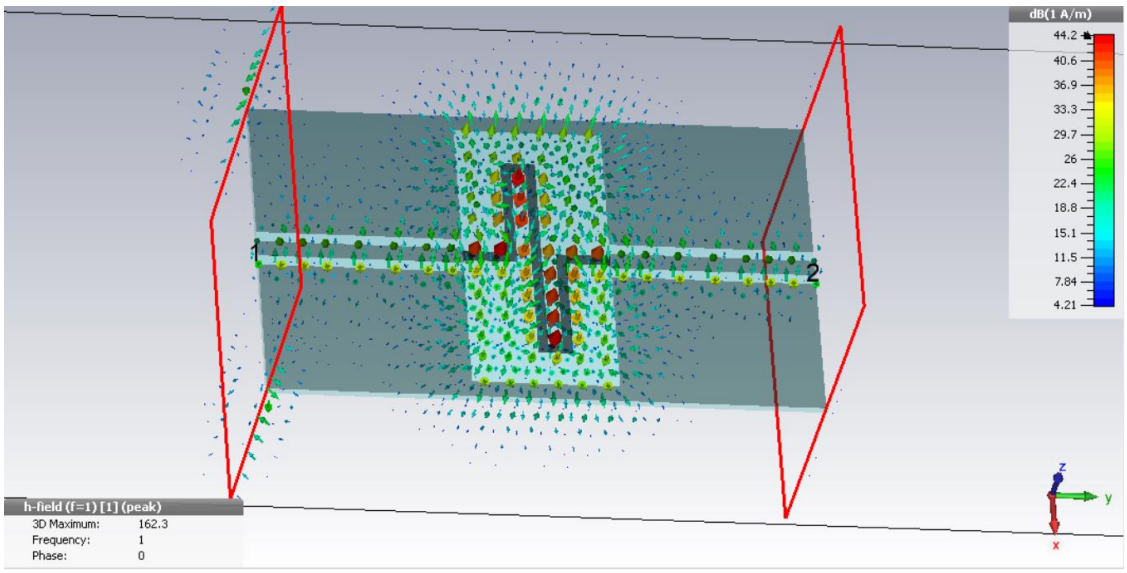

Figure 76. Magnetic field distribution when spacing is narrow in meandered inductor simulated in CST.

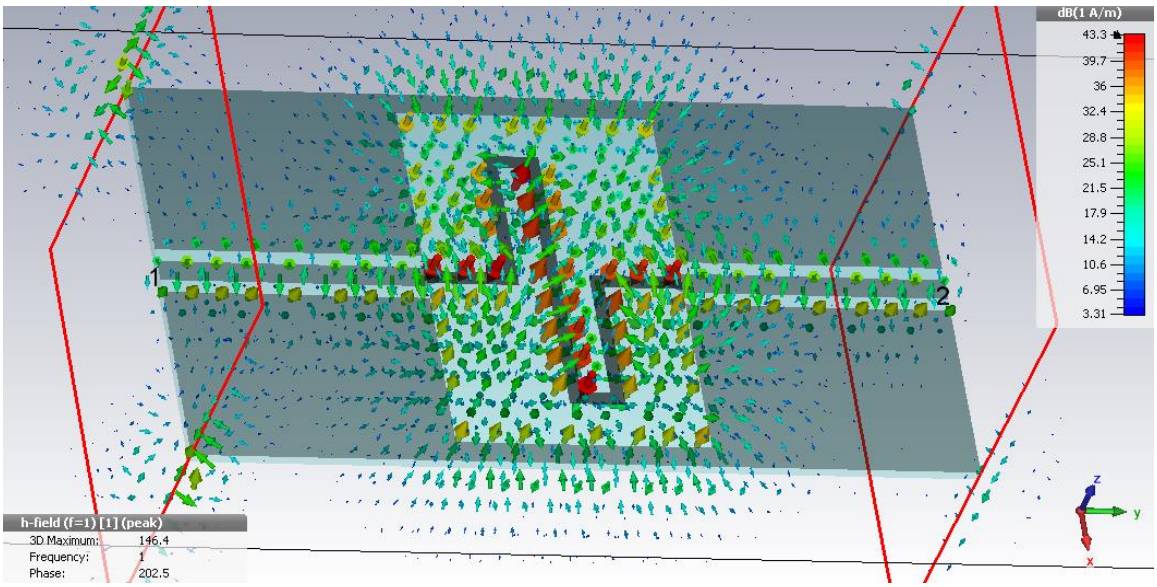

Figure 77. Magnetic field distribution when spacing is wider in meandered inductor simulated in CST.

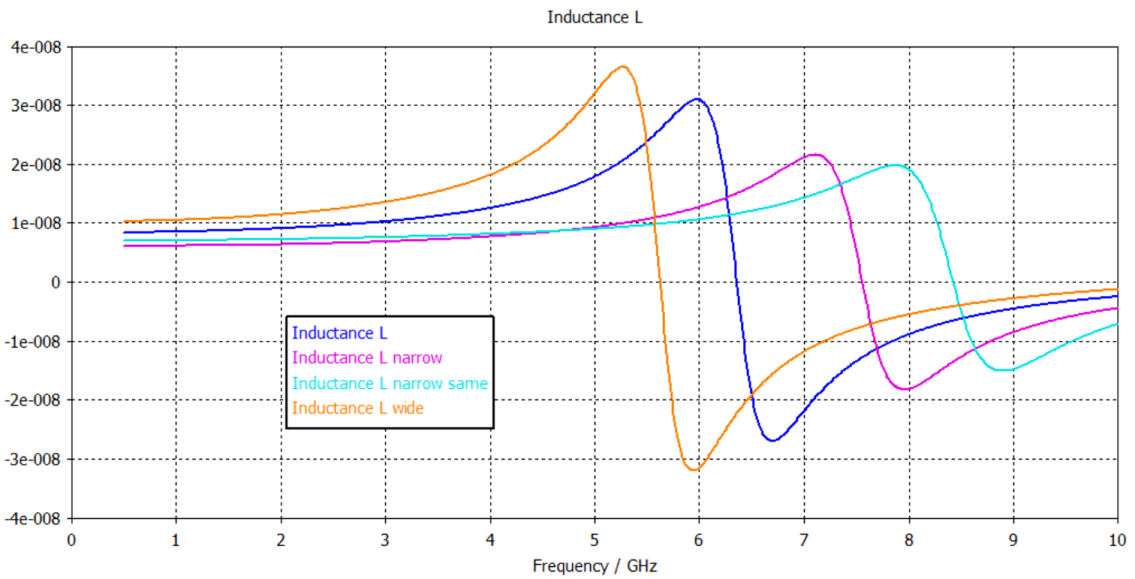

Figure 78. Inductance as spacing in inductor is varied.

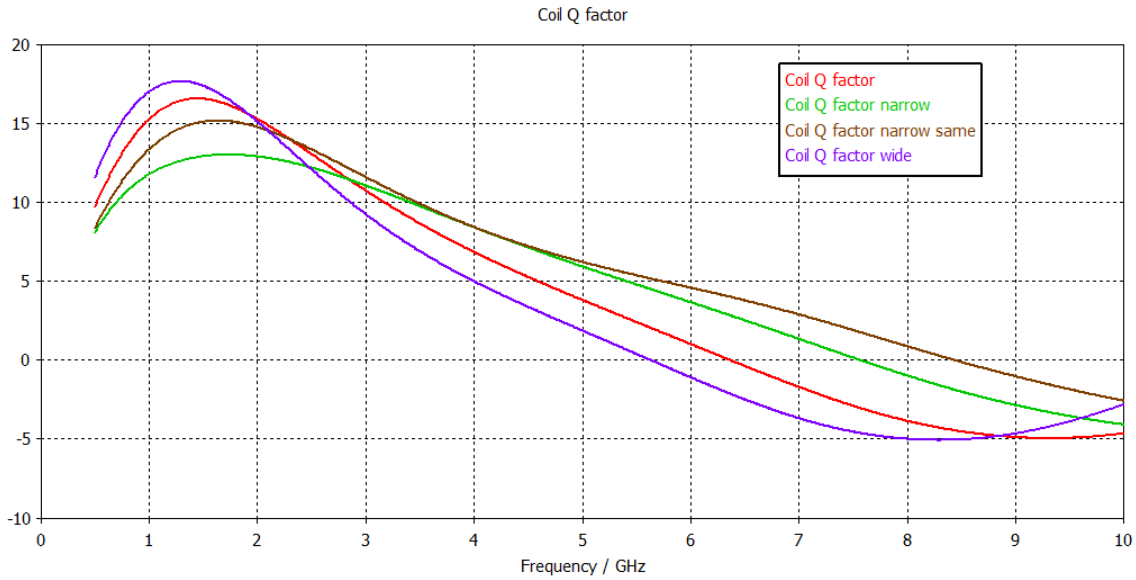

Figure 79. Quality factor as spacing in inductor is varied. Negative regions pertain to the inductor becoming capacitive as the frequency is greater than the self-resonance frequency.

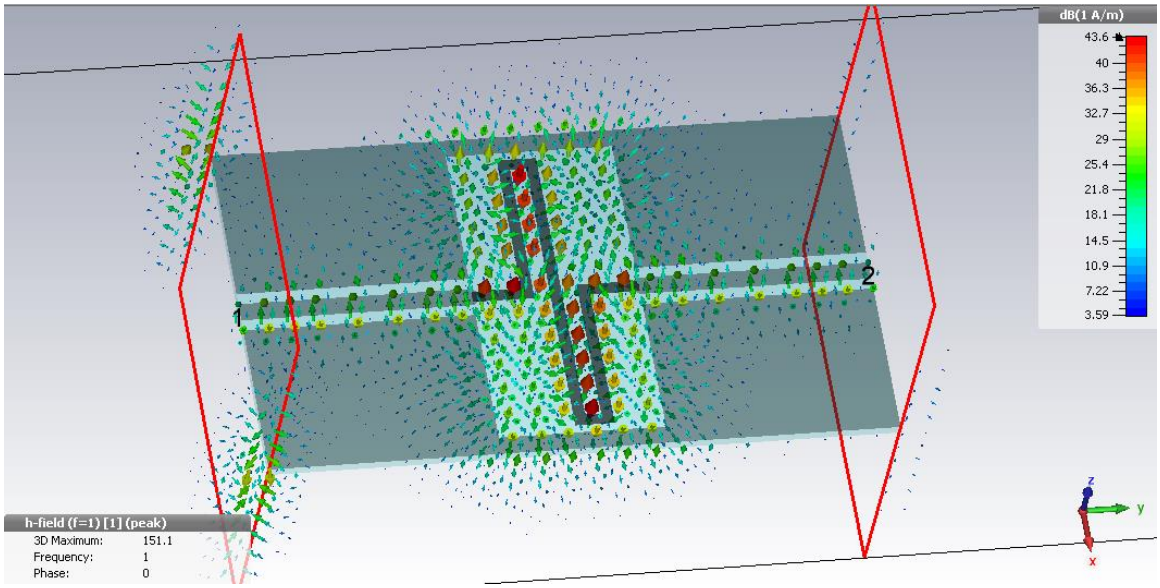

Figure 80. Magnetic field distribution when inductor height is lengthened in meandered inductor simulated in CST.

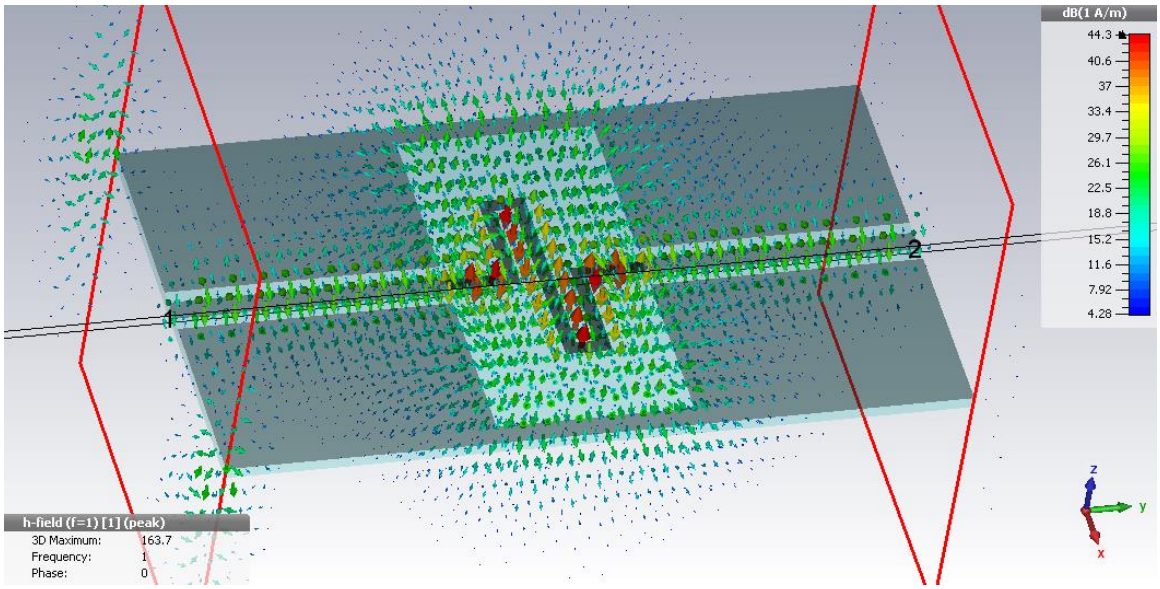

Figure 81. Magnetic field distribution when inductor height is shortened in meandered inductor simulated in CST.

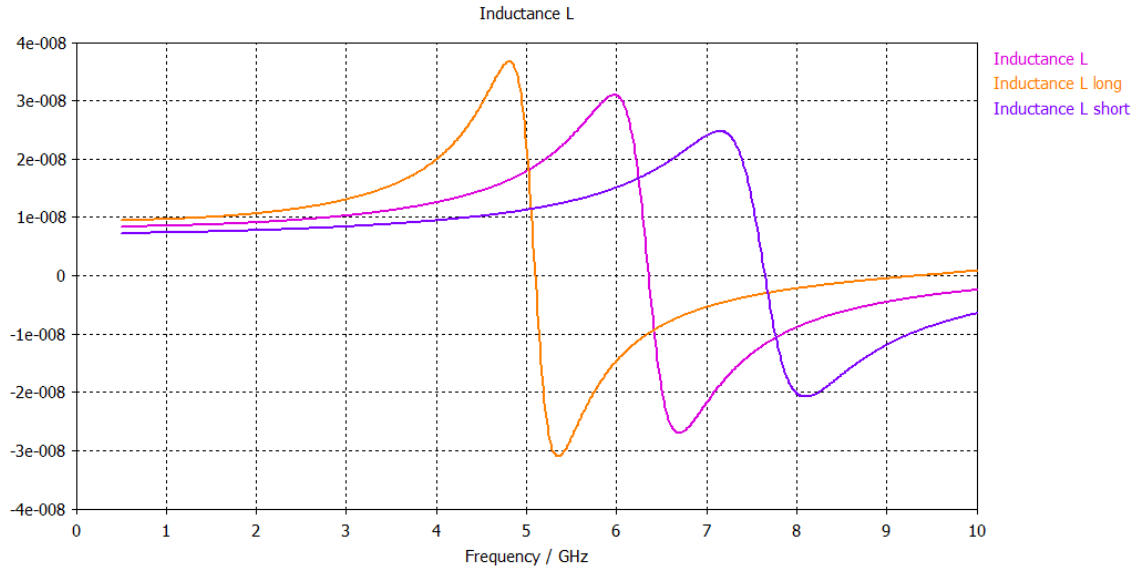

Figure 82. Inductance as height of inductor is varied.

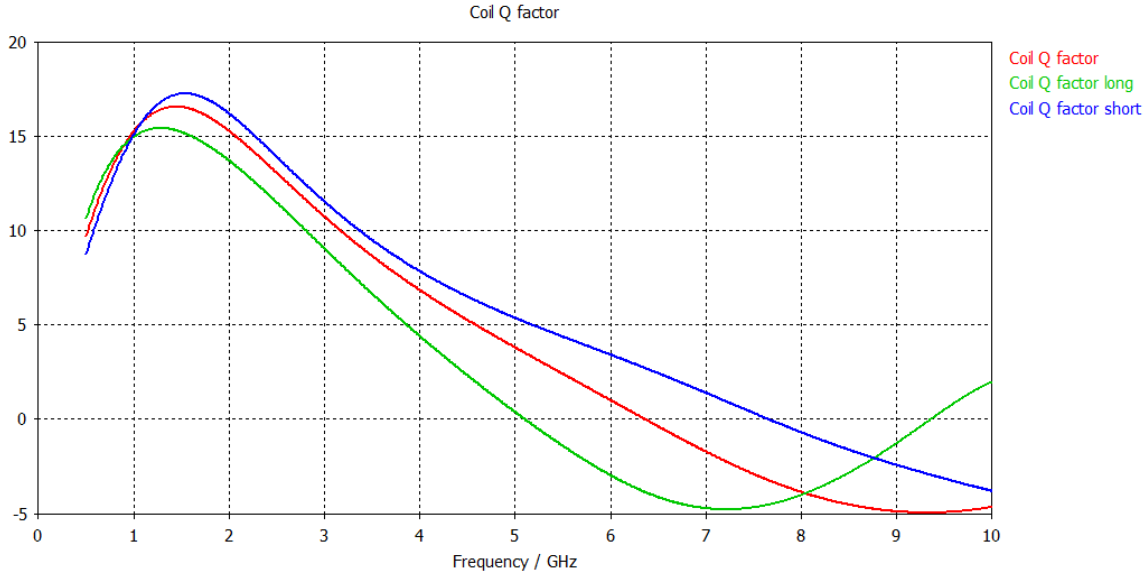

Figure 83. Quality factor as height of inductor is varied.

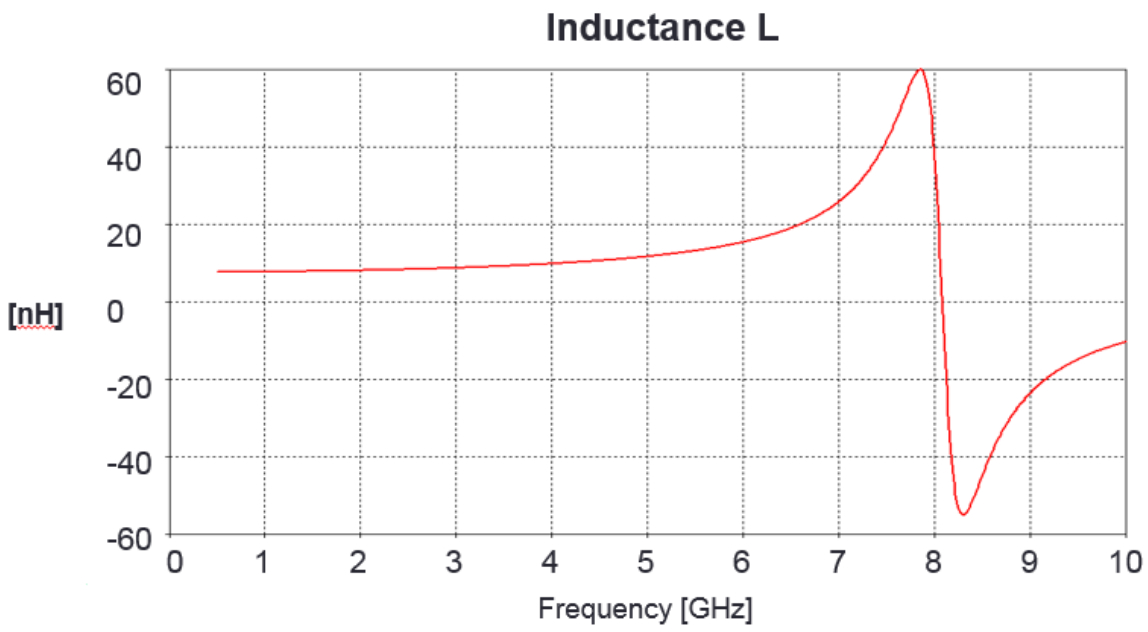

Figure 84. Optimized inductance of meandered inductor in CST.

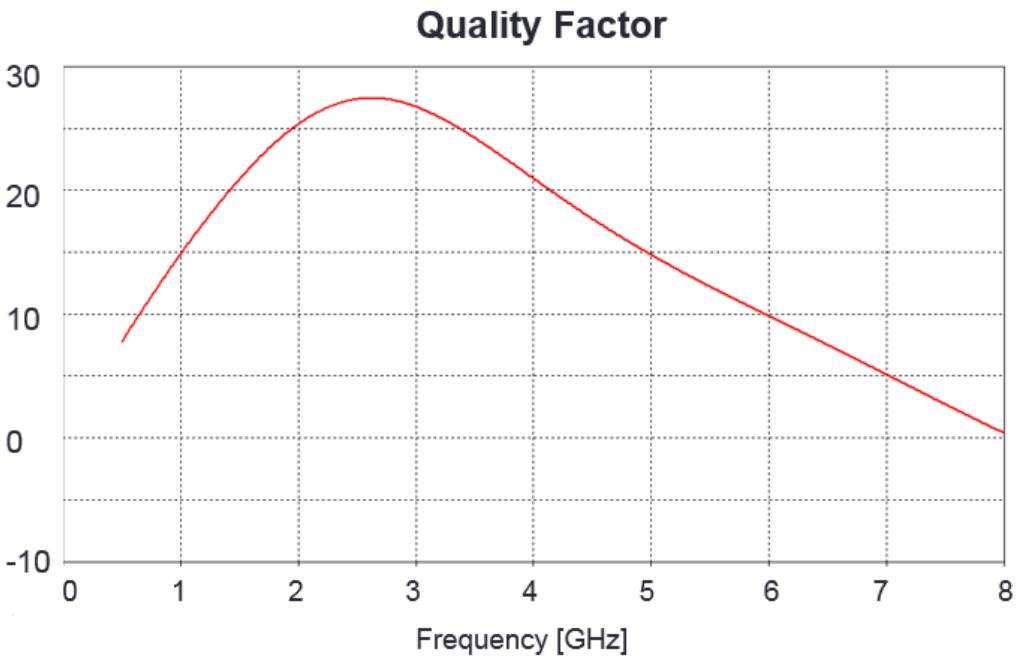

Figure 85. Optimized quality factor of meandered inductor in CST

5.5 Fabrication & Measurement

To fabricate the inductors, four layers of Cabot CCI-300 silver nanoparticle ink are printed onto the paper substrate and then cured in an oven at 150°C for one hour to sinter the nanoparticles. The magnetic nano-ink, sonicated for 1 hour before printing, is then printed on top of the inductor with 1, 3, 5, and 10 layers. Unlike the case with the carbon nanotubes, the cobalt nanoparticles are spherical in shape and were approximately 5um in diameter, which lead to a good jetting profile. The main fabrication challenge was preventing the magnetic nanoparticles from being oxidated during the curing process, despite the protection of the polymers. To prevent this oxidation during curing, the inductors were placed in a nitrogen oven at 150°C for one hour to cure the magnetic nanoparticles. Figure 86 shows a picture of the fabricated inductors. The area of the thin film over the inductor was maximized to maximize the increase of inductance.

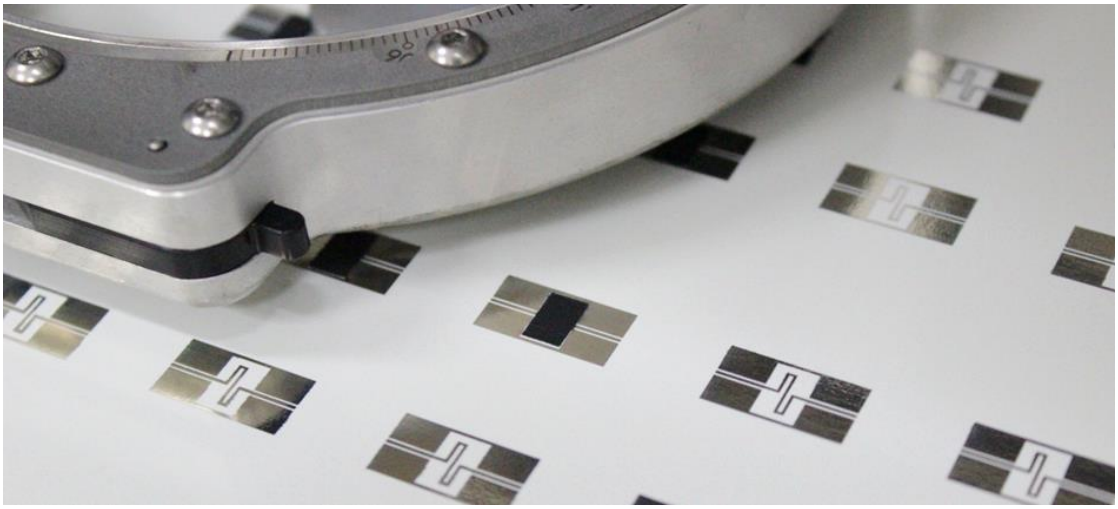

Figure 86. Fabricated inductor with and without the ferromagnetic material.

In the fabrication process, one important phenomena that can affect the uniformity of the surface of the printed thin film is the coffee stain effect.[139] When a drop of liquid dries on a solid surface, the composites are pushed to the edge of the drop circumference, creating a coffee stain-like shape, which would make the surface thicker at the edges. The

Dimatix Materials Printer has 16 nozzles and a subset of these nozzles is used to jet the drops of liquid simultaneously onto the substrate with a pre-defined spacing between the droplets. For high uniformity it is important to have an optimized overlap between the drops. There were some important factors that help reduce the coffee stain effect. First, the surface tension of the material and the substrate plays an important role of how easily the solute particles can be transported to the periphery of the drop. By optimizing these factors, the spread of the ink could be minimized, and the solute particles could be directly deposited onto the surface of the substrate. Secondly, the platen onto which the paper substrate is placed can be heated up to 60^{o}C. By heating up the substrate prior to deposition, the solvent in each picoliter droplet could be evaporated quickly upon contact, thus affecting the thermal and concentration gradients, that can interfere with the outward flow of the particles, thus mitigating the coffee stain effect. Thirdly, the acceleration of the droplets can be programmed in the Dimatix printer. Unlike a droplets that drops naturally onto the surface, an accelerated droplet makes contact with the surface with a higher force, which also helps to mitigate the natural outward flow of the particles to the periphery. Lastly, increasing the number of layers printed also increased surface roughness which also helps to decrease the spread of the particles.

Measurements are performed on a Cascade probe station, shown in Figure 87. To mitigate effects from the metal ground, the inductor was placed on top of a hard foam chuck. The measured S-Parameters are de-embedded using a printed TRL calibration kit which was subjected to the same processing conditions as the printed inductors. The de-embedded S-parameters are then used to extract the differential inductance and Q using the following equations.[8] The measured inductance and quality factor are shown in Figure 88,Figure 89Figure 90.

$$L_{diff} = \frac{\mathrm{Im}\left(\frac{4}{Y_{11}+Y_{22}-Y_{12}-Y_{21}}\right)}{\omega}$$ **Equation 2**

$$Q_{diff} = -\frac{\mathrm{Im}\left(Y_{11}+Y_{22}-Y_{12}-Y_{21}\right)}{\mathrm{Re}\left(Y_{11}+Y_{22}-Y_{12}-Y_{21}\right)}$$ **Equation 3**

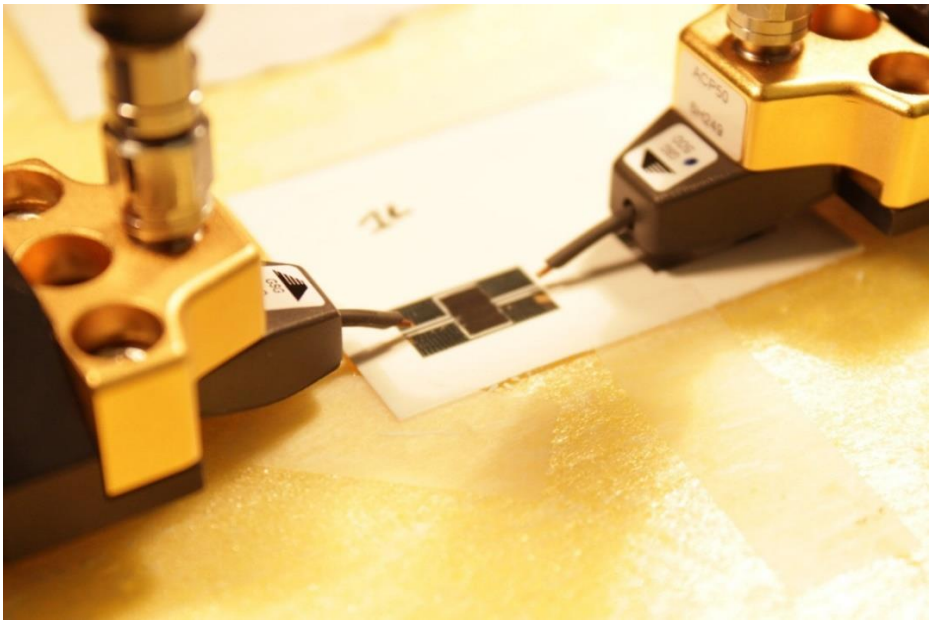

Figure 87. Measurement of inductor on cascade probe station.

Measurement Results

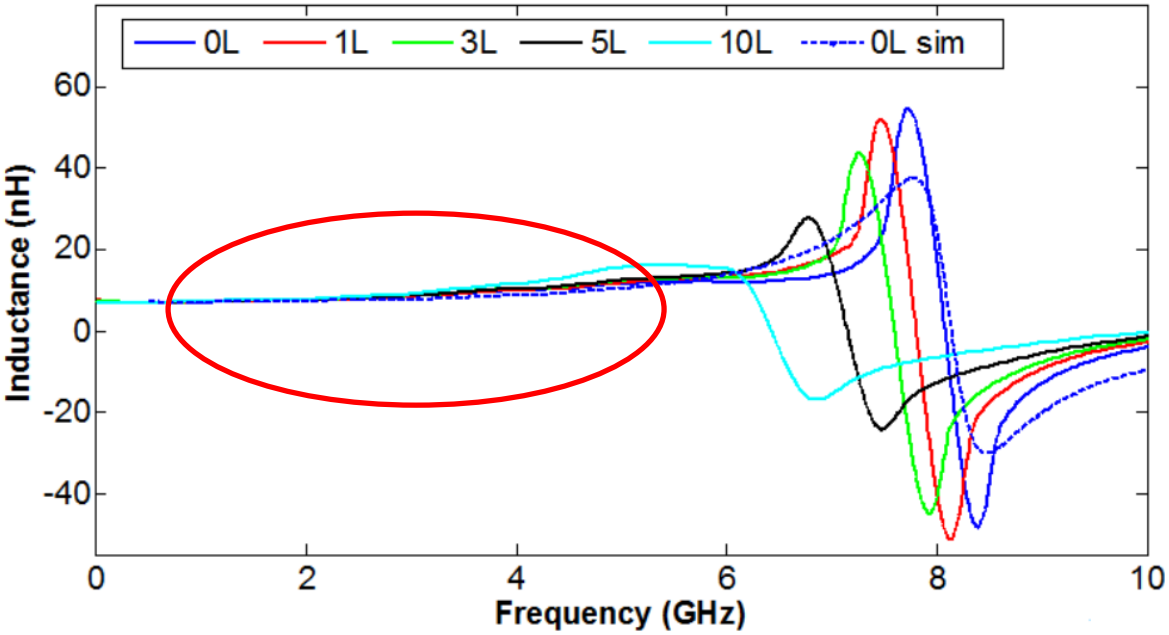

Figure 88. Measured inductance (top) magnification of inductance (bottom).

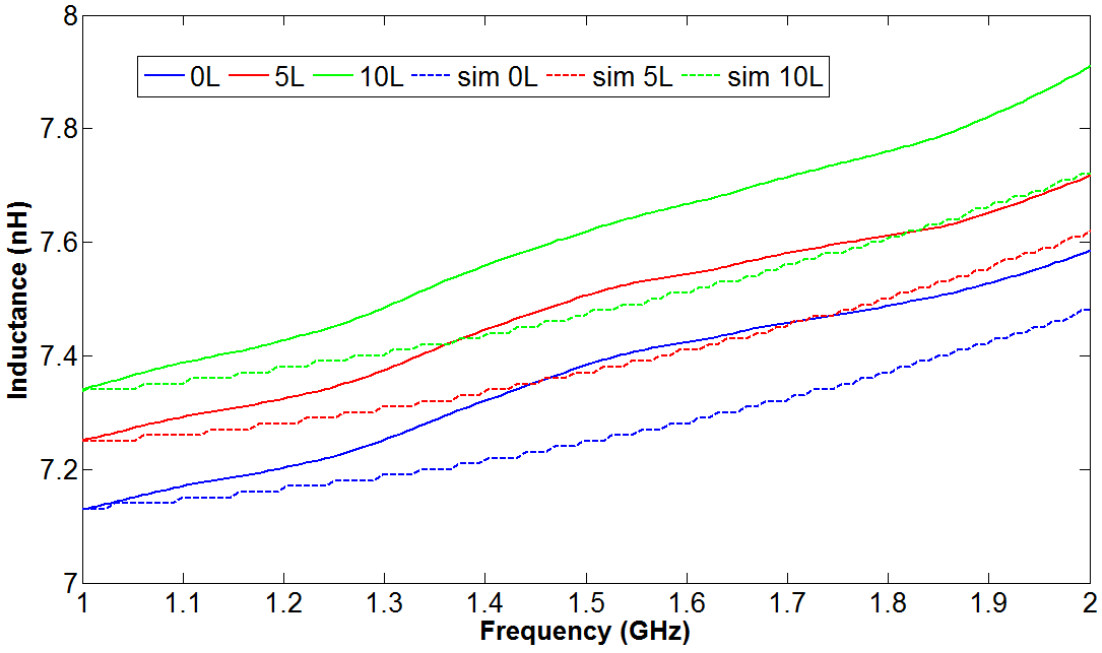

Figure 89. Measured inductance (magnified).

The measured inductance of the inductor topology without the magnetic nanomaterial has a value of 7.5nH and SRF of 8 GHz, which matches closely with the simulated

inductor shown in Figure 84. For measurements that included the magnetic thin film, the high permittivity of 7.3 and the permeability of 2.6 shifted the self resonance frequency down from 8GHz to 6.44GHz depending on the number of layers used. This downward shift in the SRF is due to the added capacitance from the high permittivity as well as the added inductance from the permeability. The effect of the permeability on the inductance value can be seen in Figure 89, in which added layers of magnetic thin film increased the inductance incrementally. The baseline is 0L which corresponds to no layers of magnetic thin film on the inductor.

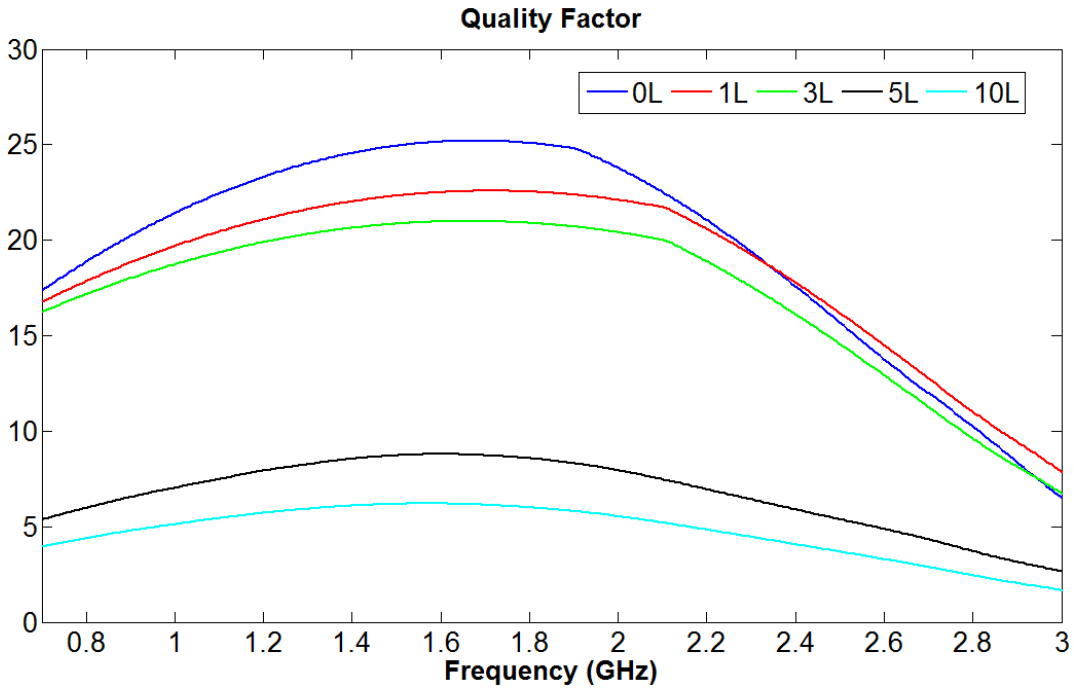

Figure 90. Measured quality factor.

The measured quality factor of the inductors shown in Figure 90 shows high Q values up to 25 without the printed magnetic nanomaterial. This is approximately 10 times higher than previous works for inkjet printed passives.[119] It can be noticed that as more layers of magnetic material are printed, the quality factor decreases. This is found to be caused by cracking of the silver traces when the solvent for the magnetic ink is absorbed by the paper, which causes the paper to expand. Conducting DC measurements across the inductor showed resistance of 2.9 to 3.1 ohms for 0, 1, and 3 layers respectively, and

from 10 ohms to 15 ohms for 5 and 10 layers. This effect can be mitigated in future work by printing a dielectric layer over the metallization as demonstrated in [140] to hinder solvent absorption into the paper substrate.

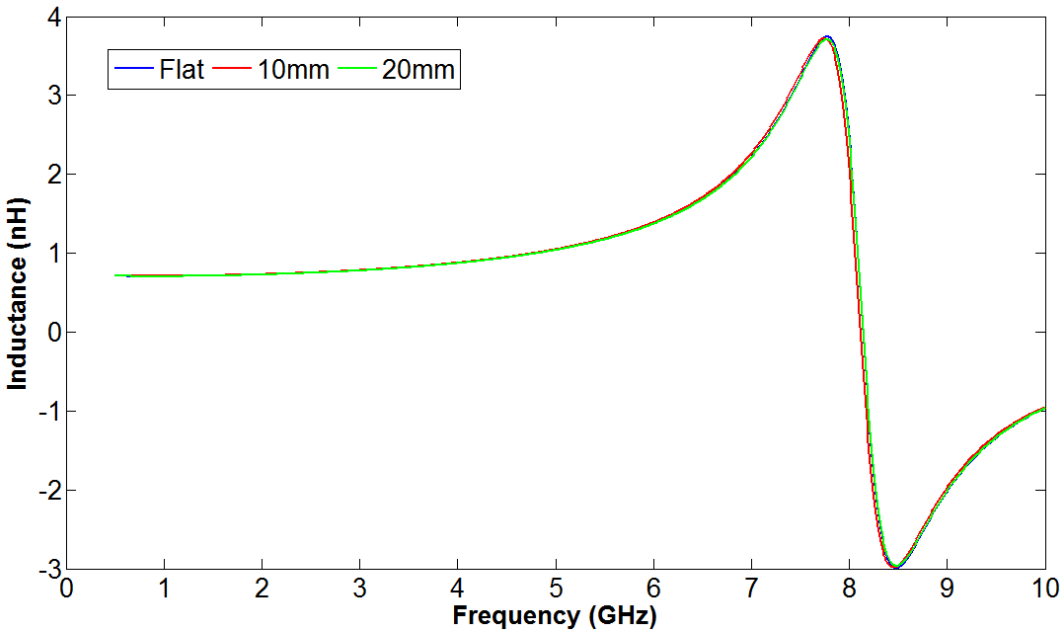

Figure 91. Simulated inductance for inductors flexed with varying radii.

To investigate the feasibility for flexible and wearable applications, further simulations were conducted, shown in

Figure 91, with the inductor curved around a cylinder of radii 10mm and 20mm. The inductance changed by 0.01nH and 0.03nH, the quality factor decreased by 1 and 2, and the SRF shifted by 3MHz and 25MHz for radii 20mm and 10mm, respectively. Since the change to inductance, Q, or SRF is minimal, this makes it possible for the inductor to be used in conformal applications such as inkjet-printed LC tanks for wearable biosensors.

5.6 Chapter Summary

High Q inkjet printed inductors utilizing magnetic nanomaterial are demonstrated for the first time. Maximum quality factors of 25 are obtained from measurement, which is the highest quality factor to date for inkjet printed passives. Increased inductance by 3-4% with increased number of layers of magnetic nanomaterial is observed which opens a path to future work in inkjet printed component miniaturization. Further steps to increase the quality factor by insulating the metallization from the magnetic ink solvent can be implemented to mitigate metallization cracking due to paper expansion. The promising results create new possibilities for inkjet-printed high-Q miniaturized flexible and wearable components operating above 5 GHz.

The impact of this work is to hopefully open the door to inkjet-printed integration of magnetic nanomaterial with RF modules for the following applications:

- Enable a cost-effective, vertical integration of controlled magnetic thin film deposition as another design parameter to control inductance value for printed electronics in the future.
- Create low-cost, flexible, inkjet-printed LC tanks for wearable bio-sensors utilizing the resonance shift of LC tanks.

5.7 Support

- This research was supported by Georgia Tech Packaging Research Center
    - Material support
    - Received cobalt-based magnetic nanomaterial
- This research was supported by Georgia Tech Research Institute
    - Received support for characterization of material
    - People who helped:
        - Kathleen G. Silver
    - Network analyzer and test heads for extracting characterization information

CHAPTER VI

CONTRIBUTIONS AND PUBLICATIONS TO DATE

This work has explored the systematic design and development of novel RF modules integrating nano-material that exhibit good performance characteristics on flexible substrates for conformal applications. There have been many contributions both to the academic and industry communities, mostly in helping better understand advantages and challenges brought by this technology. Perhaps the most substantial of these contributions are the following:

• The first inkjet-printed carbon nanotube-based wireless gas sensor on paper-based substrate

- Acknowledged by *International Symposium on Antennas and Propagation 2011* "Honorable Mention Award"

• First inkjet-printed AMC-backed flexible RFID

- Acknowledged by *IEEE International Microwave Symposium 2012*

"Finalist for Best Student Paper Award"

This work and other related research in my PhD has led to the following publications:

Book Chapter

- Rushi Vyas, Vasileios Lakafosis, **Hoseon Lee**, Sangkil Kim, Taoran Le,and Manos M. Tentzeris, "Powering and Integration Issues in Biomedical Telemetry," chapter contribution for 'Handbook of Biomedical Telemetry', Wiley-IEEE (in press)

Journal Publications

[1] **Hoseon Lee**, Benjamin S. Cook, Markondeya Raj, K. P. Murali, M. M. Tentzeris, "Inkjet Printed High-Q RF Inductors on Paper Substrate with Ferromagnetic Nanomaterial," submitted to IEEE Microwave and Wireless Components letters 2013

[2] Sangkil Kim, Yu-Jiun Ren, **Hoseon Lee**, Amin Rida, Symeon Nikolaou, and Manos M. Tentzeris, "Monopole Antenna with Inkjet Printed EBG Array on Paper Substrate for Wearable Applications," *IEEE Antennas and Wireless Propagation Letters*, 2012

[3] Rushi Vyas, Vasileios Lakafosis, **Hoseon Lee**, Anya Traille, George Shaker, Giulia Orrechini, Manos Tentzeris, "Inkjet Printed, Self-Powered, Wireless Sensors for Environmental, Gas and Authentication Based Sensing" S*pecial Anniversary Issue of IEEE Sensors*, 2011

[4] **Hoseon Lee**, George Shaker, Krishna Naishadham, Judy Song, Michael McKinley, Brent Wagner, Manos Tentzeris, "Carbon Nanotube Loaded Antenna-Based Ammonia Gas Sensor" *IEEE Transactions on Microwave Theory and Techniques*, 2011

[5] Vasileios Lakafosis, Anya Traille, **Hoseon Lee**, Edward Gebara, Manos Tentzeris, Gerald DeJean, Darko Kirovski, "RF Fingerprinting Physical Objects for Anti-counterfeiting Applications", *IEEE Transactions on Microwave Theory and Techniques,* 2011

[6] Vasileios Lakafosis, Anya Traille, **Hoseon Lee**, Giulia Orecchini, Edward Gebara, Manos Tentzeris, Joy Laskar, Gerald DeJean, Darko Kirovski, "An RFID system with enhanced hardware-enabled authentication and anti-counterfeiting capabilities", *IEEE MTT-S International*, 2010

Conference Publications

[1] **Hoseon Lee**, Manos Tentzeris, Yoshihiro Kawahara, Markondeya Pulugurtha, K. P. Murali, “Inkjet-Printed Ferromagnetic Nanoparticles for Miniaturization of Flexible Printed RF Inductors," *IEEE International Symposium on Antennas and Propagation, 2013.*

[2] **Hoseon Lee**, Sangkil Kim, Danilo de Donno, “A Novel “Universal” Inkjet-Printed EBG-Backed Flexible RFID for Rugged On-Body and Metal Mounted Applications,” *IEEE International Microwave Symposium 2012,* Finalist for Student Paper Competition

[3] A. Georgiadis, A. Collado, S. Kim, **Hoseon Lee**, M. M. Tentzeris, “UHF Solar Powered Active Oscillator Antenna on Low Cost Flexible Substrate for Wireless Identification Applications,” *IEEE International Microwave Symposium 2012*

[4] **Hoseon Lee**, G. Shaker, V. Lakafosis, R. Vyas, T. Thai, S. Kim, X. Yi, Y. Wang, M. Tentzeris, ”Antenna-based “Smart Skin” Sensors for Sustainable, Wireless Sensor Networks,” *2012 IEEE International Conference on Industrial Technology*, pp.1-4, 2012

[5] R. Vyas, V. Lakafosis, A. Traille, **Hoseon Lee**, E. Gebara, M. Marroncelli, M. Tentzeris, “Inkjet-Printed RFIDs for Wireless Sensing and Anti-counterfeiting,” *EuCAP 2012*

[6] George Shaker, **Hoseon Lee**, Safieddin Safavi-Naeini, Manos Tentzeris, "Printed Electronics for Next Generation Devices" *Loughborough Antennas & Propagation Conference*, 2011

[7] **Hoseon Lee**, George Shaker, Krishna Naishadham, Manos Tentzeris, “A Novel Highly Sensitive Antenna-Based “Smart Skin” Gas Sensor Utilizing Carbon Nanotubes and Inkjet Printing” accepted by *Antennas and Propagation Symposium*, 2011, Honorable Mention Award*

[8] Li Yang, Giulia Orecchini, George Shaker, **Hoseon Lee**, Manos Tentzeris, "Battery-free RFID-enabled wireless sensors", *IEEE MTT-S International*, 2010

[9] George Shaker, **Hoseon Lee**, Kate Duncan, Manos Tentzeris, "Integrated antenna with inkjet-printed compact artificial magnetic surface for UHF applications" *IEEE International Conference Wireless Information Technology and Systems (ICWITS)*, 2010

References

[1] Reuben Lee, "Samsung Shows Off Flexible Display Phones at Ces Keynote," *CNET*(2013), http://asia.cnet.com/samsung-shows-off-flexible-display-phones-at-ces-keynote-62220087.htm.
[2] Donald Melanson, "Hp Flexible Display Unfurled on Video," (2010), http://www.engadget.com/2010/03/20/hp-flexible-display-unfurled-on-video/.
[3] David Pierce, Samsung Introduces 'World's First' Curved Oled Tv, (www.theverge.com: The Verge, 2013), http://www.theverge.com/2013/1/8/3851310/samsung-curved-oled-tv.
[4] BCC Research, "Global Market for Sensors to Be Worth $91.5 Billion in 2016," (2011), http://www.bccresearch.com/pressroom/report/code/IAS006D.
[5] "Sensors Worth $91.5b in 2016; Bio/Chemical Sensing Tops Growth," (2011), http://www.electroiq.com/articles/stm/2011/05/sensors-worth-91b-in-2016-bio-chemical-sensing-tops-growth.html.
[6] "Global Biosensors Market Is Expected to Reach Usd 18.9 Billion in 2018 - Transparency Market Research," *PR Web*(2013), http://www.prweb.com/releases/2013/7/prweb10923056.htm.
[7] "Whms - Wearable Health Monitoring Systems," (2006), http://www.ece.uah.edu/~jovanov/whrms/.
[8] "What Is Eeg Signal," (2012), http://zavidparvez.blogspot.com/2012/09/medical-signal-processing-especially.html.
[9] "Peripheral Artery Disease in-Depth Report ", http://health.nytimes.com/health/guides/disease/arteriosclerosis-of-the-extremities/print.html.
[10] "Rae Systems Delivers Industry's First Integrated Wireless Solution for Portable Gas Monitors," (2011), http://www.raesystems.fr/press-room/news-releases/201108/rae-systems-delivers-industry-s-first-integrated-wireless-solution-.
[11] "Attacking Ied Networks," (2011), http://www.army.mil/article/49978/.
[12] "Bw Technologies by Honeywell - Portable Gas Detectors," http://www.pksafety.com/bw-technologies-by-honeywell-portable-gas-detectors.html.
[13] H. Lee et al., "A Novel Highly-Sensitive Antenna-Based “Smart Skin” Gas Sensor Utilizing Carbon Nanotubes and Inkjet Printing" (paper presented at the Antennas and Propagation (APSURSI), 2011 IEEE International Symposium on, 3-8 July 2011 2011).
[14] A. Mehdipour et al., "Advanced Conductive Carbon Fiber Composite Materials for Antenna and Microwave Applications" (paper presented at the Antennas and Propagation Society International Symposium (APSURSI), 2012 IEEE, 8-14 July 2012 2012).
[15] "Wireless Sensor Network (Wsn)," (2010), http://embedsoftdev.com/embedded/wireless-sensor-network-wsn/.
[16] "First Printed Electronics Seminar at the Cetemmsa Facilities in Mataró (Barcelona)," *packaging europe*(2012), http://www.packagingeurope.com/Packaging-Europe-

News/48558/First-printed-electronics-seminar-at-the-CETEMMSA-facilities-in-Matar-Barcelona.html.

[17] "Bemis Selects Thin Film Electronics to Develop Intelligent Packaging Platform," (2012), http://www.thinfilm.no/news/bemis-selects-thin-film-electronics-to-develop-intelligent-packaging-platform/.

[18] "Pe8xx Series Delivers 20 Percent or More Savings Vs. Conventional Silver-Based Conductors," *DuPont Microcircuit Materials*(2012), http://www2.dupont.com/MCM/en_US/news_events/article20121130.html.

[19] "Bend Me, Shape Me: Flexible Phones 'out by 2013'," *BBC News Technology*(2012), http://www.bbc.co.uk/news/technology-20526577.

[20] Jeff Kelly, "Radio Frequency Identification (Rfid) for Birds," *Radar Aeroecology*, http://www.animalmigration.org/RFID/index.htm.

[21] "Dimatix Materials Printer Dmp-2831," http://www.fujifilmusa.com/products/industrial_inkjet_printheads/deposition-products/dmp-2800/index.html.

[22] R. Vyas et al., "Paper-Based Rfid-Enabled Wireless Platforms for Sensing Applications," *Microwave Theory and Techniques, IEEE Transactions on* 57, no. 5 (2009).

[23] Amin Rida Li Yang, Rushi Vyas, Vasileios Lakafosis, Giulia Orecchini, "Inkjet-Printing Technology - Printer," http://www.athena-gatech.org/research/PRINTED%20ELECTRONICS/.

[24] Ying Ying Lim, Yee Mey Goh, and Changqing Liu, "Surface Treatments for Inkjet Printing onto a Ptfe-Based Substrate for High Frequency Applications," *Industrial & Engineering Chemistry Research* 52, no. 33 (2013).

[25] Yu-Feng Liu et al., "Low Temperature Fabricated Conductive Lines on Flexible Substrate by Inkjet Printing," *Microelectronics Reliability* 52, no. 2 (2012).

[26] Unnat S. Bhansali, M. A. Khan, and H. N. Alshareef, "Organic Ferroelectric Memory Devices with Inkjet-Printed Polymer Electrodes on Flexible Substrates," *Microelectronic Engineering* 105, no. 0 (2013).

[27] Lim, Goh, and Liu, "Surface Treatments for Inkjet Printing onto a Ptfe-Based Substrate for High Frequency Applications."

[28] B. K. Lok et al., "Effect of Plasma Treated Ito Substrate on Inkjet Printing of Conductive Ink" (paper presented at the Electronics Packaging Technology Conference, 2006. EPTC '06. 8th, 6-8 Dec. 2006 2006).

[29] Lisa Whitaker, "Rotary Printing," *Commercial print*(2011), http://l-whitaker1013-dc.blogspot.com/2011/10/commercial-print.html.

[30] Rushi Vyas Manos M Tentzeris, Vasileios Lakafosis, Taoran Le, Amin Rida, Sangkil Kim, "Conformal 2d/3d Wireless Modules Utilizing Inkjet Printing and Nanotechnology," *Microwave Journal* 55, no. 2 (2012).

[31] G. Shaker et al., "Inkjet Printing of Ultrawideband (Uwb) Antennas on Paper-Based Substrates," *Antennas and Wireless Propagation Letters, IEEE* 10(2011).

[32] Manos M Tentzeris, "Uwb Antennas on Flexible Organic Substrates," http://www.athena-gatech.org/research/COMPLETED%20RESEARCH/index.html.

[33] Jing Kong et al., "Nanotube Molecular Wires as Chemical Sensors," *Science* 287, no. 5453 (2000).

[34] Philip G. Collins et al., "Extreme Oxygen Sensitivity of Electronic Properties of Carbon Nanotubes," ibid., no. 5459.
[35] Akihiko Fujiwara et al., "Gas Adsorption in the inside and Outside of Single-Walled Carbon Nanotubes," *Chemical Physics Letters* 336, no. 3 (2001).
[36] C. Marliere et al., "Effect of Gas Adsorption on the Electrical Properties of Single-Walled Carbon Nanotubes Mats" (1999).
[37] Varghese O.K.; Kichambre P.D.; Gong D.; Ong K.G.; Dickey E.C.; Grimes C.A., "Gas Sensing Characteristics of Multi-Wall Carbon Nanotubes," *Sensors and Actuators B: Chemical* 81, no. 1 (2001).
[38] B. Zhao, H. Hu, and R. C Haddon, "Synthesis and Properties of a Water-Soluble Single-Walled Carbon Nanotube–Poly(M-Aminobenzene Sulfonic Acid) Graft Copolymer," *Advanced Functional Materials* 14, no. 1 (2004).
[39] Ting Zhang et al., "Poly (M-Aminobenzene Sulfonic Acid) Functionalized Single-Walled Carbon Nanotubes Based Gas Sensor," *Nanotechnology* 18, no. 16 (2007).
[40] Ya-Ping Sun et al., "Functionalized Carbon Nanotubes: Properties and Applications," *Accounts of Chemical Research* 35, no. 12 (2002).
[41] Elena Bekyarova et al., "Mechanism of Ammonia Detection by Chemically Functionalized Single-Walled Carbon Nanotubes: In Situ Electrical and Optical Study of Gas Analyte Detection," *Journal of the American Chemical Society* 129, no. 35 (2007).
[42] "Super-Sensitive and Small: New Mit Detector Uses Nanotubes to Sense Deadly Gases," MIT Press Release, http://web.mit.edu/newsoffice/2008/nanotube-0605.html.
[43] A. Pham, "Carbon Nanotube Resonator Sensors for Remote Sensing Systems" (paper presented at the Wireless Communication Technology, 2003. IEEE Topical Conference on, 15-17 Oct. 2003 2003).
[44] Eduardo Gracia-Espino et al., "Electrical Transport and Field-Effect Transistors Using Inkjet-Printed Swcnt Films Having Different Functional Side Groups," *ACS nano* 4, no. 6 (2010).
[45] Hyoungki Park, Jijun Zhao, and Jian Ping Lu, "Effects of Sidewall Functionalization on Conducting Properties of Single Wall Carbon Nanotubes," *Nano Letters* 6, no. 5 (2006).
[46] Hong-Zhang Geng et al., "Effect of Acid Treatment on Carbon Nanotube-Based Flexible Transparent Conducting Films," *Journal of the American Chemical Society* 129, no. 25 (2007).
[47] Takao Someya et al., "Alcohol Vapor Sensors Based on Single-Walled Carbon Nanotube Field Effect Transistors," *Nano Letters* 3, no. 7 (2003).
[48] S. Chopra et al., "Carbon-Nanotube-Based Resonant-Circuit Sensor for Ammonia," *Applied Physics Letters* 80, no. 24 (2002).
[49] K. G. Ong, Kefeng Zeng, and Craig A. Grimes, "A Wireless, Passive Carbon Nanotube-Based Gas Sensor," *Sensors Journal, IEEE* 2, no. 2 (2002).
[50] M. Dragoman et al., "Experimental Determination of Microwave Attenuation and Electrical Permittivity of Double-Walled Carbon Nanotubes," *Applied physics letters* 88, no. 15 (2006).
[51] K. Grenier M. Dragoman, D. Dubuc, L. Bary, E. Fourn , R. Plana, and E. Flahaut, "The Experimental Determination of Microwave Attenuation and Electrical Permittivity of Double Walled Carbon Nanotubes," *Appl. Phys. Letter* 88(2006).

[52] R. Zhang L. Yang, D. Staiculescu, C.P. Wong, M.M. Tentzeris, "A Novel Conformal Rfid-Enabled Module Utilizing Inkjet-Printed Antennas and Carbon Nanotubes for Gas Detection Applications," *IEEE Antennas Wireless Propagat. Lett.* 8(2009).
[53] H. Lee et al., "A Novel Highly-Sensitive Antenna-Based "Smart Skin" Gas Sensor Utilizing Carbon Nanotubes and Inkjet Printing" (paper presented at the Antennas and Propagation (APSURSI), 2011 IEEE International Symposium on, 3-8 July 2011 2011).
[54] Zhou Yijun et al., "Polymer-Carbon Nanotube Sheets for Conformal Load Bearing Antennas," *Antennas and Propagation, IEEE Transactions on* 58, no. 7 (2010).
[55] Ong, Zeng, and Grimes, "A Wireless, Passive Carbon Nanotube-Based Gas Sensor."
[56] Sanghun Kim et al., "Effects of Polymer Coating on the Adsorption of Gas Molecules on Carbon Nanotube Networks," *Applied Physics Letters* 91, no. 9 (2007).
[57] Yang Li et al., "A Novel Conformal Rfid-Enabled Module Utilizing Inkjet-Printed Antennas and Carbon Nanotubes for Gas-Detection Applications," *Antennas and Wireless Propagation Letters, IEEE* 8(2009).
[58] S Dag S Ciraci, T Yildirim, O Gülseren, R T Senger, "Functionalized Carbon Nanotubes and Device Applications," *Journal of Physics: Condensed Matter* 16, no. 29 (2004).
[59] Elena Bekyarova et al., "Electronic Properties of Single-Walled Carbon Nanotube Networks," *Journal of the American Chemical Society* 127, no. 16 (2005).
[60] Yang Li et al., "Rfid Tag and Rf Structures on a Paper Substrate Using Inkjet-Printing Technology," *Microwave Theory and Techniques, IEEE Transactions on* 55, no. 12 (2007).
[61] G. Shaker et al., "Integrated Antenna with Inkjet-Printed Compact Artificial Magnetic Surface for Uhf Applications" (paper presented at the Wireless Information Technology and Systems (ICWITS), 2010 IEEE International Conference on, Aug. 28 2010-Sept. 3 2010 2010).
[62] Vivek Subramanian et al., "Printed Organic Transistors for Ultra-Low-Cost Rfid Applications," *Components and Packaging Technologies, IEEE Transactions on* 28, no. 4 (2005).
[63] G. Shaker, M. Tentzeris, and Safieddin Safavi-Naeini, "Low-Cost Antennas for Mm-Wave Sensing Applications Using Inkjet Printing of Silver Nano-Particles on Liquid Crystal Polymers" (paper presented at the Antennas and Propagation Society International Symposium (APSURSI), 2010 IEEE, 11-17 July 2010 2010).
[64] J H Choi Seong Chan Jun, S N Cha, C W Baik, Sanghyo Lee, H Jin Kim, James Hone, and J M Kim, "Radio-Frequency Transmission Characteristics of a Multi-Walled Carbon Nanotube," *Nanotechnology* 18, no. 25 (2007).
[65] Cattien V Nguyen Lance Delzeit, Ramsey M Stevens, Jie Han, and M Meyyappan, "Growth of Carbon Nanotubes by Thermal and Plasma Chemical Vapour Deposition Processes and Applications in Microscopy," ibid.13, no. 3 (2002).
[66] J. Krupka et al., "Split Post Dielectric Resonator Technique for Precise Measurements of Laminar Dielectric Specimens-Measurement Uncertainties" (paper presented at the Microwaves, Radar and Wireless Communications. 2000. MIKON-2000. 13th International Conference on, 2000 2000).
[67] Shaker et al., "Inkjet Printing of Ultrawideband (Uwb) Antennas on Paper-Based Substrates."
[68] Ibid.

[69] Roger B. Marks, "A Multiline Method of Network Analyzer Calibration," *Microwave Theory and Techniques, IEEE Transactions on* 39, no. 7 (1991).
[70] Mario W. Cardullo. Transponder Apparatus and System. USA Patent 3713148, 1973.
[71] Bob Violino, "Genesis of the Versatile Rfid Tag," *RFID Journal*(2003), http://www.rfidjournal.com/articles/view?392.
[72] Jeremy Landt, "Shrouds of Time the History of Rfid," *AIM* (2001).
[73] Charles A. Walton. Portable Radio Frequency Emitting Identifier. USA Patent US4384288 A, 1983.
[74] "Radio-Frequency Identification," Wikipedia, http://en.wikipedia.org/wiki/Radio-frequency_identification.
[75] J. T. Prothro, G. D. Durgin, and J. D. Griffin, "The Effects of a Metal Ground Plane on Rfid Tag Antennas" (paper presented at the Antennas and Propagation Society International Symposium 2006, IEEE, 9-14 July 2006 2006).
[76] Mo Lingfei and Zhang Hongjian, "Rfid Antenna near the Surface of Metal" (paper presented at the Microwave, Antenna, Propagation and EMC Technologies for Wireless Communications, 2007 International Symposium on, 16-17 Aug. 2007 2007).
[77] J. E. Ruyle, "Investigation on Placement Sensitivity of Meandered Dipole Performance for Rfid Systems" (paper presented at the Antennas and Propagation Society International Symposium (APSURSI), 2012 IEEE, 8-14 July 2012 2012).
[78] Jennifer T. Bernhard et al., "Small, Dual Band, Placement Insensitive Antennas," (2012).
[79] Chen Min et al., "A 2g-Rfid-Based E-Healthcare System," *Wireless Communications, IEEE* 17, no. 1 (2010).
[80] Li Cheng-Ju et al., "Mobile Healthcare Service System Using Rfid" (paper presented at the Networking, Sensing and Control, 2004 IEEE International Conference on, 2004 2004).
[81] Chen Sung-Lin, "A Miniature Rfid Tag Antenna Design for Metallic Objects Application," *Antennas and Wireless Propagation Letters, IEEE* 8(2009).
[82] K. V. S. Rao, S. F. Lam, and P. V. Nikitin, "Wideband Metal Mount Uhf Rfid Tag" (paper presented at the Antennas and Propagation Society International Symposium, 2008. AP-S 2008. IEEE, 5-11 July 2008 2008).
[83] Gao Bo et al., "Low Cost Passive Uhf Rfid Packaging with Electromagnetic Band Gap (Ebg) Substrate for Metal Objects" (paper presented at the Electronic Components and Technology Conference, 2007. ECTC '07. Proceedings. 57th, May 29 2007-June 1 2007 2007).
[84] Chen Sung-Lin and Lin Ken-Huang, "A Slim Rfid Tag Antenna Design for Metallic Object Applications," *Antennas and Wireless Propagation Letters, IEEE* 7(2008).
[85] Dong-Uk Sim et al., "Design of Novel Dipole-Type Tag Antennas Using Electromagnetic Bandgap (Ebg) Surface for Passive Rfid Applications" (2007).
[86] Yang Li et al., "Wearable Rfid-Enabled Sensor Nodes for Biomedical Applications" (paper presented at the Electronic Components and Technology Conference, 2008. ECTC 2008. 58th, 27-30 May 2008 2008).
[87] Shaker et al., "Integrated Antenna with Inkjet-Printed Compact Artificial Magnetic Surface for Uhf Applications."
[88] Li et al., "Rfid Tag and Rf Structures on a Paper Substrate Using Inkjet-Printing Technology."

[89] Cecilia Occhiuzzi, Stefano Cippitelli, and Gaetano Marrocco, "Modeling, Design and Experimentation of Wearable Rfid Sensor Tag," *Antennas and Propagation, IEEE Transactions on* 58, no. 8 (2010).
[90] S. Manzari, S. Pettinari, and G. Marrocco, "Miniaturized and Tunable Wearable Rfid Tag for Body-Centric Applications" (2012).
[91] Jae Han Choi et al., "Various Wearable Embroidery Rfid Tag Antenna Using Electro-Thread" (2008).
[92] Elham Moradi, "Characterization of Embroidered Dipole-Type Rfid Tag Antennas," (2012).
[93] Tiiti Kellomaki, "On-Body Performance of a Wearable Single-Layer Rfid Tag," *Antennas and Wireless Propagation Letters, IEEE* 11(2012).
[94] Sari Merilampi et al., "Printed Passive Uhf Rfid Tags as Wearable Strain Sensors" (2010).
[95] K. Koski et al., "Practical Read Range Evaluation of Wearable Embroidered Uhf Rfid Tag" (paper presented at the Antennas and Propagation Society International Symposium (APSURSI), 2012 IEEE, 8-14 July 2012 2012).
[96] Sim et al., "Design of Novel Dipole-Type Tag Antennas Using Electromagnetic Bandgap (Ebg) Surface for Passive Rfid Applications."
[97] Hoseon Lee et al., "A Novel "Universal" Inkjet-Printed Ebg-Backed Flexible Rfid for Rugged on-Body and Metal Mounted Applications" (2012).
[98] L. Zhang D. Sievenpiper, R. F. J. Broas, N. G. Alexopoulos, and E. Yablonovich, "High-Impedance Electromagnetic Surfaces with Forbidden Frequency Band," *IEEE Transactions on Microwave Theory and Techniques* 47, no. 11 (1999).
[99] Daniel Frederic Sievenpiper, "High-Impedance Electromagnetic Surfaces" (University of California Los Angeles, 1999).
[100] V. Radonic, B. Jokanovic, and V. Crnojevic-Bengin, "Different Approaches to the Design of Metamaterials," *Microwave Review* 13, no. 2 (2007).
[101] J. R. Sohn et al., "Comparative Study on Various Artficial Magnetic Conductors for Low-Profile Antenna," *Progress In Electromagnetics Research* 61(2006).
[102] R. Marques et al., "Comparative Analysis of Edge- and Broadside- Coupled Split Ring Resonators for Metamaterial Design - Theory and Experiments," *Antennas and Propagation, IEEE Transactions on* 51, no. 10 (2003).
[103] Rao, Lam, and Nikitin, "Wideband Metal Mount Uhf Rfid Tag."
[104] Zhang Ying et al., "Planar Artificial Magnetic Conductors and Patch Antennas," *Antennas and Propagation, IEEE Transactions on* 51, no. 10 (2003).
[105] D. J. Kern et al., "The Design Synthesis of Multiband Artificial Magnetic Conductors Using High Impedance Frequency Selective Surfaces," ibid.53, no. 1 (2005).
[106] J. B. Pendry et al., "Magnetism from Conductors and Enhanced Nonlinear Phenomena," *Microwave Theory and Techniques, IEEE Transactions on* 47, no. 11 (1999).
[107] J. Garcia-Garcia et al., "On the Resonances and Polarizabilities of Split Ring Resonators," *Journal of Applied Physics* 98, no. 3 (2005).
[108] M. K. Taher Al-Nuaimi, "Low Profile Dipole Antenna Design Using Square Srrs Artificial Ground Plane" (paper presented at the Wireless Conference (EW), 2010 European, 12-15 April 2010 2010).

[109] Yang Fan and Y. Rahmat-Samii, "Reflection Phase Characterizations of the Ebg Ground Plane for Low Profile Wire Antenna Applications," *Antennas and Propagation, IEEE Transactions on* 51, no. 10 (2003).
[110] Cuming Microwave, "C-Foam Pf-2 and Pf-4," (Technical Bulletin 210-6).
[111] Huang Ying et al., "Design of a Low Profile End-Fire Antenna Using Split-Ring Resonators" (paper presented at the Antennas and Propagation Society International Symposium, 2008. AP-S 2008. IEEE, 5-11 July 2008 2008).
[112] Dan Sievenpiper et al., "High-Impedance Electromagnetic Surfaces with a Forbidden Frequency Band," *Microwave Theory and Techniques, IEEE Transactions on* 47, no. 11 (1999).
[113] D. De Donno et al., "Design and Applications of a Software-Defined Listener for Uhf Rfid Systems" (paper presented at the Microwave Symposium Digest (MTT), 2011 IEEE MTT-S International, 5-10 June 2011 2011).
[114] Italian National Research Council, "Dielectric Properties of Body Tissues," (Institute for Applied Physics).
[115] B. Viala et al., "Rf Planar Ferromagnetic Inductors on Silicon," *Magnetics, IEEE Transactions on* 40, no. 4 (2004).
[116] P. Markondeya Raj et al., "Magnetic Nanocomposites for Organic Compatible Miniaturized Antennas and Inductors" (2005).
[117] H. W. Zhang, X. L. Tang, and H. Su, "Rf Integrated Planar Inductor Fabricated on Ferrite Substrates" (2006).
[118] Byung Ju Kang, Chang Kyu Lee, and Je Hoon Oh, "All-Inkjet-Printed Electrical Components and Circuit Fabrication on a Plastic Substrate," *Microelectronic Engineering* (2012).
[119] Aleksandar Menicanin et al., "Ink-Jet Printed Cpw Inductors in Flexible Technology" (2012).
[120] Viala et al., "Rf Planar Ferromagnetic Inductors on Silicon."
[121] Zhang, Tang, and Su, "Rf Integrated Planar Inductor Fabricated on Ferrite Substrates."
[122] J. L. Snoek, "Dispersion and Absorption in Magnetic Ferrites at Frequencies above One Mc/S," *Physica* 14, no. 4 (1948).
[123] P. Jeppson et al., "Cobalt Ferrite Nanoparticles: Achieving the Superparamagnetic Limit by Chemical Reduction," *Journal of Applied Physics* 100, no. 11 (2006).
[124] K. I. Arai and K. Ishiyama, "Recent Developments of New Soft Magnetic Materials," *Journal of Magnetism and Magnetic Materials* 133, no. 1–3 (1994).
[125] Peng Kun et al., "Synthesis and Magnetic Properties of Ni–Sio2 Nanocomposites," *Materials Chemistry and Physics* 111.
[126] N. J. Tang et al., "Synthesis and Complex Permeability of Co/Sio2 Nanocomposites," *Materials Letters* 59.
[127] N. J. Tang et al., "Complex Permeability of Feni3/Sio2 Core-Shell Nanoparticles," *Solid State Communications* 132.
[128] Markondeya Raj et al., "Magnetic Nanocomposites for Organic Compatible Miniaturized Antennas and Inductors."
[129] P. Markondeya Raj et al., "Novel Nanomagnetic Materials for High-Frequency Rf Applications" (2011 2011).
[130] Y. D. Zhan et al., "Nanocomposite Co/Sio2 Soft Magnetic Materials," *Magnetics, IEEE Transactions on* 37, no. 4 (2001).

[131] Soshin Chikazumi and C. D. Graham Jr, *Physics of Ferromagnetism 2e*, vol. 94 (Oxford University Press, 2009).
[132] An-Hui Lu, E. L Salabas, and Ferdi Schüth, "Magnetic Nanoparticles: Synthesis, Protection, Functionalization, and Application," *Angewandte Chemie International Edition* 46, no. 8 (2007).
[133] G. Guerrero, P. H. Mutin, and A. Vioux, "Anchoring of Phosphonate and Phosphinate Coupling Molecules on Titania Particles," *Chemistry of Materials* 13, no. 11 (2001).
[134] Lu, Salabas, and Schüth, "Magnetic Nanoparticles: Synthesis, Protection, Functionalization, and Application."
[135] J. P. Jakubovics, *Magnetism and Magnetic Materials / J.P. Jakubovics*, Book: 573 (London ; Institute of Materials, 1994.
2nd ed., 1994).
[136] L. Thourel, *The Use of Ferrites at Microwave Frequencies / L. Thourel ; Translated by J. B. Arthur*, International Series of Monographs on Electronics and Instrumentation ; V. 26 (New York : Macmillan, 1964., 1964), Bibliographies
Non-fiction.
[137] Maurice H. Francombe, *Handbook of Thin Film Devices / Handbook Edited by Maurice H. Francombe* (San Diego, CA : Academic, c2000., 2000).
[138] Raj et al., "Novel Nanomagnetic Materials for High-Frequency Rf Applications."
[139] Olgica Bakajin Robert D. Deegan, Todd F. Dupont, Greb Huber, Sidney R. Nagel, and Thomas A. Witten, "Capillary Flow as the Cause of Ring Stains from Dried Liquid Drops," *Nature* (1997).
[140] J. R. Cooper B. S. Cook, and M. M. Tentzeris, "A Novel Inkjet-Printed Passive Microfluidic Rfid-Based Sensing Platform," in *International Microwave Symposium* (2013).